The Effect of Atmosphere-Snow-Ice-Ocean Coupling on Hexachlorocyclohexane (HCH) Pathways within the Arctic Marine Environment

by Monika Agnieszka Pucko

A Thesis submitted to the Faculty of Graduate Studies of the University of Manitoba

in partial fulfillment of the requirements for the degree of

Doctorate of Philosophy

Department of Environment and Geography

University of Manitoba

Abstract

The importance of the cryosphere, and of sea ice in particular, for contaminant transport and redistribution in the Arctic was pointed out in the literature. However, studies on contaminants in sea ice are scarce, and entirely neglect the sea ice geophysical and thermodynamic characteristics as well as interactions between various cryospheric compartments. This thesis addresses those gaps. Ice formation was shown to have a significant concentrating impact on the levels of HCHs in the water just beneath the ice. Both geophysical and thermodynamic conditions in sea ice were shown to be crucial in understanding pathways of accumulation or rejection of HCHs. Although HCH burden in the majority of the ice column remains locked throughout most of the season until the early spring, upward migration of brine from the ice to the snow in the winter has an effect on levels of HCHs in the snow by up to 50 %. In the spring, when snow melt water percolates into the ice delivering HCHs to the upper ocean via desalination by flushing, levels of HCHs in the ice can increase by up to 2 %-18 % and 4 %-32 % for α- and γ-HCH, respectively. Brine contained within sea ice currently exhibits the highest HCH concentrations in any abiotic Arctic environment, exceeding under-ice water concentrations by a factor of 3 in the spring. This circumstance suggests that the brine ecosystem has been, and continues to be, the most exposed to HCHs. α-HCH levels were shown to decrease rapidly in the last two decades in the Polar Mixed Layer (PML) and the Pacific Mode Layer (PL) of the Beaufort Sea due to degradation. If the rate of degradation does not change in the near future, the majority of α-HCH could be eliminated from the Beaufort Sea by 2020, with concentrations in 2040 dropping to < 0.006 ng/L and < 0.004 ng/L in the PML and the PL, respectively. Elimination of α-HCH from sea water takes significantly longer than from the atmosphere, with a lag of approximately two decades.

Acknowledgements

First, I would like to thank my supervisors, Dr. Gary Stern and Dr. David Barber for enabling me to do the PhD research in the Arctic as part of the International Polar Year (IPY) Circumpolar Flaw Lead (CFL) System Study. I highly appreciate their help and encouragement throughout the process of completing my degree. I greatly thank Dr. Robie Macdonald for inspiring me to always do better. I also thank my Advisory Committee members, Dr. Fei Wang and Dr. Jay Doering, for their comments and suggestions. I am grateful to Wojtek for his help and support, and to Zoyka for being. Finally, I thank the Canadian program office of the International Polar Year, the Natural Sciences and Engineering Research Council (NSERC), Canada Foundation for Innovation (CFI), Canada Research Chairs (CRC), the Department of Fisheries and Oceans Canada, ArcticNet, the Nahidik program, and the University of Manitoba for funding. More detailed acknowledgements are to be found by the end of chapters 2-5.

List of figures

List of tables

Thesis format and manuscript claims

This Ph.D. thesis contains four manuscripts (chapters 2-5), each consisting of Abstract, Introduction, Materials and Methods, and Results and Discussion sections. A general introduction is presented in chapter 1, and a synopsis of research in chapter 6.

Chapter 2: Pućko, M.; G. A. Stern; D. G. Barber; R. W. Macdonald, and B. Rosenberg. 2010. The International Polar Year (IPY) Circumpolar Flaw Lead (CFL) System Study: The Importance of Brine Processes for α- and γ-Hexachlorocyclohexane (HCH) Accumulation or Rejection in Sea Ice. *Atmosphere-Ocean.* **48:** 244-262.

M. Pućko planned the field sampling, and collected and analyzed samples with help of B. Rosenberg. B. Rosenberg analyzed samples for EF values. M. Pućko analyzed data and prepared the manuscript with the participation of co-authors.

Chapter 3: Pućko, M.; G. A. Stern; R. W. Macdonald, and D. G. Barber. 2010. α- and γ-Hexachlorocyclohexane Measurements in the Brine Fraction of Sea Ice in the Canadian High Arctic Using a Sump-Hole Technique. *Environ. Sci. Technol.* **44:** 9258-9264.

M. Pućko planned and organized the field sampling. M. Pućko collected and analyzed samples, analyzed data and prepared the manuscript with the participation of co-authors.

Chapter 4: Pućko, M.; G. A. Stern; R. W. Macdonald; B. Rosenberg, and D. G. Barber. 2011. The Influence of the Atmosphere-Snow-Ice-Ocean Interactions on the Levels of Hexachlorocyclohexanes (HCHs) in the Arctic Cryosphere. *J. Geophys. Res.* **116:** C02035, doi:10.1029/2010JC006614.

M. Pućko planned and organized the field sampling. M. Pućko collected and analyzed samples, analyzed data and prepared the manuscript with the participation of co-authors. B. Rosenberg analyzed samples for EF values.

Chapter 5: Pućko, M.; G. A. Stern; R. W. Macdonald; D. G. Barber; B. Rosenberg, and W. Walkusz. When will α-HCH disappear from the Arctic Ocean? Accepted with minor revisions to *J. Mar. Syst.*

M. Pućko collected and analyzed samples for α-HCH from the CFL cruise (with help of B. Rosenberg) and from the Nahidik cruise (with help of W. Walkusz). B. Rosenberg collected and analyzed samples for α-HCH from the CASES cruise and analyzed samples for EF values. M. Pućko analyzed data and prepared the manuscript with the participation of co-authors.

Chapter 1

General introduction

1.1 Research background

1.1.1 *Sources and pathways of HCHs to the Arctic environment*

Hexachlorocyclohexane (HCH), also known as benzene hexachloride (BHC) in the past, is an organochlorine insecticide which was used heavily worldwide since the 1940s (Li *et al.,* 1998). HCH was available in two commercial products: technical HCH and lindane. Technical HCH consists of 5 stable geometric isomers: α-HCH (55 %-80 %), β-HCH (5 %-14 %), γ-HCH (8 %-15 %), δ-HCH (2 %-16 %) and ε-HCH (3 %-5 %), whereas lindane contains more than 90 % of γ-HCH, the only isomer with insecticidal properties (Metcalf, 1955; Barrie *et al.,* 1992). Technical HCH was the dominating contributor of γ-HCH to the environment until the late 1970s, and thereafter lindane became the major source of this isomer. Canada banned use of technical HCH in 1971, followed by United States in 1978 and many European countries (Jantunen and Bidleman, 1995; Breivik *et al.*, 1999). Use of lindane is currently banned in over 50 countries around the world (e.g. in Canada since 2004), but its usage continues in many parts of the world especially in some Asian and African countries, e.g. India (US EPA, 2006). In 2005, Hung *et al.* classified γ-HCH as a 'current-use insecticide' due to its elevated levels in the Arctic in the spring, referred to as 'spring maximum events' (SMEs).

Total global emissions in the 1980s and 1990s are estimated at 228 kt for α-HCH, and 76 kt for γ-HCH (Macdonald *et al.,* 2000). HCHs were transported to the Arctic through a combination of solvent switching and solvent depleting/enhancing processes (Li and Macdonald, 2005). Their travel was initiated at the place of application from soil via entering surface water through runoff or air through volatilization. Solvent switching between air and water occurred continuously along the

transport pathway, and acted differentially on α- and γ-HCH due to differences in their physical-chemical parameters. A large database for α-HCH, together with multimedia models showed this chemical to exhibit classical "cold condensation" behavior (Li *et al.*, 2002). The surface water of the Arctic Ocean became loaded between 1950 and 1990 because atmospheric transport of α-HCH from source regions to the Arctic was rapid (highest Henry's Law Constant, HLC, and vapour pressure of all three HCH isomers favoring airborne transport), and because α-HCH partitioned strongly into cold water of the Arctic Ocean due to HLC decrease with temperature. γ-HCH was transported to the Arctic via a combination of atmospheric and ocean currents (HLC and vapour pressure lower than α-HCH). HCHs provide an important lesson that environmental pathways must be comprehensively understood and linked to physical-chemical properties before attempting to predict the behavior of one chemical by extrapolation from a seemingly similar chemical. It is also a good example of how current and historical biological exposures to different HCH isomers in the Arctic were determined by their physical-chemical characteristics affecting their pathways into the North, mainly through atmosphere-ocean processes.

1.1.2 *Structures of HCH isomers*

Hexachlorocyclohexane is a derivative of cyclohexane, in which 6 hydrogen atoms are substituted by chlorine atoms. Hexachlorocyclohexane isomers are stereoisomers, and in particular diastereomers or geometric isomers. They are isomeric molecules that have the same molecular formula ($C_6H_6Cl_6$) and sequence of bonded atoms (constitution) but which differ only in the three-dimensional orientations of their atoms in space, and have a plane or axis of symmetry.

In general, substituents in cyclohexane are most stable when in equatorial positions which is strictly connected to sterics. Axial bonds are more hindered than the corresponding equatorial bonds, because the substituents in the axial position are relatively close to two other axial substituents. Proximity of the axial substituents, especially if they are relatively large, can result in various strains and, thus, more energy will be required to keep such a conformation. The preference of a substituent towards the equatorial position is measured in terms of its A-Value, which is the Gibbs free energy difference (ΔG^0) between the equatorial and the axial conformers. A positive A-Value indicates preference towards the equatorial position. Chlorine, a substituent found in hexachlorocyclohexane, has the A-Value of 0.43 kcal/mol. Structures of the two most abundant HCH isomers in the Arctic (α and γ) including α-HCH enantiomers are shown in the Figure 1.1.

Figure 1.1 Chemical structures of two most common HCH isomers (α and γ) including α-HCH enantiomers; bold represents chlorines substituted in equatorial positions

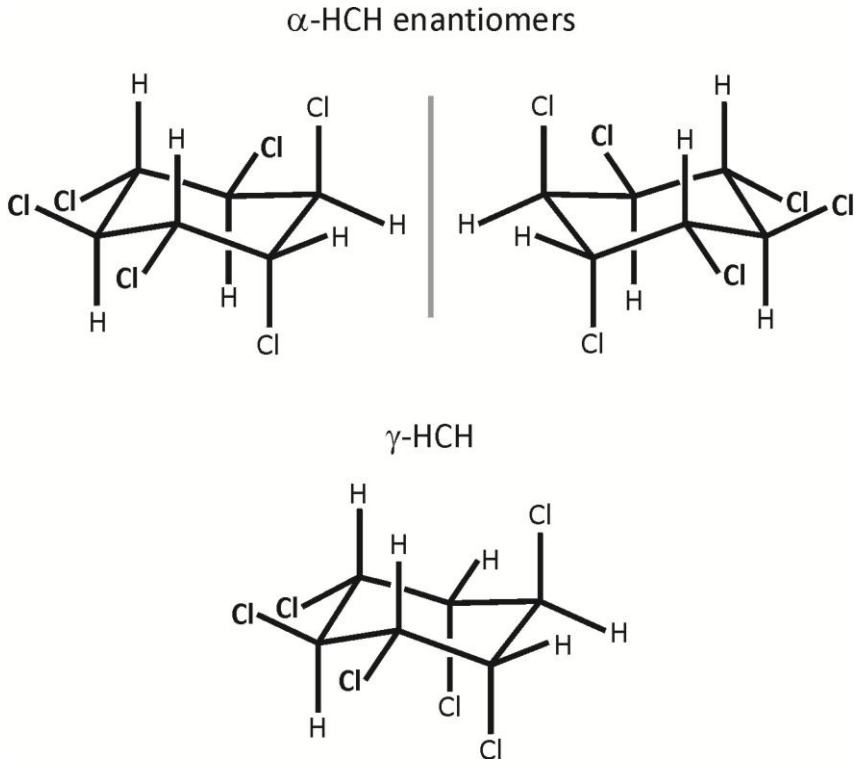

α-HCH consists of two mirror-image enantiomers, termed (+) and (-). Enantiomers (optical isomers) are two stereoisomers that are related to each other by a reflection. They are mirror images of each other which are not superimposable, and every stereogenic center in one has the opposite configuration in the other. A symmetry of a molecule determines whether it will form enantiomers (chirality). A chiral molecule lacks the plane of symmetry. Although enantiomers exhibit identical basic physical and chemical properties, they behave differently when degraded by microbes because enzymes exhibit stereo selectivity (Müller and Kohler, 2004). Accordingly, the racemic (1:1) mixture of α-HCH released into the environment undergoes enantioenrichment when enantioselective processes come into play (microbial breakdown, selective biological uptake, biotransformation and elimination pathways in food webs (Faller *et al.*, 1991a; Falconer *et al.*, 1995; Wiberg *et al.*, 2000)). On the other hand, abiotic transformations of HCHs such as transport, hydrolysis or photolysis are not enantioselective. Change in the enantiomer fraction (EF), which is therefore a good indicator of biological processes (Hühnerfuss *et al.*, 1992), can be expressed as:

$$EF = (+)\alpha\text{-HCH}/[(+)\alpha\text{-HCH}+(-)\alpha\text{-HCH}] \quad \text{(eq. 1.1)}.$$

Jantunen and Bidleman (1998) determined spatial and vertical distribution of α-HCH EFs across the Arctic Ocean from the Bering and Chukchi Seas, through the North Pole, to a station north of Spitsbergen, and then to the south into the Greenland Sea. Preferential enantioselective degradation of (-)α-HCH, indicated by surface water EFs > 0.5, was found in the Bering and Chukchi Seas, whereas the (+) enantiomer was depleted in the Arctic Ocean and Greenland Sea with EFs < 0.5. Reasons for the opposite depletion patterns are not well understood. One hypothesis is that different microbial populations in those regions are responsible. As first pointed out in Faller *et al.* (1991b), (+)α-HCH is preferentially degraded in some regions of the North Sea

whereas (-)α-HCH is depleted in others. Even though HCHs are > 99 % in the dissolved phase, Jantunen and Bidleman (1998) were able to measure EF values of the filtered particles of large volume samples. Their observations suggest that α-HCH enantioselective degradation in the dissolved and particulate phase are decoupled and may involve different microbial populations. α-HCH EFs generally decrease with depth in the Arctic Ocean. Two explanations were suggested to account for the greater enantioselectivity with depth (Jantunen and Bidleman, 1998). As particles settle from the surface, the sorbed α-HCH is metabolized and released back into the dissolved phase. Alternatively, EFs decreasing with depth may reflect older, Atlantic-layer water, which lies below the pycnocline.

1.1.3 *Physical-chemical properties of α- and γ-HCH*

Physical-chemical properties of α- and γ-HCH are summarized in Table 1.1. The vapour pressure (p^0) describes the tendency of a chemical to transfer to and from gaseous environmental phases. p^0 is defined as the pressure of the vapour of a compound at equilibrium with its pure condensed phase, be it liquid or solid (Schwarzenbach *et al.*, 1993). One approach is to extrapolate the p^0 measured above the melting point to lower temperatures while another way is to use a thermodynamic relationship to estimate the liquid-phase p^0 at temperatures below the melting point (Bidleman, 1999). The uncertainty in each of these approaches increases as the difference between ambient temperature and the melting point becomes greater. The relationship between p^0 and temperature (T) can be expressed by the Clausius-Clapeyron equation:

$$\ln p^0 = m/T + b \quad \text{(eq. 1.2)}$$

where m and b are constants.

Table 1.1 Physical-chemical properties of α- and γ-HCH

Property	α-HCH	γ-HCH	Summary
Molecular weight (g/mol)	290.83	290.83	α = γ
Color	Brownish to white	White	
Physical state	Crystalline solid		
Melting point (°C)	159-160	112.5	α > γ
Boiling point (°C) at 760 mm Hg	288	323.4	
Aqueous solubility (mol/m^3) At 25 °C ([c])	0.333	0.247	α > γ
HLC (Pa m^3/mol) at 20 °C ([a]) and 25 °C ([b])	0.36[a] 1.24[b]	0.16[a] 0.52[b]	α > γ
K_{OA} at 25 °C ([c])	2.91 10^7	5.50 10^7	γ > α
p^0 (Pa) at 25 °C ([c])	0.245	0.0757	α >> γ
K_{OW} ([d])	3.8	3.72	α = γ
Microbial degradation, Arctic Ocean, $t_{1/2}$ (years) ([e])	5.9 (+)α-HCH 23.1 (-)α-HCH	18.8	(-)α > γ > (+)α

[a]Sahsuvar *et al.*, 2003; [b]Altschuh *et al.*, 1999; [c]Xiao *et al.*, 2004; [d]Hansch and Leo, 1995; [e]Harner *et al.*, 1999

Henry's Law Constant (HLC) defines how a chemical partitions at equilibrium between gas and liquid phases. It can be thought of as simply the ratio of a compound's abundance in the gas phase to that in the aqueous phase at equilibrium. The abundance of a chemical in the gas phase is commonly expressed as its partial pressure, *p*, and its abundance in the aqueous solution as a molar concentration, C*w* (Schwarzenbach *et al.*, 1993). Thus:

$$HLC = p/Cw \text{ (Pa m}^3\text{/mol)} \qquad \text{(eq. 1.3).}$$

HLC can be estimated by ratioing a chemical's liquid phase saturation vapour pressure (usually the sub-cooled liquid vapour pressure) over its aqueous solubility, at some reference temperature (Halsall, 2007). Vapour pressure is defined above, and the aqueous solubility is commonly defined as the abundance of the chemical per unit volume in the aqueous phase when the solution is in equilibrium with the pure compound in its actual aggregation state (gas, liquid, solid) at a specified temperature and pressure (Schwarzenbach *et al.*, 1993).

Air-water partition coefficient (K_{AW}) is a 'dimensionless' HLC (Halsall, 2007), and can be defined by the ratio of chemical's concentration in gas phase (C*a*) and liquid phase (C*w*) expressed in the same units:

$$K_{AW} = Ca/Cw \quad \text{(eq. 1.4)}.$$

K_{AW} is derived from HLC by converting vapour pressure into 'solubility' with units of molar concentration by applying the ideal gas law:

$$p\,V = n\,R\,T \quad \text{(eq. 1.5)},$$

where V is the volume (m^3), n is the amount of substance (mol), R is the gas constant (8.314 Pa m^3/mol K), and T is the temperature (K). Rearranging the equation 1.5 to n/V = *p*/R T, allows the following expression:

$$K_{AW} = Ca/Cw = p/R\,T\,Cw = HLC/R\,T \quad \text{(eq. 1.6)}.$$

Air-water partition constant quantifies the relative escaping tendency (fugacity) of a compound existing as vapour molecules as opposed to being dissolved in water (Schwarzenbach *et al.*, 1993). Thus, compounds with high vapour pressures (low fugacity in the gas phase) and low solubility in water (high fugacity in aqueous solution) should partition appreciably from water into air (high HLC and K_{AW}). The opposite would be true for the water-air partition coefficient describing, for example, a tendency of a compound to be scavenged from the atmosphere by rain.

Temperature is a key parameter for controlling HLC or K_{AW}. HLCs of organochlorines decrease with temperature (T), and thus will tend to partition more strongly into cold, Arctic waters than in the warmer oceans at temperate latitudes. For example, at equilibrium the ratio of α-HCH concentration in seawater to that in air is 3,000 at 25 °C, but 22,000 at 0 °C (Macdonald *et al.*, 2000). The effects of salt should also be taken into consideration when describing HLC or K_{AW}. In general, seawater

solubilities are smaller, but within a factor of 2 of distilled water values, thus the air-water ratios will be enhanced in the seawater.

Henry's Law Constant dependence on temperature is relatively well described for HCHs. HLC values for α- and γ-isomers versus reciprocal temperature are described using the following equation for temperatures of 5 °C to 35 °C (Sahsuvar *et al.*, 2003):

$$\text{Log HLC} = b + m/\text{T} \quad \text{(eq. 1.7)}.$$

Parameters (± standard deviation) of equation 1.7 for α- and γ-HCH isomers are:

$$\text{Log HLC}_{\alpha} = 10.13\ (\pm\ 0.29) - 3098\ (\pm\ 84)/\text{T} \quad \text{(eq. 1.8)},$$

$$\text{Log HLC}_{\gamma} = 10.14\ (\pm\ 0.55) - 3208\ (\pm\ 161)/\text{T} \quad \text{(eq. 1.9)}.$$

Octanol-air partition coefficient (K_{OA}) is used as a proxy to model partitioning between air and organic phases such as vegetation, soil, and particles in air and water.

Particle-gas partition coefficient (K_P) is the ratio of chemical concentration on atmospheric particles (ng/μg) to concentration in the gas phase (ng/m^3). Exchange of atmospheric compounds between the atmosphere and the Earth's surface takes place by rain and snow scavenging of gaseous and particulate species and transfer of gaseous compounds across air-water and air-solid surfaces. Flux equations used to describe these processes take into account the partitioning of the compound between the particle and gas phases in air (Cotham and Bidleman, 1991). Estimates of the atmospheric phase distribution are frequently made with the Junge-Pankow (J-P) adsorption model (Pankow, 1987):

$$\varphi = c\theta/(p^0 + c\theta), \quad \text{(eq. 1.10)},$$

where φ is the fraction of the total airborne compound sorbed to aerosols, p^0 is the supercooled liquid-phase vapour pressure at the ambient temperature, and θ is the aerosol surface area (cm^2 aerosol surface per cm^3 air). Parameter c depends on the thermodynamics of adsorption and varies with compound and aerosol type.

The octanol-water partition coefficient (K_{OW}) is used to represent the equilibrium distribution of organic contaminants between lipid phases and water, and is widely applied as a correlation parameter for bioaccumulation and sediment sorption. It can be defined as a ratio of chemical solubility in octanol and water, which both increase with temperature. However, K_{OW} varies weakly with temperature.

In general, octanol-air and octanol-water partition coefficients for HCHs increase with temperature.

1.1.4 *Mass balance model of HCHs in the Arctic Ocean*

The first mass balance for HCHs in the Arctic Ocean was based on limited data in air, ocean and rivers in the mid-1980s (Barrie *et al.*, 1992). Barrie and colleagues also assumed that atmospheric levels remained constant over the year. The estimated standing stock of HCHs in the upper 200 m of the water column was 8,100 tonnes with a residence time of 20-30 years. Major inputs to the Arctic Ocean were by ocean currents (63 %), atmospheric deposition (30 %) and river runoff (7 %). Losses were mainly by outflow of water to the North Atlantic through the Canadian Archipelago (78 %), the East Greenland Current (16 %), and to a lesser extent by other currents (4 %) and ice export (2 %).

In 2000, Macdonald and colleagues published revised HCH budget by: using new atmospheric HCH measurements; estimating atmospheric fluxes on a monthly basis rather than biannually; incorporating new data on the spatial variability of HCHs in the Arctic Ocean; making use of more detailed information on the circulation, ice cover and water budget of the Arctic Ocean; updating estimates on the input of HCHs by rivers and ocean currents; and accounting for the degradation of HCHs by hydrolysis and microbial action.

The estimated standing stock of HCHs in the upper 200 m of the water column was 2,910 tonnes. The total annual inputs were estimated at 186 tonnes of α-HCH and 83 tonnes of γ-HCH. The following percentages of total of α-HCH and γ-HCH were estimated to enter the Arctic Ocean via ocean currents (58 % and 39 %), atmospheric deposition (28 % and 12 %), and rivers (13 % and 49 %). Total annual losses were 555 tonnes of α-HCH and 79 tonnes of γ-HCH. Removal was taking place by water outflow (49 % and 58 %), degradation (43 % and 34 %), volatilization (7.2 % and 6.6 %), and ice export (1.2 % and 1.3 %). Microbial degradation accounted for about 85 %, and hydrolysis for about 15 %, of the total degradation of HCHs.

The output/input ratio for α-HCH in the budget by Macdonald et al. (2000) was 3, indicating net removal from the Arctic Ocean, whereas the budget was balanced for γ-HCH. In 2004, Li *et al.* developed an Arctic Mass Balance Box Model (AMBBM) to calculate a sequential historical α-HCH budget in the Arctic Ocean from its introduction in the 1940s up to the 2000. The results of the model compared well with the previously published budgets, and showed that the α-HCH burden in the Arctic Ocean started to accumulate in the early 1940s and reached the highest value of 6,670 tonnes in 1982, 1 year before China banned the use of technical HCH. Since then the burden of α-HCH in Arctic waters has decreased quickly by an average of approximately 270 t/yr during the 1990s, decreasing from 4,220 tonnes in 1990 to 1,550 tonnes in 2000. Authors predicted that the complete elimination of α-HCH from Arctic waters would require another two decades.

1.1.5 *Biological exposures to HCHs in the Arctic*

HCHs were classified as contaminants of concern due to their persistent, bioaccumulative and toxic properties (Prasad *et al.*, 1995; Magnusson *et al.*, 1996;

Möller *et al.*, 1996; Hargrave *et al.*, 2000; Macdonald *et al.*, 2000). Although α- and γ-HCH were shown to be toxic and tumor-promotive in rats through hepatotoxicity as evidenced by increased activity of cytochrome P450 monooxygenase, hepatocarcinogenic risk in the case of human exposure was not proven for either α- or γ-HCH (Schulte-Hermann and Parzefall, 1981; Pereira *et al.*, 1982; Möller *et al.*, 1996). A significant difference between the α-HCH enantiomers was observed concerning the cytotoxic effect as well as the growth stimulation with greater effectiveness of (+)α-HCH (Möller *et al.*, 1996). Thus, the enantioselective enrichment of (-)α-HCH is associated with a lower risk factor than the bioaccumulation of (+)α-HCH. Also, α-HCH is the only HCH isomer that can cross blood-brain barrier (Mössner *et al.*, 1992). The study was done on neonatal northern fur seals (*Callorhinus ursinus*), where both α- and γ-HCH isomers gave a tissue specific distribution with a rather constant α/γ ratio of 4 ± 2. Only the brain tissue had α/γ ratio of 36 ± 1.

Bioaccumulation refers to the accumulation of substances, such as pesticides, in an organism. Bioaccumulation occurs when an organism absorbs a toxic substance at a rate greater than that at which the substance is lost (Bryan *et al.*, 1979). Thus, the longer the biological half-life of the substance the greater the risk of chronic poisoning, even if environmental levels of the toxin are not very high. Bioaccumulation is described by Bioaccumulation Factor (BAF) defined as a concentration of a chemical in tissue divided by its concentration in the diet (on a wet or lipid weight basis). BAF is strongly correlated to the chemical K_{OW} (Mackay, 1982). α- and γ-HCH have very similar K_{OW} values (Table 1.1). In general, bioaccumulation factors, particularly in lower trophic levels (e.g. plankton), reflect seawater concentrations in the case of α- and γ-isomer (Hargrave *et al.*, 1992). Levels of HCHs (Σ) in polar bear (*Ursus maritimus*) adipose

tissue and ringed seal (*Phoca hispida*) blubber were found to be well correlated with the geographical distribution of HCHs in the seawater as well (Muir and Norstrom, 2000).

Once HCHs enter organisms, they are subject to biotransformation pathways that can change concentrations, ratios of isomers and α-HCH EFs. For example, α-HCH was reported to be present in human placentas, with EFs close to racemic at higher concentrations and different from racemic at lower concentrations which was attributed to faster metabolism of (+)α-HCH (Shen *et al.*, 2006). Another example of enantioselective transport of α-HCH was presented by Mössner *et al.* (1992). They found ratios of (+)α-HCH/(-)α-HCH in the blubber, liver, lung, and milk tissues of neonatal northern fur seals within a range of 1.2-1.9, whereas the brain samples showed surprisingly high ratio of 30 ± 2. The high α-HCH ratio in brain tissues may be a result of the blood-brain barrier, which in the case of α-HCH can probably be crossed selectively by one enantiomer.

1.1.6 *Air-water gas exchange of HCHs in the Arctic*

The fugacity of a component in a mixture is essentially the pressure that it exerts in the vapour phase when in equilibrium with the liquid mixture. To describe the saturation state of water relative to the partial pressure in air, the fugacity ratios (f_w/f_a) are implemented according to the following formulas (Jantunen and Bidleman, 1995):

$$f_w = 10^{-9} C_w \, HLC / M \quad \text{(eq. 1.11)},$$

$$f_a = 10^{-9} C_a \, R \, T_a / M \quad \text{(eq. 1.12)},$$

$$f_w / f_a = C_w \, HLC / C_a \, R \, T_a \quad \text{(eq. 1.13)},$$

where C_w and C_a are the concentrations of dissolved and gaseous HCHs in water and air (ng/m^3), R is the gas constant (8.314 Pa m^3/mol K), T is the air temperature in K, M is the molecular weight (290.83 g/mol), and HLC is the Henry's Law Constant (Pa

m^3/mol) as a function of the surface water temperature. A fugacity ratio = 1, > 1 and < 1 indicates equilibrium state, potential for volatilization and deposition, respectively. Fugacity ratio indicates only the direction of spontaneous net exchange and the flux, which takes into account the mass transport and the sea ice concentration (SIC), is used to estimate air-water exchange rates.

Fluxes of HCHs (F) are calculated using the two-film model and the following relationships (Mackay and Yeun, 1983; Hinckley *et al.*, 1991; Jantunen and Bidleman, 1996; Jantunen and Bidleman, 1997):

$$F_p = 10^9 \, M \, D_{AW} \, (f_w - f_a) \quad \text{(eq. 1.14)},$$

$$F = F_p \, (1 - SIC / 100) \quad \text{(eq. 1.15)},$$

$$D_{AW} = (86400 \, k_a) / (R \, T_a) \quad \text{(eq. 1.16)},$$

$$k_a = 10^{-3} + 4.62 \, 10^{-4} \, (6.1 + 0.63 \, u_{10})^{0.5} \, u_{10} \, Sc_g^{-0.67} \quad \text{(eq. 1.17)},$$

$$u_{10} = 10.4 \, u_z / (\ln(z) + 8.1) \quad \text{(eq. 1.18)},$$

where F_p is the potential HCH flux in ng/m^2 day (for 100 % of open water), F is the actual HCH flux in ng/m^2 day (adjusted for the sea ice concentration), D_{AW} is the transport parameter (mol/m^2 day Pa), k_a is the transport velocity in gas phase (m/s), Sc_g is the Schmidt number in gas phase, u_{10} is the wind speed at 10 m above the sea surface (m/s), u_z is the wind speed at z m above the sea surface (m/s), and SIC is the sea ice concentration (%). Fluxes > 0 imply volatilization, and < 0 deposition.

The actual flux of HCHs between air and surface sea water will depend on the HCH concentrations in the air and water, air and water temperatures, wind speed and sea ice concentration. Thus, air-water gas exchange will be controlled to a great extent by ocean processes determining HCH distribution in the sea water, particularly in the surface layer, as well as it strongly depends on season through temperature, sea ice concentration and differences within ocean processes determining the distribution of

HCHs in the surface layer. Below, the main mechanisms contributing to the Arctic Ocean functioning are reviewed from a seasonal perspective and linked to the air-water exchange of HCHs.

Water mass circulation and vertical distribution in the Arctic Ocean are strongly connected to its complex bathymetry (Aagaard, 1989). The Ocean interior is divided by the Lomonosov Ridge into two main basins: the Canadian and Eurasian Basin. The Canadian Basin is further divided into the Canada and Makarov Basins by the Alpha-Mendeleyev Ridge. The Eurasian Basin consists of the Amundsen and Nansen Basins divided by the Nansen-Gakkel Ridge. These Basins are surrounded by broad (600-800 km), shallow (30-200 m) continental shelves along the Barents, Kara, Laptev, East Siberian and Chukchi Seas. The two main basins maintain distinct circulations separated by a front in the central region over the Lomonosov Ridge (Anderson *et al.*, 1994).

Sea water enters the Arctic Ocean from the Pacific Ocean through the Bering Strait, and from the Atlantic Ocean through the Fram Strait. Much of the water entering from the Pacific escapes through the Canadian Archipelago, while some exits through the Fram Strait (Macdonald and Bewers, 1996). One branch of the Atlantic water passes over the Barents Shelf, where it is modified and rejoins the less modified branch that enters in the West Spitsbergen current. The Atlantic layer circulates counter-clockwise around the Arctic Ocean basins while being modified by shelf water to escape eventually in the East Greenland current.

The main parameter controlling the distribution of contaminants in the Arctic Ocean is vertical stratification (Macdonald and Bewers, 1996). The Arctic Ocean is vertically stratified into layers that owe their origin to water masses entering from the Pacific and the Atlantic. The surface layer is termed the Polar Mixed Layer (PML). It

includes approximately the top 40 m, and has a residence time of about 5 years. In the summer, there is a 5-10 m layer of fresher surface water from melting sea ice, river runoff and precipitation, which is creating stratification of this layer. In the winter, relatively saline and dense brine expelled during the initial stages of sea ice formation destabilizes the PML allowing it to mix. Beneath the PML, a halocline is found. Halocline is a cline of a strong vertical salinity (and density) gradient, which prevents the surface ocean layer from mixing with the deeper ocean. Within the Canada and Makarov Basins, the halocline is dominated by water from the Pacific Ocean that entered through the Bering Strait and has been modified by sea-ice formation and runoff on the Chukchi Shelf. Below this layer there is a region called the lower halocline which is of Atlantic origin modified by the brine drainage water mainly on the Barents Shelf. In the Amundsen and Nansen Basins, the halocline region is of Atlantic origin. Below the halocline, there is the Atlantic water layer from about 225 m to approximately 1000 m with the residence time of roughly 25-30 years. Below the Atlantic layer, there is a deep layer with the residence time of up to 300 years depending on the basin. Basic arrangement or vertical stacking of water masses, also called water mass assembly, found in the Arctic Ocean is distinct for the two major basins mainly due to the presence or absence of the relatively fresh, high-nutrient Pacific origin water (McLaughlin *et al.*, 1996). The Western Arctic (WA) assembly, which contains a halocline of Pacific origin, is characteristic for the Canadian Basin. The Eastern Arctic (EA) assembly, in which the halocline is of Atlantic origin, is typical for the Eurasian Basin; however, it was shown that EA assembly pertains into the Makarov Basin during the highly positive AO index (Macdonald and Bewers, 1996). In the WA assembly, the Atlantic layer has a core temperature of generally below 0.5 °C (McLaughlin *et al.*, 1996). In the EA assembly, the core of the Atlantic

layer is as warm as 2 °C – 3 °C. The deep and more saline layer in the WA assembly is about -0.5 °C, and -0.9 °C in the EA assembly.

Large continental shelves comprise over 30 % of the surface area of the Arctic Ocean and play a key role in establishing property distributions within the Arctic Basin. The main mechanisms recognised to drive shelf/basin exchange (SBE) are: brine drainage, river discharge and the associated estuarine circulation, and wind forcing leading mainly to upwelling (Carmack and Chapman, 2003). Although downwelling can occur in the Canada Basin, upwelling is more prevalent due to easterly and northeasterly winds. The primary signature of the upwelling is the appearance of salty Atlantic water at shallow depths. More precisely the upwelled water is from the lower halocline Atlantic water. The efficiency of the upwelling formation depends strongly on the location of the ice edge relative to underlying topography. Upwelling-favorable winds generate very little SBE so long as the ice edge remains shoreward of the shelf break, but an abrupt onset of shelf-break upwelling takes place when the ice edge retreats beyond the shelf break.

Air-water gas exchange of HCHs occurs exclusively at the ocean-air interface. HCH levels in the air and water will tend to equal the partitioning equilibrium value described by Henry's Law Constant (HLC). This process will strongly depend on the HCH fugacity differences between the gas and the dissolved phase. Ocean processes influencing water masses distribution, and thus HCH concentrations in the surface water, will have a major impact on the HCH air-water exchange. They are summarized separately for the winter and summer season in Figure 1.2.

In the winter, air-water exchange of HCHs will be remarkably limited mainly due to the ice cover barrier (Figure 1.2A). The exchange will only take place in the leads and polynyas regions. The rejection of brine with relatively high salinity and HCH

concentrations will promote mixing of the PML unifying the HCH concentrations in the PML at the beginning of the ice formation. Winter stratification of the Arctic Ocean will limit the mixing of surface water with deeper ocean layers by the presence of the halocline below 40 m, and the wind-driven mixing of the PML will be further dramatically limited due to the extensive ice cover. In general, the processes that may change HCH concentrations in the surface water and affect the limited air-water exchange include ocean currents, exchange between the PML and deeper ocean layers and shelf/basin water exchange (SBE). Exchange of HCHs between the PML and deeper layers could potentially occur through the organic and mineral matter sedimentation or biota migrations (e.g. zooplankton).

In the summer, mixing of the surface water with the deeper water in the PML will be limited by the presence of the fresher water from the ice melt, river runoff and precipitation resulting in the PML stratification (Figure 1.2B). However, air-water exchange of HCHs will take place over the vast area due to the reduction in the sea ice extent. Higher air temperatures and rougher sea surface will both enhance the HCH exchange process. Also, higher productivity will promote zooplankton migrations with the potential to influence the HCH vertical distribution by HCH release/uptake in different water masses. HCH concentrations in the surface water may also be affected by uptake by biota (primary producers, zooplankton, etc.) and subsequent release in the deeper layers during particulate organic matter sedimentation. The main SBE processes influencing the HCH distribution in the surface water of the Arctic Basin in the summer include river runoff, upwelling, and wind-enforced mixing.

Figure 1.2 Basin and shelf processes in the Arctic Ocean affecting air-water gas exchange of HCHs in the winter (A) and summer (B)

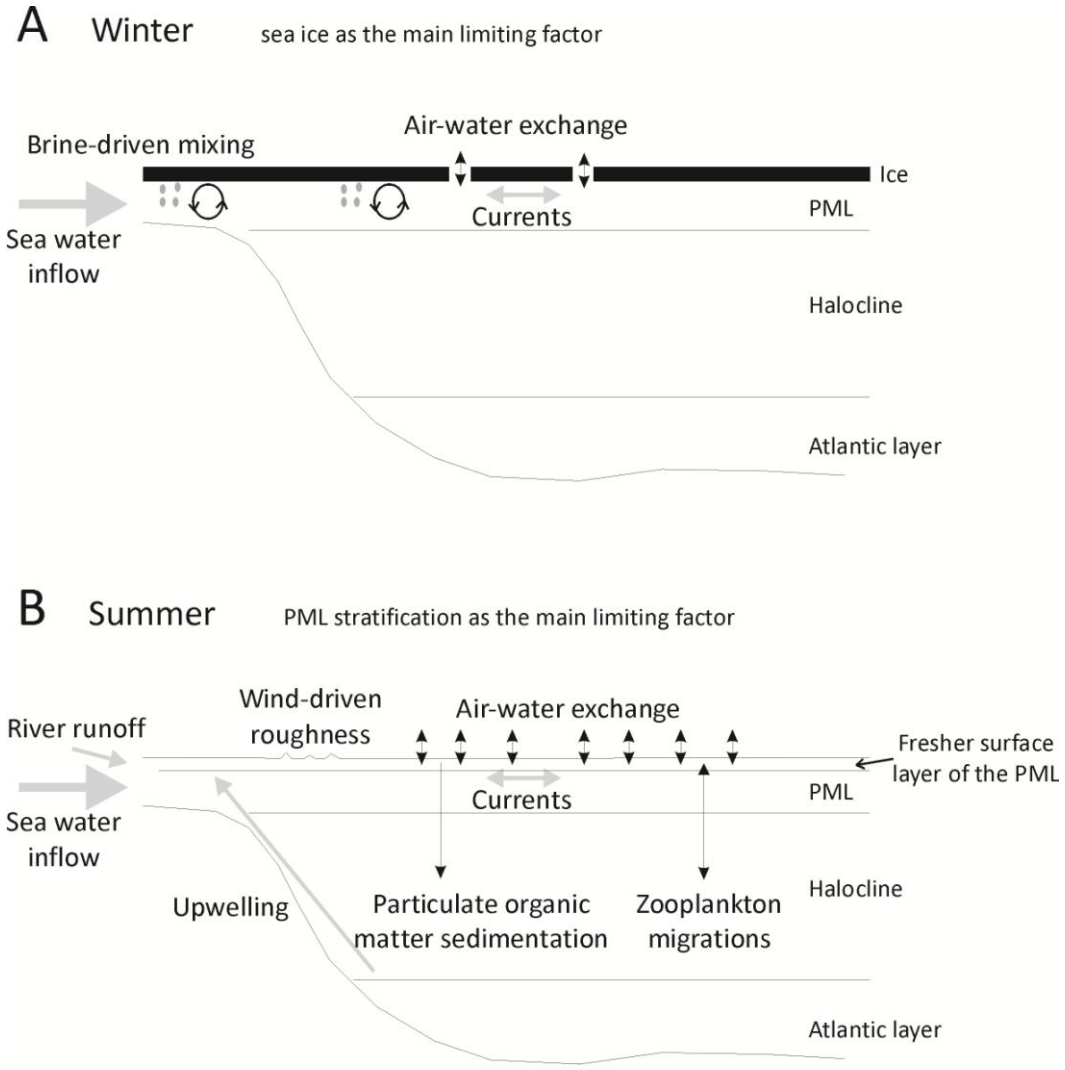

α-HCH accumulated in the cold surface water in the Arctic Ocean and, with the reversal of the air-water gas exchange direction for this isomer in the Arctic Ocean (Jantunen and Bidleman, 1995), is currently being volatilized back to the atmosphere due to decreased air concentrations. According to the same authors, γ-HCH was near the equilibrium state.

1.1.7 *Degradation of HCHs in the water*

Removal of HCHs from subsurface waters in the Arctic Ocean occurs by three main mechanisms: biological degradation, hydrolysis, and removal by partitioning to settling particles (sedimentation), with the latter playing much less important role (Harner *et al.*, 1999). For example, the half-life of α-HCH due to sedimentation in the Arctic Ocean was estimated at > 700 years. Photolysis of HCHs can be neglected when compared to biological and hydrolytic degradation due to the prolonged winter darkness period and limited light penetration due to the ice and snow cover (Helm *et al.*, 2000). Harner *et al.* (1999) estimated the degradation rates due to hydrolysis and microbial activity for (+)α-HCH, (-)α-HCH, and γ-HCH in the eastern Arctic Ocean based on the vertical profiles of EF and concentration, initial concentration data from 1979 and the "ventilation" age of water at a particular depth. The ventilation age, defined as the time since the water was last at the surface and able to exchange gases with the atmosphere, at 250-1000 m in the eastern Arctic Ocean was estimated at 12-20 years (Wallace *et al.*, 1992). Harner *et al.* (1999) assumed that over the years the water has subsided from the surface, there have been no further inputs or losses through atmospheric processes, and the levels of α- and γ-HCH decreased only due to hydrolysis and microbial degradation.

Removal of HCHs from the water column may be represented by the following equation (Harner *et al.*, 1999):

$$C = C^0 e^{-(kd)\,t} \qquad \text{(eq. 1.19)}$$

where C is the concentration at a certain depth, C^0 is the initial concentration at the surface water, t is the ventilation age, and k_d is the degradation rate constant due to hydrolysis and microbial processes ($k_d = k_m + k_h$). The degradation half-life due to basic hydrolysis in sea water was estimated from the second-order rate constant at 0 °C, and equaled 64 and 110 years for α- and γ-HCH, respectively. Accordingly, γ-HCH half-life

due to microbial degradation was estimated at 19 ± 10 years. The situation is more complex for α-HCH since microbes can discriminate between the (+) and (-) enantiomers. In this case, the enantiomers were treated separately as the solution required information about the selectivity of the microbial process.

Removal of the two enantiomers can be described by:

$$C_{(+)} = C^{0}_{(+)}\, e^{-(kd1)\, t} \quad \text{(eq. 1.20)}$$

$$C_{(-)} = C^{0}_{(-)}\, e^{-(kd2)\, t} \quad \text{(eq. 1.21)}$$

where $C^{0}_{(+)}$ and $C^{0}_{(-)}$ represent the initial (surface water) concentrations of (+) and (-)α-HCH in 1979, and $C_{(+)}$ and $C_{(-)}$ are the respective concentrations 17 years later in water at 250-1000 m depth. It was assumed that α-HCH was racemic at the time of input. The pseudo-first order rate constants K_{d1} and k_{d2} are the sum of microbial and hydrolysis removal rates. The half-lives of (+)α-HCH and (-)α-HCH due to microbial degradation were calculated at 6 ± 1 and 23 ± 5 years.

(+)α-HCH degrades faster than γ-HCH by a factor of approximately 3.2. The relative microbial removal rate for (+)α-HCH and (-)α-HCH was 3.9 which was in good agreement with other studies, e.g. by Buser and Müller (1995) where they estimated it at 2.9 in sewage sludge under anaerobic conditions in 25 °C. However, rates of removal of different HCH isomers could easily be changed by rate-determining conditions such as temperature.

1.1.8 *HCH levels and pathways in the Arctic snow and sea ice*

Snow plays an important role in providing atmospherically derived semi-volatile organic compounds like HCHs to the arctic marine environment (reviewed by Herbert *et al.*, 2006). It can be considered as a porous homogenous surface (relative to snow-free surfaces), with a large internal surface area suitable for sorption of vapour-phase

chemicals. The winter snowpack then serves as a reservoir for semi-volatile organic contaminants with Henry's Law Constants low enough for them to be retained in snow (for example HCHs). Spring melt can deliver HCHs in rapid pulses to the sea water, thus influencing biological exposures to a great extent.

Scavenging of semi-volatile organic contaminants by snow is a depositional process (Wania *et al.*, 1998). To quantify snow scavenging, the concepts conventionally applied to rain scavenging have been adopted, notably the total scavenging ratio W_T which is defined as the ratio of concentrations:

$$W_T = C_s / C_a \quad \text{(eq. 1.22)}$$

where C_s is the total mass of chemical per volume of melt water, and C_a is the total mass of chemical per volume of air.

Numerically, W_T can be interpreted as the number of volumes of air which is scavenged of chemical by one volume of snow melt water. Relatively few data for W_T exist for snow scavenging of semi-volatile organic compounds, and there are no published data available for HCHs.

Total scavenging of semi-volatile compounds by snow is a combination of chemical's sorption to air-ice interface (quasi-liquid layer, QLL) and aerosol scavenging. Relative importance of these two processes will depend on the compound's physical-chemical properties. In the case of HCHs, the major process contributing to its scavenging from the atmosphere by snow will be sorption to air-ice interface since the portion of HCHs sorbed to particles in the air is negligible. Thus, physical-chemical properties of HCHs that will affect its scavenging by snow in the Arctic, involve these influencing the partitioning between snow/ice and air.

Hoff *et al.* (1995) examined the partitioning of a number of chlorinated volatile/semi-volatile chemicals to snow, and concluded that partitioning at the ice-air

interface (through derivation of experimental interfacial/air partition coefficients, K_{IA}) was akin to that of water surfaces and could be estimated at temperatures near melting by extrapolating adsorption constants for the air-water interface. In this case, an interfacial/air partition coefficient for snow ($K_{IA\ snow}$) can be calculated according to chemical's aqueous solubility (subcooled) (C_w) and HLC according to:

$$\text{Log } K_{IA\ snow} = -0.769 \text{ Log } C_w - 5.97 + \text{Log R T/HLC} \quad \text{(eq. 1.23)}$$

where R is the gas constant, and T is temperature (293 K).

Another potential form of scavenger of HCHs from the atmosphere is diamond dust, which is a ground-level cloud composed of tiny ice crystals, also referred to as clear-sky precipitation. Diamond dust is most commonly observed in the polar regions, under stable boundary layer with a deep surface-based temperature inversion (Girard and Blanchet, 2001). Similar to ice fog, diamond dust forms directly as ice, whereas ice fog is formed as liquid water which then freezes. Variables distinguishing diamond dust from ice fog in the Arctic are the cloud particle mean diameter (> 30 μm for diamond dust and < 30 μm for ice fog) and the cloud particle number concentration (< 4000/L for diamond dust and > 1000/L for ice fog) (Girard and Blanchet, 2001). Observations show a frequency of up to 50 % of diamond dust and ice fog north of the Arctic circle from November to May (Maxwell, 1982). The main formation mechanism of diamond dust and ice fog in the Arctic is the advection of warm air from midlatitudes and its subsequent radiative cooling at constant pressure (Curry *et. al.*, 1990). However, other mechanisms such as condensation over open leads in the sea ice can contribute locally to the formation. Diamond dust and ice fog play an important role by controlling the radiation and moisture budget of the arctic lower troposphere and thus they affect ice thickness and snow cover (Beesley and Moritz, 1999). A surface cooling of about 5 °C over 5 days is obtained due to increased precipitation efficiency during a diamond dust

event, while ice fogs lead to long-lived ice crystal clouds without any significant precipitation (Blanchet and Girard, 1995).

Once deposited to the snowpack, fate of HCHs will depend on the atmospheric conditions known to influence HCHs dynamics to a great extent (Cabanes *et al.*, 2002; Halsall, 2004). As much as 75 % of a semi-volatile organic contaminant can be lost from the fresh snowpack under windy conditions (~10 m/s) over 24 hours, and only 5 % in the case of calm atmospheric conditions (< 5 m/s) as shown for γ-HCH. This discrepancy is caused by the fact that ventilation of the snowpack greatly reduces snow specific surface area (SSA) which leads to increased snow density (ρ) and reduced snow capacity to hold sorbed chemicals effectively according the following equations (Herbert *at al.*, 2006; Burniston *et al.*, 2007):

$$K_{sa} = K_{IA\ snow}\ SSA\ \rho \qquad \text{(eq. 1.24)}$$

$$\rho = (591 \pm 40)\ \exp\ (-(0.0120 \pm 0.0007)\ (SSA) \qquad \text{(eq. 1.25)}$$

where K_{sa} is a snow sorption coefficient. As a result, chemicals re-partition back into the interstitial pore spaces and are subsequently out-gassed back into the atmosphere. Efficiency of this process is determined by the rapidity of decrease in SSA, which is only high enough in the beginning of winter when the snowpack is still shallow (Hansen *et al.*, 2005). Throughout the rest of the season, relatively constant SSA prevails (250 – 50 cm^2/g) and the temperature-driven changes in snow sorption dominate the snow-air exchange of semi-volatile compounds by reduced snow sorptive capacities (K_{sa}) with increasing temperature. Hansen *et al.* (2005) suggested that HCHs experience the strongest rate of re-evaporation during the last part of the winter when the snowpack warms up due to their relatively strong sorption to snow. In this case, temperature will influence partitioning between different compartments of a snowpack

favoring air pore space by the end of winter season, and will be described in detail below (reviewed by Meyer and Wania, 2008).

Physical-chemical properties influence contaminant behavior in snow primarily by determining how a contaminant is distributed between the various components of a snowpack. In dry snow organic chemicals can reside as gases in the pore space, attached to particles present in the snow, or adsorbed at the air-ice interface, while in wet snow they can also be dissolved in melt water (Meyer and Wania, 2008).

The distribution in dry snow thus depends on the chemical's relative affinity for the gas phase, the ice surface QLL, and the particles contained in the snow, which are controlled by specific partition coefficients. Meyer and Wania (2008) assumed that the organic matter contributes most of the sorptive capacity of the particles in snow, and humic acid is a good surrogate for organic matter. As a result, they expressed affinity to the particles in snow with humic acid-air ($K_{HA\ A}$), humic acid-ice ($K_{HA\ I}$), and humic acid-water ($K_{HA\ W}$) partition coefficients. By plotting the equilibrium phase distribution of α- and γ-HCH in a two-dimensional chemical partitioning space defined by K_{IA} and $K_{HA\ A}$, they obtained the regions of predominant sorption for two different types of snowpack.

In recently fallen snow with a high SSA (1000 cm^2/g), a low density (0.05 g/cm^3), and a moderate organic matter content (0.009 μg/mL snow volume), HCHs partition into the QLL at the ice-air interface within the range of 0 to -20 °C (Meyer and Wania, 2008). Physical changes in aged snow due to snow compaction and dry deposition during aging, resulting in low SSA (125 cm^2/g), high density (0.40 g/cm^3), and a larger organic matter concentration (0.18 μg/mL snow volume), shift the chemical partitioning of HCHs, in particular of the γ-isomer, towards the air pore space with

temperature being the controlling factor of the air-ice interface equilibrium (Meyer and Wania, 2008).

In spring, snow melt water can deliver HCHs to the aquatic ecosystem in the form of short and concentrated pulses. In general, two essential patterns of organic contaminant enrichment in snow melt water have been described (Meyer and Wania, 2008). Type 1 enrichment, leading to a "first flush" of organic contaminants in early melt water fractions, mimicks the melt behaviour of inorganic ions. This early release is attributed to a freezing-out of chemicals and small particles from the ice lattice during snow metamorphism occurring prior to snow melt or during melt/freeze cycles. A downward-percolating melt water front picks up the contaminants concentrated on the ice surface and thus becomes enriched. HCHs exhibit type 1 enrichment, especially under strong temperature fluctuations causing intense melt/freeze cycles. Under gradual spring warming, HCHs are washed out more uniformly, indicating that intense melting at the onset of melt leads to strong preferential flow in confined flow fingers bypassing other areas of the bulk snow (Meyer and Wania, 2008). Type 2 enrichment leads to the late elution of particle-bound substances, and is generally attributed to the filtering of particles by the snowpack.

Of note, it was recently reported that the fraction of γ-HCH estimated to be associated with particles in the snow may have been underestimated by 33 %–75 % (Meyer *et al.*, 2009a). This discrepancy may be caused by an incorrect estimation of organic matter in the snow, phase exchange after melting, and/or by the increasing relative proportion of particles during melting.

HCH levels and pathways in the sea ice are very problematic to discuss due to the fact that studies are scarce, and interpretations are plagued by a complete inattention to sea ice physical and thermodynamic conditions (Hargrave *et al.*, 1988; Gaul, 1989;

Melnikov *et al.*, 2003). Although brine is thought to provide a critical component of the water-soluble compound pathway within the sea ice, there appears to be no detailed study of this subject (Weeks, 1994).

The most common classifications of sea ice in the literature are based on the World Meteorological Organization (WMO) developmental stage (new and young ice <30 cm, first year ice 30-200 cm and old ice > 200 cm that survived at least one melt season), mechanism of formation and crystalline structure (frazil ice – individual unconsolidated ice crystals resulting from the water supercooling, and congelation/fast ice – consolidated sheets of thicker ice), and large-scale form of the ice (landfast or free drifting) (WMO, 1970; Weeks and Ackley, 1986). Often, there are openings in the ice cover, commonly termed leads. Within the ice itself, the orientation and size of ice crystals are broadly classified as granular, transitional/intermediate and columnar (Weeks and Ackley, 1986; Eicken and Lange, 1989).

As the ice grows, it undergoes natural desalination processes by brine pocket migration, brine expulsion, gravity drainage and flushing. Brine expulsion dominates only for the first few hours of ice growth. Gravity drainage dominates for the remainder of the ice growth period, and flushing during the transition from first year to old ice (Cox and Weeks, 1975). Flushing is a form of gravity brine drainage above sea level forced by snow or surface ice melt (Eide and Martin, 1975).

Sea ice consists of ice crystals with pockets of liquid water (brine) and air (Bock and Eicken, 2005). The brine pores vary in size, distribution and degree of connectivity within the ice column depending on ice texture, temperature and growth rate (Weeks and Ackley, 1986; Bock and Eicken, 2005). Brine processes have a major impact on the biological exposure in the Arctic as the HCHs become concentrated in the relatively

small volume of brine (below 5 % in the case of winter arctic sea ice) according to the following equation (after Frankenstein and Garner, 1967):

$$\upsilon b = S\,(49.185 / |T| + 0.532) \cdot 0.1 \quad \text{(eq. 1.26)} \qquad \text{for } -0.5\ ^{\circ}C \geq T \geq -22.9\ ^{\circ}C,$$

where υb is a brine volume fraction (%) (± 0.06 %), S is ice salinity, and T is ice temperature (°C). When υb reaches a critical value of < 5 %, vertical movement of liquids within the sea ice column can occur (Golden *et al.*, 2006).

Both α- and γ-HCH isomers were detected in the dissolved phase of the first year, 140 cm thick, sea ice in the Canadian High Arctic in 3 samples from May-June 1986 (Hargrave *et al.*, 1988). These authors reported mean α- and γ-HCH concentrations of 1.321 ng/L and 0.186 ng/L, respectively.

1.2 Research motivation

1.2.1 *The role of sea ice in contaminant redistribution*

Most ionic species dissolved in sea water are too large to be incorporated into the crystal lattice of ice as a solid solution, thus, only between 15 % and 30 % of the salt contained in sea water is retained in the corresponding volume of newly grown ice (Weeks and Ackley, 1986). Because many dissolved contaminants are excluded with brine during the freezing process, sea ice may be less contaminated than the water from which it forms (Macdonald *et al.*, 2002). Highly saline water, possibly with relatively high levels of contaminants, is formed in this way in many shelf regions allowing for surface to bottom convection (Pfirman *et al.*, 1995). Also, shelf brine runs off the banks and flows into neighbouring depressions carrying associated contaminants along the way. Process of contaminant amplification in the sea water during intense ice formation could be particularly important in the ice production ‘hot spots’ such as Kara and

Laptev Seas (Pfirman *et al.*, 1997; Macdonald *et al.*, 2010). The export of ice from the Kara Sea has been shown to be nine times larger than the import (Korsnes *et al.*, 2002), with the net export equaling 240 km^3/yr (Macdonald *et al.*, 2010). Ice export from the Laptev Sea is even greater with a net value reaching 670 km^3/yr (Macdonald *et al.*, 2010).

A portion of contaminants entrained in sea ice as well as accumulated in the overlying snow over the winter will be released directly into the surface water in the spring. Dynamics of the release will depend on the contaminant physical-chemical properties (Meyer and Wania, 2008; Meyer *et al.*, 2009a, 2009b). For example, more water-soluble contaminants will be released in high pulses at the beginning of the spring in the process of brine flushing. This could be of particular importance in the marginal ice zones (Pfirman *et al.*, 1995). This is a region of intense biological activity, thus contaminants released directly into the surface water from sea ice in the process of spring brine flushing may easily enter the food chain.

As discussed above, there is certainly a potential for sea ice formation, transport and melting to impact contaminant levels in the Arctic, however, virtually no data are available to assess its relative importance. As pointed out by Pfirman *et al.* (1995), future studies should focus on the entrainment, transport and release of contaminants by sea ice. The same authors suggest sea ice should also be investigated in terms of its potential to contribute contaminants to higher trophies levels in the Arctic food web as well as to the ice-associated biota.

1.2.2 *Climate change and its implications for contaminant exposures and pathways*

There is now a general consensus amongst the scientific community and the general public that climate change is one of the greatest global challenges of the future.

Temperatures have risen greatly over the last two decades in air and water (Tett *et al.*, 1999; Barnett *et al.*, 2005), and the consequences of those changes for ecosystems are first to be observed in the Arctic environment (Hansen *et al.*, 2007).

In the era of global warming Arctic is undergoing rapid changes. The extent of sea ice cover decreases gradually as well as the average ice age and thickness (Parkinson *et al.*, 1999; Comiso, 2002; Rigor, 2005). Satellite data show that between 1981 and 2000 the Arctic sea ice extent was declining at a rate of 2 % per decade, however, the extent of perennial ice cover (measured in September) was shrinking at a much faster rate of 7 % per decade (Comiso, 2002). In September 2007, Arctic sea ice extent reached its lowest on record since 1979, opening the Northwest Passage completely for the first time in human history. Ice extent in 2007 averaged 1.65 million square miles (4.28 million square kilometres) shattering the previous record from 2005 by 23 % and the long-term average from 1979-2000 by 39 %. Also, as concluded from the International Arctic Buoy Program, age and thickness of Arctic sea ice has decreased dramatically since 1987, particularly in the Eurasian sector (Rigor, 2005). Figure 1.1 summarizes the changes in the extent and age (thickness) of perennial ice cover in the Arctic in the past two decades using the satellite data. However, recent studies suggest that satellite observations may underestimate the rate of ice thinning in the Canadian Arctic (Barber *et al.*, 2009). In September 2009, Radarsat derived ice charts predicted 7 to 9 tenths multi-year (MY) or thick first-year (FY) sea ice throughout most of the Southern Beaufort Sea in the deep water of the Canada Basin. *In situ* observations found heavily decayed, very small remnant MY and FY floes interspersed with new ice (< 5 cm thick) and open water (about 25 %), which was termed ‘rotten’ ice regime. Discrepancy between satellite and *in situ* observations was further attributed to very similar near-surface physical characteristics of MY and

'rotten' ice regimes, subsequently resulting in almost identical radiometric and scattering characteristics.

There are several model projections of seasonally ice-free Arctic by the end of this century (Flato and Boer, 2001; Comiso, 2002; Holland *et al.*, 2006). Comparison of the Arctic sea ice cover extent projected for 2045 by Comiso (2002) and the sea ice extent minimum observed for 2007 reveals that Arctic sea ice may continue to shrink at a much faster rate than those predicted by numerous model projections. The most commonly mentioned reason for that is the impact of sea ice-albedo feedback. It was suggested that the Arctic sea ice cover might have reached a tipping point as the impact of sea ice-albedo feedback starts to dominate (Lindsay and Zhang, 2005). There are also suggestions that the Arctic sea ice extent decline simulation models do not include the impact of cloud cover on the incident solar radiance and, subsequently, on the rate of sea ice shrinkage due to the relatively low resolution (Mackay D., personal communication). An unusually cloud-free Arctic in the summer has been pointed out among three main reasons for a dramatic drop in the Arctic sea ice extent in 2007 (Cressey, 2007).

Despite numerous discrepancies regarding the date when the Arctic will become seasonally ice-free, such a scenario seems to be likely especially if the levels of greenhouse gasses increase at the currently observed rate in the atmosphere. Although a warming Arctic impacts the cryosphere in the most pronounced way, numerous consequences for Arctic ecosystems, including contaminant exposure and pathways are like to follow.

Climate change can have direct impact on organisms' susceptibility to contaminant exposure or indirect impact on contaminant exposure through effects on ecosystems (Schiedek *et al.*, 2007). In the case of direct impact of climate change on

organisms' susceptibility, contaminant exposure interacts with direct and indirect stresses on ecosystems and biota, thus altering contaminant bioavailability, toxicity or biological effects. In the case of indirect impact on contaminant exposure through effects on ecosystems, change in environmental conditions and pathways will alter the transport, transfer, deposition and fate of contaminants, thus affecting biological exposure. Of all the contaminants, the organochlorines (OCs) provide the greatest challenge to predict consequences of change because they have been so widely released, comprise so many compounds and exhibit such a wide range of chemical properties (Macdonald *et al.*, 2005). However, change of organochlorine contaminant pathways should be attributed mainly to the global warming impact on physical-chemical properties sensitive to temperature change. They include vapour pressure, Henry's Law Constant (alternatively expressed as the air-water partition coefficient), octanol-air partition coefficient, octanol-water partition coefficient and particle-gas partition coefficient (Macdonald *et al.*, 2005).

1.3 Thesis hypotheses and objectives

The null hypothesis of this thesis is that the cryospheric processes have no significant potential to impact HCH levels in the Arctic marine environment. The alternative hypothesis states that sea ice, brine and snow processes can significantly alter levels of HCHs in the Arctic marine environment. Thus, the overall goal of this thesis was to gain the first insight into the HCH pathways within the Arctic marine cryosphere. The major emphasis was put on the interactions between various abiotic compartments. Putting those objectives in a broader context, observed and projected climate change will have cascading effects on many aspects of the environment including contaminants (Schiedek *et al.*, 2007). Advancing our understanding of HCH

pathways in the Arctic cryosphere represents the necessary baseline to predict if and how contaminant pathways will respond to unprecedented environmental change. Below, a detailed outline of thesis chapters' objectives designed to test the null hypothesis is presented.

In chapter 2, concentrations of α-HCH, γ-HCH and enantiomer composition of α-HCH are determined in sea ice from the Canadian High Arctic over a complete season. It is also shown how ice thickness, bulk salinity, and ice crystal structure influence vertical distribution of HCHs. The role of brine in the entrapment and rejection of HCHs in sea ice is investigated. Finally, the effect of biological processes at the bottom of the ice on HCH concentration and α-HCH enantiomer fraction during spring is examined.

In chapter 3, the concentrations of α- and γ-HCH measured directly in the brine using an ice sump are reported. Reliability of this sampling technique for HCHs under winter and spring ice conditions is discussed. Based on total ice measurements, the partitioning of HCHs between the brine and ice crystal matrix is estimated. Finally, the potential for ice crystal melting and sea water replenishment to dilute the HCH in brine during spring is described with respect to the measured decrease of HCH brine concentrations.

In chapter 4, the interaction between snow and sea ice in the Arctic Ocean is examined, focusing in particular on how the exchange of salt and HCH is affected during early growth (brine rejection) and mid-season temperature minimums (isolation of brine channels).

In chapter 5, levels of α-HCH in the southern Beaufort Sea region in 2003/2004 (CASES) and 2007/2008 (CFL/ NAHIDIK) are reported. Further, inventories of α-HCH in the Polar Mixed Layer (PML) and the Pacific Mode Layer (PL) of the Beaufort Sea

are calculated between 1986 and 2007 based on available data. Particular emphasis is put on the influence of ice formation on the vertical distribution of α-HCH in the PML. Inputs and outputs of α-HCH to/from the PML and PL are discussed and the time necessary to eliminate the majority of α-HCH burden from the Beaufort Sea is predicted.

1.4 References

Aagaard, K. A. 1989. A synthesis of the Arctic Ocean circulation. *Rapp. P. V. Reun.Cons. Int. Explor. Mer Mediter.* **188:** 11-22.

Altschuh, J.; R. Brüggemann; H. Santl; G. Eichinger, and O. G. Pringer. 1999. Henry's law constants for a diverse set of organic chemicals: experimental determination and comparison of estimation methods. *Chemosphere.* **39:** 1871-1887.

Anderson, L. G.; G. Bjork; O. Holby; E. P. Jones; G. Kattner; K. P. Koltermann; B. Liljeblad; R. Lindegren; B. Rudels, and J. H. Swift. 1994. Water masses and circulation in the Eurasian Basin: Results from the ODEN 91 expedition. *J. Geophys. Res.* **99:** 3273-3283.

Barber, D. G.; R. Galley; M. G. Asplin; R. De Abreu; K.-A. Warner; M. Pućko; M. Gupta; S. Prinsenberg, and S. Julien. 2009. Perennial pack ice in the southern Beaufort Sea was not as it appeared in the summer of 2009. *Geophys. Res. Lett.* **36:** L24501.

Barnett, T. P.; D. W. Pierce; K. M. AchutaRao; P. L. Gleckler; B. D. Santer; J. M. Gregory, and W. M. Washington. 2005. Penetration of human-induced warming into the world's oceans. *Science.* **309:** 284-287.

Barrie, L. A.; D. Gregor; B. Hargrave; R. Lake; D. Muir; R. Shearer; B. Tracey, and T. Bidleman. 1992. Arctic contaminants: sources, occurrence and pathways. *Sci. Total Environ.* **122:** 1-74.

Beesley, J. A. and R. E. Moritz. 1999. Toward an explanation of the annual cycle of cloudiness over the Arctic Ocean. *J. Climate.* **12:** 395-415.

Bidleman, T. F. 1999. Atmospheric transport and air-surface exchange of pesticides. *Water Air Soil Pollut.* **115:** 115-166.

Bock, C. and H. Eicken. 2005. A magnetic resonance study of temperature-dependent microstructural evolution and self-diffusion of water in Arctic first-year sea ice. *Ann. Glaciol.* **40:** 179-184.

Breivik, K.; J. M. Pacyna, and J. Münch. 1999. Use of α-, β- and γ-hexachlorocyclohexane in Europe, 1970-1996. *Sci. Total Environ.* **239:** 151-163.

Bryan, G. W.; M. Waldichuk; R. J. Pentreath, and A. Darracott. 1979. Bioaccumulation of Marine Pollutants [and Discussion]. *Philosphical Transactions of the Royal Society of London, Series B, Biological Sciences.* **286:** 483-505.

Burniston, D. A.; W. J. M. Strachan; J. T. Hoff, and F. Wania. 2007. Changes in Surface Area and Concentrations of Semivolatile Organic Contaminants in Aging Snow. *Environ. Sci. Technol.* **41:** 4932-4937.

Buser, H.-R. and M. D. Müller. 1995. Isomer and Enantioselective Degradation of Hexachlorocyclohexane Isomers in Sewage Sludge under Anaerobic Conditions. *Environ. Sci. Technol.* **29:** 664-672.

Cabanes, A. ; L. Legagneux, and F. Dominé. 2002. Evolution of the specific surface area and morphology of Arctic fresh snow during the ALERT 2000 campaign. *Atmos. Environ.* **36:** 2767-2777.

Carmack, E. and D. C. Chapman. 2003. Wind-driven shelf/basin exchange on an Arctic shelf: The joint roles of ice cover extent and shelf-break bathymetry. *Geophys. Res. Lett.* **30:** 1778. Doi: 10.1029/2003GL017526.

Comiso, J.C. 2002. A rapidly declining perennial sea ice cover in the Arctic. *Geophys. Res. Lett.* **29:** 1956.

Cotham, W and T. F. Bidleman. 1991. Estimating the atmospheric deposition of organochlorine contaminants to the Arctic. *Chemosphere.* **22:** 165-188.

Cox, G. F. N. and W. F. Weeks. 1975. Brine drainage and initial salt entrapment in sodium chloride ice.; CRREL Res Rep 345, Cold Reg Res Eng Lab: Hanover; pp. 88.

Cressey, D. 2007. Arctic sea ice at record low. *Nature.* doi: 10.1038/news070917-3.

Curry, J. A.; F. G. Meyers; L. F. Radke; C. A. Brock, and E. E. Ebert. 1990. Occurrence and characteristics of lower tropospheric ice crystals in the Arctic. *Int. J. Climatol.* **10:** 749-764.

Eicken, H. and M. A. Lange. 1989. Development and properties of sea ice in the coastal regime of the southeastern Weddell Sea. *J. Geophys. Res.* **94:** 8193-8206.

Eide, I. E. and S. Martin. 1975. The formation of brine drainage features in young sea ice. *J. Glaciol.* **14:** 137-154.

Faller, J.; H. Hühnerfuss; W. A. König; R. Krebber, and P. Ludwig. 1991a. Do Marine Bacteria Degrade α-Hexachlorocyclohexane Stereoselectively? *Environ. Sci. Technol.* **25:** 676-678.

Faller, J.; H. Hühnerfuss; W. A. König, and P. Ludwig. 1991b. Gas Chromatographic Separation of the Enantiomers of Marine Organic Pollutants. Distribution of α-HCH Enantiomers in the North Sea. *Mar. Pollut. Bull.* **22:** 82-86.

Falconer, R. L.; T. F. Bidleman; D. J. Gregor; R. Semkin, and C. Teixeira. 1995. Enantioselective Breakdown of α-Hexachlorocyclohexane in a Small Arctic Lake and Its Watershed. *Environ. Sci. Technol.* **29:** 1297-1302.

Flato, G. M. and G. J. Boer. 2001. Warming asymmetry in climate change simulations. *Geophys. Res. Lett.* **28:** 195-8.

Frankenstein, G. E. and R. Garner. 1967. Equations for Determining the Brine Volume of Sea Ice from -0.5 to -22.9 °C. *J. Glaciol.* **6:** 943-944.

Gaul, H. 1989. Organochlorine compounds in water and sea ice of the European Arctic Sea. The 8th International Conference of Comite Arctique International. Oslo. 18-22 September 1989. pp. 10.

Girard, E. and J.-P. Blanchet. 2001. Microphysical Parametrization of Arctic Diamond Dust, Ice Fog, and Thin Stratus for Climate Models. *J. Atmos. Sci.* **58:** 1181-1198.

Golden, K. M; A. L. Heaton; H. Eicken, and V. I. Lytle. 2006. Void bounds for fluid transport in sea ice. *Mech. Mater.* **38:** 801-817.

Halsall, C. J. 2004. Investigating the occurrence of persistent organic pollutants (POPs) in the arctic: their atmospheric behavior and interaction with the seasonal snow pack. *Environ. Pollut.* **128:** 163-175.

Halsall, C. J. 2007. Environmental Organic Chemistry. In *Principles of Environmental Chemistry*; Harrison, R. M., Ed.; RSC Publishing: Cambridge; pp. 363.

Hansch, C. and A. Leo. 1995. *Exploring QSAR: fundamentals and applications in chemistry and biology,* American Chemical Society, Washington, pp. 557.

Hansen, K. M.; C. J. Halsall, and J. H. Christensen. 2005. A dynamic model to study the exchange of gas-phase persistent organic pollutants between air and a seasonal snowpack. *Environ. Sci. Technol.* **39:** 2644-2652.

Hansen, J.; M. Sato; P. Kharecha; G. Russell, and D. W. Lea. 2007. Climate change and trace gases. *Philos. Transact. A Math. Phys. Eng. Sci.* **365:** 1925-1954.

Hargrave, B. T.; G. C. Harding; W. P. Vass; P. E. Erickson; B. R. Fowler, and V. Scott. 1992. Organochlorine Pesticides and Polychlorinated Biphenyls in the Arctic Ocean Food Web. *Arch. Environ. Contam. Toxicol.* **22:** 41-54.

Hargrave, B. T.; G. A. Phillips; W. P. Vass; P. Bruecker; H. E. Welch, and T. D. Siferd. 2000. Seasonality in Bioaccumulation of Organochlorines in Lower Trophic Level Arctic Marine Biota. *Environ. Sci. Technol.* **34:** 980-987.

Hargrave, B. T.; P. Vass; P. E. Erickson, and B. R. Fowler. 1988. Atmospheric transport of organochlorines to the Arctic Ocean. *Tellus.* **40B:** 480-493.

Harner, T.; H. Kylin; T. F. Bidleman, and W. M. J. Strachan. 1999. Removal of α- and γ-hexachlorocyclohexanes and enantiomers of α-hexachlorocyclohexane in the eastern Arctic Ocean. *Environ. Sci. Technol.* **33:** 1157-1164.

Helm, P. A.; M. L. Diamond; R. Semkin, and T. F. Bidleman. 2000. Degradation as a Loss Mechanism in the Fate of α-Hexachlorocyclohexane in Arctic Watersheds. *Environ. Sci. Technol.* **34:** 812-818.

Herbert, B. M. J.; S. Villa, and C. J. Halsall. 2006. Chemical interactions with snow: Understanding the behavior and fate of semi-volatile organic compounds in snow. *Ecotox. Environ. Safe.* **63:** 3-16.

Hinckley, D. A.; T. F. Bidleman, and C. P. Rice. 1991. Atmospheric Organochlorine Pollutants and Air-Sea Exchange of Hexachlorocyclohexane in the Bering and Chukchi Seas. *J. Geophys. Res.* **96:** 7201-7213.

Holland, M. M.; C. M. Bitz, and B. Tremblay. 2006. Future abrupt reductions in the summer Arctic sea ice. *Geophys. Res. Lett.* **33:** L23503.

Hoff, J. T.; F. Wania; D. Mackay, and R. Gillham. 1995. Sorption of Nonpolar Organic Vapors by Ice and Snow. *Environ. Sci. Technol.* **29:** 1982-1989.

Hühnerfuss, H.; J. Faller; W. A. König, and P. Ludwig. 1992. Gas Chromatographic Separation of the Enantiomers of Marine Pollutants. 4. Fate of Hexachlorocyclohexane Isomers in the Baltic and North Sea. *Environ. Sci. Technol.* **26:** 2127-2133.

Hung, H.; P. Blanchard; C. J. Halsall; T. F. Bidleman; G. A. Stern; P. Fellin; D. G. C. Muir; L. A. Barrie; L. M. Jantunen; P. A. Helm; J. Ma, and A. Konoplev. 2005. Temporal and spatial variabilities of atmospheric polychlorinated biphenyls (PCBs), organochlorine (OC) pesticides and polycyclic aromatic hydrocarbons (PAHs) in the Canadian Arctic: results from a decade of monitoring. *Sci. Total Environ.* **342:** 119-144.

Jantunen, L. M. and T. F. Bidleman. 1995. Reversal of the Air-Water Gas Exchange Direction of Hexachlorocyclohexanes in the Bering and Chukchi Seas: 1993 versus 1988. *Environ. Sci. Technol.* **29:** 1081-1089.

Jantunen, L. M. and T. F. Bidleman. 1996. Air-water gas exchange of hexachlorocyclohaxanes (HCHs) and the enantiomers of α-HCH in arctic regions. *J. Geophys. Res.* **101:** 28837-28846.

Jantunen, L. M. and T. F. Bidleman. 1997. Correction to "Air-water gas exchange of hexachlorocyclohaxanes (HCHs) and the enantiomers of α-HCH in arctic regions". *J. Geophys. Res.* **102:** 19279-19282.

Jantunen, L. M. M. and T. F. Bidleman. 1998. Organochlorine Pesticides and Enantiomers of Chiral Pesticides in Arctic Ocean Water. *Arch. Environ. Contam. Toxicol.* **35:** 218-228.

Korsnes, R.; O. Pavlova, and F. Godtliebsen. 2002. Assessment of potential transport of pollutants into the Barents Sea via sea ice – an observational approach. *Mar. Pollut. Bull.* **44:** 861-869.

Li, Y.-F.; T. F. Bidleman; L. A. Barrie, and L. L. McConnell. 1998. Global hexachlorocyclohexane use trends and their impact on the arctic atmospheric environment. *Geophys. Res. Lett.* **25:** 39-41.

Li, Y.-F. and R. W. Macdonald. 2005. Sources and pathways of selected organochlorine pesticides to the Arctic and the effect of pathway divergence on HCH trends in biota: a review. *Sci. Total Environ.* **342:** 87-106.

Li, Y.-F.; R. W. Macdonald; L. M. M. Jantunen; T. Harner; T. F. Bidleman, and W. M. J. Strachan. 2002. The transport of β-hexachlorocyclohexane to the western Arctic Ocean: a contrast to α-HCH. *Sci. Total Environ.* **291:** 229-246.

Li, Y.-F.; R. W. Macdonald; J. M. Ma; H. Hung, and S. Venkatesh. 2004. Historical α-HCH budget in the Arctic Ocean: the Arctic Mass Balance Box Model (AMBBM). *Sci. Total Environ.* **324:** 115-139.

Lindsay, R. W. and J. Zhang. 2005. The thinning of arctic sea ice, 1988-2003: have we passed a tipping point? *J. Climate*. **18:** 4879-4894.

Macdonald, R. W.; L. G. Anderson; J. P. Christensen; L. A. Miller; I. P. Semiletov, and R. Stein. 2010. The Arctic Ocean. In *Carbon and Nutrient Fluxes in Continental Margins*; Liu, K.-K.; L. Atkinson; R. Quinones, and L. Talaue-McManus, Eds.; Springer-Verlag: Berlin; pp. 744.

Macdonald, R. W.; L. A. Barrie; T. F. Bidleman; M. L. Diamond; D. J. Gregor; R. G. Semkin; W. M. J. Strachan; Y. F. Li; F. Wania; M. Alaee; L. B. Alexeeva; S. M. Backus; R. Bailey; J. M. Bewers; C. Gobeil; C. J. Halsall; T. Harner; J. T. Hoff; L. M. M. Jantunen; W. L. Lockhart; D. Mackay; D. C. G. Muir; J. Pudykiewicz; R. J.

Reimer; J. N. Smith; G. A. Stern; W. H. Schroeder; R. Wagemann, and M. B. Yunker. 2000. Contaminants in the Canadian Arctic: 5 years of progress in understanding sources, occurrence and pathways. *Sci. Total Environ.* **254:** 93-234.

Macdonald, R. W. and J. M. Bewers. 1996. Contaminants in the arctic marine environment: priorities for protection. *ICES J. Mar. Sci.* **53:** 537-563.

Macdonald, R. W.; T. Harner, and J. Fyfe. 2005. Recent climate change in the Arctic and its impact on contaminant pathways and interpretation of temporal trend data. *Sci. Total Environ.* **342:** 5-86.

Macdonald, R. W.; D. Mackay, and B. Hickie. 2002. Contaminant amplification in the environment. *Environ. Sci. Technol.* **36:** 456A-462A.

Mackay, D. 1982. Correlation of Bioconcentration Factors. *Environ. Sci. Technol.* **16:** 274-278.

Mackay, D. and A. T. K. Yeun. 1983. Mass Transfer Coefficient Correlations fo Volatilization of Organic Solutes from Water. *Environ. Sci. Technol.* **17:** 211-217.

Magnusson, K.; R. Ekelund; G. Dave; Å. Granmo; L. Förlin; L. Wennberg; M.-O. Samuelsson; M. Berggren, and E. Brorström-Lunden. 1996. Contamination and correlation with toxicity of sediment samples from the Skagerrak and Kattegat. *J. Sea Res.* **35:** 223-234.

Maxwell, J. B. 1982. Climate of the Canadian Arctic islands and adjacent water. *Climatol. Stud.* **30:** 34-52.

McLaughlin, F. A.; E. C. Carmack; R. W. Macdonald, and J. K. B. Bishop. 1996. Physical and geochemical properties across the Atlantic/Pacific water mass front in the southern Canadian Basin. *J. Geophys. Res.* **101:** 1183-1197.

Melnikov, S.; J. Carroll; A. Gorshkov; S. Vlasov, and S. Dahle. 2003. Snow and ice concentrations of selected persistent pollutants in the Ob-Yenisey River watershed. *Sci. Total Environ.* **306:** 27-37.

Metcalf, R. L. 1955. *Organic Insecticides, Their Chemistry and Mode of Action,* Interscience Publishers, New York, pp. 214.

Meyer, T.; Y. D. Lei; I. Muradi, and F. Wania. 2009a. Organic Contaminant Release from Melting Snow. 1. Influence of Chemical Partitioning. *Environ. Sci. Technol.* **43:** 657-662.

Meyer, T.; Y. D. Lei; I. Muradi, and F. Wania. 2009b. Organic Contaminant Release from Melting Snow. 2. Influence of Snow Pack and Melt Characteristics. *Environ. Sci. Technol.* **43:** 663-668.

Meyer, T. and F. Wania. 2008. Organic contaminant amplification during snowmelt. *Water Res.* **42:** 1847-1865.

Möller, K.; H. Hühnerfuss, and D. Wölfle. 1996. Differential Effects on the Enantiomers of α-Hexachlorocyclohexane (α-HCH) on Cytotoxicity and Growth Stimulation in Primary Rat Hepatocytes. *Organohalogen Compd.* **29:** 357-360.

Mössner, S.; T. R. Spraker; P. R. Becker, and K. Ballschmiter. 1992. Ratios of enantiomers of alpha-HCH and determination of alpha-, beta-, and gamma-HCH isomers in brain and other tissues of neonatal Northern Fur Seals (*Callorhinus ursinus*). *Chemosphere.* **24:** 1171-1180.

Muir, D. C. G. and R. J. Norstrom. 2000. Geographical differences and time trends of persistent organic pollutants in the Arctic. *Toxicol. Lett.* **112-113:** 93-101.

Müller, T. A. and H.-P. E. Kohler. 2004. Chirality of pollutants – effects on metabolism and fate. *Appl. Microbiol. Biotechnol.* **64:** 300-316.

Pankow, J. F. 1987. Review and comparative analysis of the theories on partitioning between the gas and aerosol particulate phases in the atmosphere. *Atmos. Environ.* **21:** 2275-2283.

Parkinson, C. L.; D. J. Cavalieri; P. Gloersen; H. J. Zwally, and J. C. Comiso. 1999. Arctic sea ice extents, areas and trends, 1978-1996. *J. Geophys. Res.* **104:** 20,837-20,856.

Pereira, M. A.; S. L. Herren; A. L. Britt, and M. M. Khoury. 1982. Sex difference in enhancement of GGTase-positive foci by hexachlorobenzane and lindane in rat liver. *Cancer Lett.* **15:** 95-101.

Pfirman, S. L.; H. Eicken; D. Bauch, and W. F. Weeks. 1995. The potential transport of pollutants by Arctic sea ice. *Sci. Total Environ.* **159:** 129-146.

Pfirman, S.; J. Kogler, and I. Rigor. 1997. Potential for rapid transport of contaminants from the Kara Sea. *Sci. Total Environ.* **202:** 111-122.

Prasad, A. K.; N. Pant; S. C. Srivastava; R. Kumar, and S. P. Srivastava. 1995. Effect of dermal application of hexachlorocyclohexane (HCH) on male reproductive system in rat. *Hum. Exp. Toxicol.* **14:** 484-488.

Rigor, I. G. 2005. International Arctic Buoy Programme: Monitoring the Arctic Ocean since 1979. In *Sea Ice Mass Budget of the Arctic (SIMBA), Workshop Report,* Applied Physics Laboratory, University of Washington, Seatlle, 28/02/2005-02/03/2005.

Sahsuvar, L.; P. A. Helm; L. M. Jantunen, and T. F. Bidleman. 2003. Henry's law constants for α-, β-, and γ-hexachlorocyclohexanes (HCHs) as a function of temperature and revised estimates of gas exchange in Arctic regions. *Atmos. Environ.* **37:** 983-992.

Schiedek, D.; B. Sundelin; J. W. Readman, and R. W. Macdonald. 2007. Interactions between climate change and contaminants. *Mar. Pollut. Bull.* **54:** 1845-1856.

Schulte-Hermann, R. and W. Parzefall. 1981. Failure to Discriminate Initiation form Promotion of Liver Tumors in a Long-Term Study with the Phenobarbital-type Inducer α-Hexachlorocyclohexane and the Role of Sustained Stimulation of Hepatic Growth and Monooxygenases. *Cancer Res.* **41:** 4140-4146.

Schwarzenbach, R. P.; P. M. Gschwend, and D. M. Imboden. 1993. *Environmental Organic Chemistry*, Wiley & Sons, New York, pp. 681.

Shen, H.; H. E. Virtanen; K. M. Main; M. Kaleva; A. M. Andersson; N. E. Skakkebæk; J. Toppari, and K.-W. Schramm. 2006. Enantiomeric ratios as an indicator of exposure processes for persistent pollutants in human placentas. *Chemosphere.* **62:** 390-395.

Tett, S. F. B.; P. A. Stott; M. R. Allen; W. J. Ingram, and J. F. B. Mitchell. 1999. Causes of twentieth-century temperature change near the Earth's surface. *Nature.* **339:** 569-572.

US EPA. 2006. Addendum to the 2002 Lindane Registration Eligibility Decision (RED), United States Environmental Protection Agency; Prevention, Pesticides and Toxic Substances (7508P). EPA 738-R-06-028. July 2006.

Wallace, D. W. R.; P. Schlosser; M. Krysell, and G. Bönisch. 1992. Halocarbon ration and tritium/^{3}He dating of water masses in the Nansen Basin, Arctic Ocean. *Deep-Sea Res.* **39:** S435-S458.

Wania, F.; J. T. Hoff; C. Q. Jia, and D. Mackay. 1998. The effects of snow and ice on the environmental behaviour of hydrophobic organic chemicals. *Environ. Pollut.* **102:** 25-41.

Weeks, W. F. 1994. Possible roles of sea ice in the transport of hazardous material. In *Proc. Workshop on Arctic Contamination. Interagency Arctic Research Policy Committee. Anchorage, Alaska, 1993. Arctic Res. US.* **8:** 34-52.

Weeks, W. F. and S. F. Ackley. 1986. The growth, structure and properties of sea ice. In *The geophysics of sea ice*; Untersteiner, N., Ed.; Matrinus Nijhoff: Dordrecht (NATO ASI B146); pp. 164.

Wiberg, K.; R. J. Letcher; C. D. Sandau; R. J. Norstrom; M. Tysklind, and T. F. Bidleman. 2000. The Enantioselective Bioaccumulation of Chiral Chlordane and α-HCH Contaminants in the Polar Bear Food Chain. *Environ. Sci. Technol.* **34:** 2668-2674.

WMO, 1970. WMO Sea-Ice Nomenclature. Volume 1: Terminology and Codes. Part I and II. Report 259: Geneva; pp. 14.

Xiao, H.; N. Li, and F. Wania. 2004. Compilation, Evaluation, and Selection of Physical-Chemical Property Data for α-, β-, and γ-Hexachlorocyclohexane. *J. Chem. Eng. Data.* **49:** 173-185.

Chapter 2

The importance of brine processes for α- and γ-hexachlorocyclohexane (HCH) accumulation or rejection in sea ice

2.1 Abstract

Both geophysical and thermodynamic conditions in sea ice are crucial in understanding pathways of accumulation or rejection of hexachlorocyclohexanes (HCHs). α- and γ-HCH concentrations and α-HCH enantiomer fractions have been measured in varied ice classes and ages from the Canadian High Arctic. Mean α-HCH concentrations reached 0.642 ± 0.046 ng/L in the new and young ice (< 30 cm), 0.261 ± 0.015 ng/L in the first year ice (30-200 cm) and 0.208 ± 0.045 in the old ice (> 200 cm). Mean γ-HCH concentrations were 0.066 ± 0.006 ng/L in the new and young ice, 0.040 ± 0.002 ng/L in the first year ice and 0.040 ± 0.007 ng/L in the old ice. In general, α-HCH concentrations and vertical distributions were highly dependent on the initial entrapment of brine and the subsequent desalination process. γ-HCH levels and distribution in sea ice were not as clearly related to ice formation processes. Through the year, first year ice progressed from freezing (accumulation) to melting conditions. Relations between the geophysical state of the sea ice and vertical distribution of HCHs are described as ice passes through these thermodynamic states. In melting ice, which corresponded to the algal bloom period, the influence of biological processes within the bottom part of the ice on HCH concentrations and α-HCH enantiomer fraction is discussed implementing both univariate and multivariate approaches.

2.2 Introduction

Hexachlorocyclohexanes (HCHs) are one of the most abundant organochlorine pesticides in the Arctic with the highest levels recorded in the surface layer of the Arctic Ocean (Iwata *et al.*, 1993; Harner *et al.*, 1999). HCHs were classified as contaminants of concern due to their recalcitrant, bioaccumulative and toxic properties (Prasad *et al.*, 1995; Magnusson *et al.*, 1996; Möller *et al.*, 1996; Hargrave *et al.*, 2000;

Macdonald *et al.,* 2000). HCHs were released to the environment in two main formulations: technical HCH (α isomer 60-70 %, β isomer 5-12 %, γ isomer 10-15 %) and lindane (pure γ isomer). Both formulations are presently banned in most countries.

α-HCH consists of two mirror-image enantiomers, termed (+) and (-). Although these enantiomers exhibit identical physical and chemical properties they behave differently when degraded by microbes because enzymes exhibit stereo selectivity (Müller and Kohler, 2004). Accordingly, the racemic (1:1) mixture of α-HCH released into the environment undergoes enantioenrichment when enantioselective processes come into play (microbial breakdown, selective biological uptake, biotransformation and elimination pathways in food webs (Faller *et al.*, 1991; Falconer *et al.*, 1995; Wiberg *et al.*, 2000)). On the other hand, abiotic transformations such as transport, hydrolysis or photolysis are not enantioselective. Change in the enantiomer fraction, EF, which is therefore a good indicator of biological processes (Hühnerfuss *et al.*, 1992), will be expressed here as:

$$EF = ER/[ER+1] \qquad \text{(eq. 2.1)}$$

where ER is the enantiomer ratio (+)α-HCH/(-)α-HCH.

Sea ice consists of an ice matrix with inclusions of brine and air (Perovich and Gow, 1996). Brine volume fraction, which is a function of temperature and salinity (Frankenstein and Garner, 1967), has a critical value of 5 %, above which movement of liquids within the sea ice column can occur (Cox and Weeks, 1975; Weeks and Ackley, 1986; Golden *et al.*, 1998; Golden *et al.*, 2006). Movement can result in flushing, convective drainage (exchange of the denser brine within the ice with the underlying less saline sea water) or upward movement of brine to the overlying snow (Barber *et al.*, 1995).

The most common classifications of sea ice in the literature are based on the World Meteorological Organization (WMO) developmental stage (new and young ice < 30 cm, first year ice 30-200 cm and old ice > 200 cm that survived at least one melt season), mechanism of formation and crystalline structure (frazil ice – individual unconsolidated ice crystals resulting from the water supercooling, and congelation/fast ice – consolidated sheets of thicker ice), and large-scale form of the ice (landfast or free drifting) (WMO, 1970; Weeks and Ackley, 1986). Often, there are openings in the ice cover, commonly termed leads. Within the ice itself, the orientation and size of ice crystals are broadly classified as granular, transitional/intermediate and columnar (Weeks and Ackley, 1986; Eicken and Lange, 1989).

Most ionic species dissolved in sea water are too large to be incorporated into the crystal lattice of ice as a solid solution, thus, only between 15 to 30 % of the salt contained in sea water is retained in the corresponding volume of newly grown ice (Weeks and Ackley, 1986). Salts become entrapped between ice crystals in mobile liquid brine pockets. The brine pores vary in size, distribution and degree of connectivity within the ice column depending on ice texture, temperature and growth rate (Nakawo and Sinha, 1984; Weeks and Ackley, 1986; Weissenberger *et al.,* 1992; Perovich and Gow, 1996; Bock and Eicken, 2005).

Sea ice salinity is affected by ice growth rate, ice texture and the natural rejection of salt from the ice lattice during desalination (Cox and Weeks, 1975; Krembs *et al.,* 2000). Bulk sea ice salinity decreases exponentially with ice sheet thickness (Kovacs, 1997).

Desalination occurs by brine pocket migration, brine expulsion, gravity drainage and flushing. Brine expulsion dominates only for the first few hours of ice growth. Gravity drainage dominates for the remainder of the ice growth period, and flushing

during the transition from first year to old ice (Cox and Weeks, 1975). Flushing is a form of gravity brine drainage above sea level forced by snow or surface ice melt (Eide and Martin, 1975).

HCH concentrations have been studied in arctic air, water, biota and sediments; however, studies of HCHs in sea ice are rare and interpretations are plagued by a complete inattention to sea ice physical and thermodynamic conditions (Hargrave *et al.*, 1988; Gaul, 1989; Melnikov *et al.*, 2003). Although brine is thought to provide a critical component of the water-soluble compound pathway within the sea ice, there appears to be no detailed study of this subject (Weeks, 1994; Eicken, 2004). Here, we determine concentrations of α-HCH, γ-HCH and enantiomer composition of α-HCH in sea ice from the Canadian High Arctic over a complete season. We investigate the role of brine in the entrapment and rejection of HCHs in sea ice, and the influence of ice thickness, bulk salinity, and ice crystal structure as determining factors for the vertical distribution of α-and γ-HCH in sea ice. Finally, we examine the effect of biological processes at the bottom of the ice during spring on HCH concentration and α-HCH enantiomer fraction.

2.3 Materials and methods

2.3.1 *Sampling site*

Sea ice samples were collected from the CCGS '*Amundsen*' as a part of the Circumpolar Flaw Lead System Study (CFL) of the International Polar Year (IPY) in the Canadian High Arctic (Beaufort Sea) between October 2007 and May 2008 (Figure 2.1). In general, stations provided opportunities to sample drifting ice (D), landfast ice (F), old ice (O) and ice with adjacent open leads (L).

2.3.2 *Field sampling*

Sea ice samples were obtained with a metal strainer (unconsolidated new ice), metal ice chipper (< 10 cm consolidated ice) or ice corer, 9 cm i.d., Mark II coring system, Kovacs Enterprises (> 10 cm consolidated ice). Extracted ice samples were placed in tightly closed plastic containers (< 10 cm sea ice) or sealed plastic bags (ice cores) and stored horizontally at -20 °C until further analysis. First year sea ice cores used to construct α- and γ-HCH vertical profiles were subsequently cut into 3-6 layers selected based on boundaries between ice texture classes determined prior to cutting. At all ice stations, sea water was collected from beneath the ice for α-HCH and γ-HCH determination by deploying a Kemmerer water sampler through the hole immediately after ice core extraction. In spring 2009, ice algae were collected at several stations by slurping or scraping the under-ice surface using divers, and extracting the bottom of the ice using an ice corer.

Figure 2.1 Circumpolar map of the Arctic with a study area marked (A) (AMSR-E data product prepared by Phil Hwang) and ice sampling locations (B); F – landfast ice station, O – old ice station, remaining stations – drifting and/or lead ice station

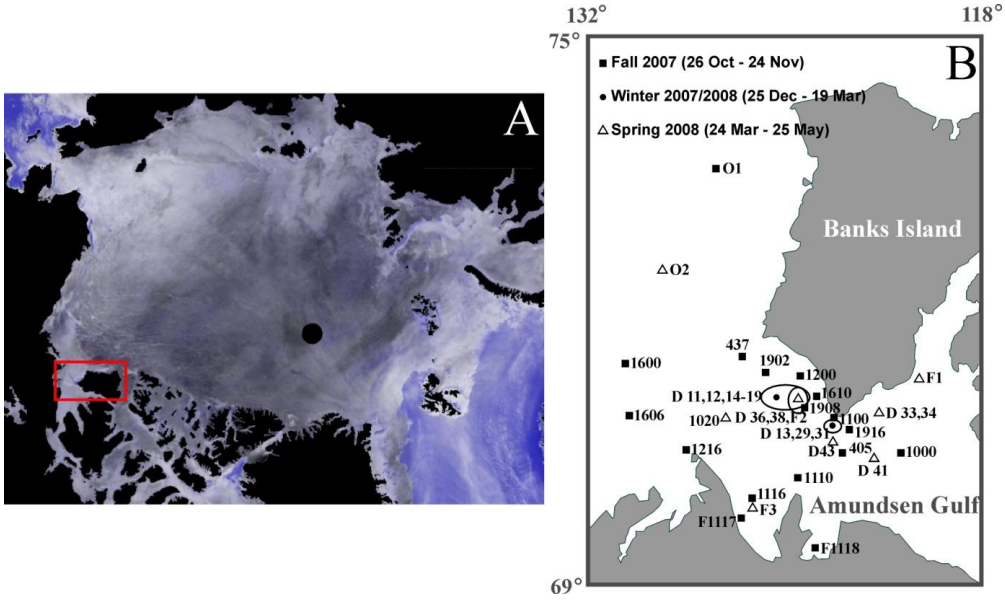

2.3.3 *Laboratory analysis*

With the exception of the two old ice stations, vertical texture of the sea ice was analyzed whenever ice thickness exceeded 3 cm using plane transmitted and cross-polarized light thin ice sections (~1 mm) to highlight ice crystal shape, size and orientation (Sinha, 1977). Sea ice vertical texture profiles were classified as: g- granular, tg- transitional granular, tc- transitional columnar and c- columnar (Figure 2.2). Granular texture included fine crystals, transitional granular texture contained ice crystals of mainly coarse structure and weak alignment with the c-axis (vertical axis in the ice column). Transitional columnar texture comprised crystals mainly of columnar shape but relatively short with strong alignment with the c axis, and columnar ice crystals were very long and very strongly aligned with the c axis. Typically, the uppermost part of the ice core contained granular or granular/transitional ice crystals whereas deeper layers primarily contained columnar ice crystals. Salinity of melted sea ice samples was calculated from conductivity and temperature using a HACH SENSION5 portable conductivity meter (± 0.01 ‰).

Melted sea ice samples (8 L) and under-ice sea water samples (4 L) were spiked with d_6-α-HCH surrogate, pumped through 0.7 μm GFF filters (Whatman) to remove particulate matter, and filtered through solid-phase extraction (SPE) cartridges (Oasis) at a flow rate < 20 mL/min. Cartridges were stored at -20 °C prior to laboratory analysis. The main steps of the laboratory procedure included elution of SPE cartridges with ~40 mL of acetone, transfer into iso-octane by adding 1 mL of this solvent to the acetone extract previously rotor-evaporated to 3 mL, vortexing and transferring the more non-polar phase (top phase) into the new test tube, rinsing the acetone phase with hexane three times, reducing the volume of the solvents mixture to 1 mL under the nitrogen flow, and cleaning-up the solution with 0.5 mL of concentrated sulphuric acid

(Mukherjee and Gopal, 1996). Ice algae samples were filtered through 0.7 μm pre-combusted and pre-weighed GFF filters (Whatman) and stored at -20 °C. Before extraction, filters were dried at 35 °C until they reached stable weight (approximately 10 hours) and the dry mass of algae was determined gravimetrically. Subsequently, filters were spiked with d_6-α-HCH surrogate, extracted using ASE 2000 Accelerated Solvent Extractor (Dionex) with about 100 mL of hexane:dichloromethane (1:1 by volume) solution, reduced to 1 mL volume by rotor-evaporation and cleaned-up on florisil columns.

Figure 2.2 Four main sea ice vertical texture types characterized in this study, cross-polarized thin ice section pictures 5 x 5 cm

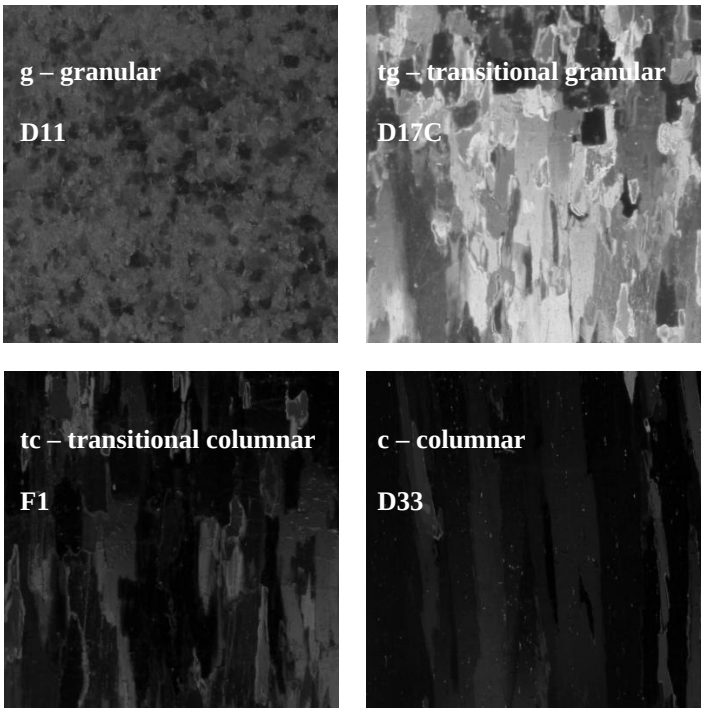

Quantitative analysis of α- and γ-HCH was performed using a Varian 3800 Gas Chromatograph-Electron Capture (GC-ECD) equipped with a 60 m, JW DB5 column (0.25 mm i.d., 0.25 μm film thickness). The oven was programmed from 80 °C (1

minute hold) to 150 °C at 15 °C/minute, and to 265 °C at 3 °C/minute with a 7.5 minute hold. External calibration standards were obtained from Cerilliant. Chiral analysis of α-HCH was carried out by GC-negative ion mass spectrometry on an Agilent 5890 GC coupled to a 5973 Mass Selective Detector (MSD) operated in Single Ion Monitoring (SIM) mode; target and qualifier ions were 255 and 257. A 30 m Supelco BetaDex 120 (0.25 mm i.d., 0.25 μm film thickness) column was used with temperature programmed from 80 °C to 160 °C at 15 °C/minute and to 180 °C at 1 °C/minute with a 3 minute hold. From multiple injections of a few samples, coefficient of variation for the EF was estimated at ± 1.2 %. The average ± SD of EFs for a racemic α-HCH standard was 0.500 ± 0.003.

α- and γ-HCH concentrations presented in this study were corrected for percent recovery but not for mean blank. Average recovery was above 80% for sea ice and under-ice sea water, and 56 % for ice algae samples. Field blanks for α-and γ-HCH were determined by placing SPE cartridges/GFF filters on the bench in the laboratory on the ship for at least 10 minutes and subsequently exposing them to identical analytical procedure as the rest of the samples. Limit of detection (LOD), defined as 3 standard deviations of the mean field blank, were 0.019 ng/L and 0.007 ng/L for α- and γ-HCH, respectively. Limit of quantification (LOQ), defined as 10 standard deviations of the mean field blank value, was estimated at 0.047 ng/L and 0.011 ng/L for α- and γ-HCH, respectively.

2.3.4 *Sea ice brine drainage experiment*

The sea ice brine drainage experiment was performed to simulate sea ice melt conditions as sampling is complicated in the spring by the presence of melt ponds and extensive brine drainage after ice core extraction. Five sea ice cores, sampled at station

D19, 24 January 2008, were placed in sealed plastic bags and hung in the laboratory at ambient temperatures between 14 °C and 17 °C. Melt water was collected in five portions over 46 hours. Temperature profiles were investigated roughly every 4 hours during the course of the experiment. Drainage started in the 6th hour of the experiment when the temperatures in the whole ice column came close to 0 ^{o}C. Salinity and α- and γ-HCH concentrations in five fractions of melt water were determined using methods described above.

2.3.5 *Calculations and data analysis*

Brine volume fraction, υ_b, was calculated following the formula by Frankenstein and Garner (1967):

$$\upsilon_b = S_{ICE} (49.185/ \left| T_{ICE} \right| + 0.532) \cdot 100 \qquad \text{for } -0.5\ °C \geq T_{ICE} \geq -22.9\ °C \quad \text{(eq. 2.2)}$$

where:

υ_b – brine volume fraction (%)

S_{ICE} – ice salinity (‰)

T_{ICE} – ice temperature (°C)

Statistical analyses include Analysis of Variance (ANOVA), one-way, post-hoc test: Tukey, $\alpha = 0.05$, ordinary least-square linear regression (SYSTAT 11, Systat Software Inc.) and Redundancy Analysis, RDA (correlation matrix, SYN-TAX 5.1. software, courtesy of Dr. N. Kenkel, University of Manitoba, Canada). Prior to RDA, ice bulk salinity and brine volume fraction were log-transformed to meet the criterion of these parametric analyses. Plots of vertical distribution of variables in the ice core as a function of time were performed using Ocean Data View software (Schlitzer, 2002). For statistical analysis, ice vertical textures classes were coded as follows: 1- granular, 1.25- transitional granular, 1.75- transitional columnar and 2- columnar. Progression of

the sea ice annual cycle is represented here as days from the beginning of freeze-up. We sampled from 26 October 2007 (day 1) to 25 May 2008 (day 184).

2.4 Results and discussion

Average concentrations of α-HCH and γ-HCH, and α-HCH EF in the sea ice column sampled over the course of this study at different stations in the Amundsen Gulf are summarized in Table 2.1. Sea ice physical parameters measured included sea ice thickness and bulk salinity. α- and γ-HCH concentrations, and α-HCH EF in the under-ice sea water were also determined at each ice sampling station.

2.4.1 *α- and γ-HCH levels in the sea ice*

Mean α-HCH concentration reached 0.642 ± 0.046 ng/L in the new and young ice (< 30 cm), 0.261 ± 0.015 ng/L in the first year ice (30-200 cm) and 0.208 ± 0.045 in the old ice (> 200 cm) (Table 2.2). Mean γ-HCH concentration equaled 0.066 ± 0.006 ng/L in the new and young ice, 0.040 ± 0.002 ng/L in the first year ice and 0.040 ± 0.007 ng/L in the old ice. Corresponding sea ice bulk salinities averaged 11.6 ± 1.2 ‰, 7 ± 0.3 ‰ and 1.6 ± 1.1 ‰, respectively.

We are aware of only three studies reporting levels of HCH in the Arctic sea ice (Hargrave *et al.*, 1988; Gaul, 1989; Melnikov *et al.*, 2003). Both α- and γ-HCH isomers were detected in the dissolved phase of the first year, 140 cm thick, sea ice in the Canadian High Arctic based on 3 ice samples from May-June 1986 (Hargrave *et al.*, 1988). These authors reported mean α- and γ-HCH concentrations of 1.321 ng/L and 0.186 ng/L, respectively. In 5 ice cores collected from April and May 2008 (mean thickness 136 cm) α-HCH and γ-HCH were approximately 5-fold lower in HCH

concentrations reflecting a similar decline in surface water during the 20-year period (4.399 versus 0.880 ng/L and 0.567 versus 0.113 ng/L for α- and γ-HCH, respectively).

2.4.2 *Entrapment of HCHs in the sea ice*

As ice forms from sea water, solute segregation takes place at the ice-water interface resulting in the entrapment of a portion of salts from the sea water (Weeks and Ackley, 1986). We collected 2 samples of new unconsolidated sea ice of about 0.5 cm thickness, one during fall 2007 freeze-up (26 Oct 2007, station 1000), and the other in the spring 2008 from a lead (7 Apr 2008, station 36A (Table 2.1)). In the case of the fall freeze-up sample, 63 % of salts, 62 % of α-HCH and 68 % of γ-HCH were entrained in the sea ice relative to the surface sea water concentrations. In the case of the spring lead sample, 64 % of salts, 50 % of α-HCH and 68 % of γ-HCH was entrapped in the sea ice. The similarity between these two samples suggests that the amount of HCH in thin new ice can be predicted based solely on the HCH concentrations and salinity of the surface water and the salinity of the sea ice.

Table 2.1 α-HCH and γ-HCH concentration, α-HCH enantiomer fraction (EF_{ICE}) and α-HCH/γ-HCH ratio in different ice samples along with sea ice physical parameters (thickness [Thick] and salinity [S]) and under-ice sea water α-HCH and γ-HCH concentration, α-HCH enantiomer fraction (EF_{WAT}) and α-HCH/γ-HCH ratio throughout the project (October 2007 to May 2008)

Date [coded*]	St.	Ice type	$Thick_{ICE}$ (cm)	S_{ICE} (‰)	α-HCH (ng/L)	EF_{ICE}	γ-HCH (ng/L)	α/γ_{ICE}	$\alpha\text{-HCH}_{WAT}$ (ng/L)	EF_{WAT}	$\gamma\text{-HCH}_{WAT}$ (ng/L)	α/γ_{WAT}
26Oct07 [1]	1000	$D_{N/Y}$	0.5	20.0	0.977	0.438	0.081	12.1	1.579	0.462	0.120	13.2
27Oct07 [2]	1110	$D_{N/Y}$	8	11.1	0.866	0.421	0.073	11.9	1.356	0.416	0.126	10.7
28Oct07 [3]	1116	$D_{N/Y}$	7	10.9	0.663	0.444	0.064	10.4	1.831	0.446	0.141	13.0
29Oct07 [4]	1216	$D_{N/Y}$	10	7.4	0.476	0.427	0.048	9.9	1.168	0.360	0.105	11.1
31Oct07 [6]	1200	$D_{N/Y}$	13	8.8	0.731	0.460	0.091	8.0	1.573	0.452	0.118	13.4
01Nov07 [7]	1600	$D_{N/Y}$	15	n/a	0.510	0.458	0.051	10.1	1.635	0.457	0.129	12.7
02Nov07 [8]	1606	$D_{N/Y}$	5.5	12.0	0.667	0.397	0.055	12.2	1.199	0.366	0.114	10.5
03Nov07 [9]	1902	$D_{N/Y}$	7	13.3	0.630	0.469	0.112	5.6	1.665	0.452	0.136	12.3
03Nov07 [10]	1902	$D_{N/Y}$	22	7.2	0.440	0.467	0.046	9.7	1.665	0.452	0.136	12.3
05Nov07 [12]	1908	$D_{N/Y}$	12	10.2	0.507	0.464	0.038	13.5	1.272	0.452	0.116	11.0
05Nov07 [12]	1908	D_{FY}	32	7.2	0.402	0.454	0.040	10.0	1.272	0.452	0.116	11.0
06Nov07 [13]	1916	$D_{N/Y}$	12	9.5	0.562	0.438	0.068	8.3	1.975	0.437	0.137	14.4
12Nov07 [19]	1118	F	34.5	5.9	0.254	0.432	0.027	9.3	1.501	0.397	0.134	11.2
16Nov07	1117	F	34	7.0	0.340	0.429	0.039	8.7	1.493	0.417	0.109	13.7

[23]												
16Nov07 [23]	1117	F	38	6.6	0.330	0.435	0.030	11.0	1.463	0.425	0.127	11.5
19Nov07 [26]	405	D_{FY}	44	7.7	0.308	0.439	0.049	6.2	1.676	0.447	0.133	12.6
20Nov07 [27]	1100	$D_{N/Y}$	5	17.3	0.677	0.431	0.062	10.9	1.595	0.458	0.105	15.2
21Nov07 [28]	1610	D_{FY}	45	10.4	0.486	0.456	0.049	9.8	1.739	0.442	0.123	14.1
22Nov07 [29]	437	D_{FY}	62	7.7	0.339	0.470	0.072	4.7	1.699	0.449	0.121	14.1
24 Nov07 [31]	O1**	O	300	0.5	0.253	0.476	0.047	5.4	1.394	0.475	0.127	11.0
25 Dec07 [62]	D11	D_{FY}	30.5	10.8	0.351	0.466	0.049	7.2	1.589	0.463	0.133	11.9
26 Dec07 [63]	D12	D_{FY}	64.5	8.5	0.276	0.447	0.045	6.1	1.346	0.458	0.100	13.4
01 Jan08 [69]	D13	D_{FY}	99.5	7.0	0.247	0.451	0.031	7.8	1.799	0.460	0.139	13.0
03 Jan08 [71]	D14	D_{FY}	100	6.7	0.245	0.457	0.032	7.6	1.730	0.447	0.140	12.3
15 Jan08 [83]	D17A	D_{FY}	46	8.0	0.261	0.478	0.027	9.7	2.003	0.467	0.150	13.3
15 Jan08 [83]	D17B	D_{FY}	68	8.1	0.229	0.448	0.032	7.2	2.003	0.467	0.150	13.3
18 Jan08 [86]	D17C	D_{FY}	95	6.8	0.215	0.451	0.033	6.4	1.261	0.467	0.112	11.2
20 Jan08 [88]	D17D	D_{FY}	92	6.8	0.213	0.444	0.028	7.6	1.012	0.461	0.108	9.4
23 Jan08 [91]	D18A	$L_{N/Y}$	1	30.2	0.470	0.467	0.076	6.2	0.843	0.458	0.086	9.8
23 Jan08 [91]	D18B	$L_{N/Y}$	3	31.4	0.439	0.465	0.064	6.9	0.817	0.459	0.074	11.0
24 Jan08 [92]	D19	D_{FY}	92	6.3	0.197	0.463	0.030	6.6	0.968	0.453	0.136	7.1
16 Mar08	D29	D_{FY}	130	6.1	0.287	0.461	0.046	6.2	1.035	0.440	0.171	6.1

[114]												
19 Mar08 [117]	D31	$L_{N/Y}$	30	11.2	0.350	0.475	0.068	5.2	1.005	0.425	0.147	6.8
24 Mar08 [122]	D34	L_{FY}	45	9.2	0.330	0.468	0.066	5.0	0.998	0.439	0.155	6.4
25 Mar08 [123]	D33	D_{FY}	138	5.3	0.232	0.484	0.048	4.9	1.073	0.440	0.164	6.5
28 Mar08 [126]	F1	F	189	5.8	0.172	0.504	0.041	4.2	0.949	0.437	0.120	7.9
04 Apr08 [132]	D33A	L_{FY}	64	8.5	0.221	0.490	0.052	4.3	0.936	0.445	0.138	6.8
07 Apr08 [135]	D36A	$L_{N/Y}$	0.5	20.6	0.446	0.462	0.074	6.0	0.908	0.448	0.113	8.0
08 Apr08 [136]	D36B	L_{FY}	70	8.4	0.207	0.448	0.047	4.4	0.892	0.450	0.133	6.7
08 Apr08 [136]	D36C	D_{FY}	164	6.1	0.192	0.440	0.047	4.0	0.870	0.451	0.141	6.2
10 Apr08 [138]	D38A	$L_{N/Y}$	2.5	11.5	0.393	0.459	0.129	3.0	0.927	0.441	0.148	6.3
12 Apr08 [140]	D38	D_{FY}	121	6.5	0.185	0.442	0.042	4.4	0.841	0.432	0.104	8.1
20 Apr08 [148]	D41	D_{FY}	129	5.4	0.153	0.388	0.035	4.4	0.885	0.447	0.122	7.3
29 Apr08 [157]	D43	D_{FY}	134	6.1	0.184	0.416	0.032	5.8	0.912	0.433	0.126	7.2
06 May08 [165]	1020	$L_{N/Y}$	2.5	18.3	0.440	0.454	0.073	6.0	0.823	0.433	0.100	8.2
09 May08 [168]	F2	F	125	5.4	0.296	0.457	0.051	5.8	0.877	0.417	0.107	8.2
14 May08 [173]	F3	F	171	5.7	0.205	0.421	0.034	6.1	0.883	0.416	0.104	8.5
25 May08 [184]	O2	O	388	2.7	0.162	0.371	0.033	4.9	0.852	0.451	0.097	8.8

St. – station; $D_{N/Y}$ – drifting new and young ice 0-30 cm thick; D_{FY} – drifting first year ice 30-200 cm thick; F – landfast first year ice 30-200 cm thick; O – old ice above 200 cm thick; $L_{N/Y}$ – lead new and young ice 0-30 cm thick; L_{FY} – lead first year ice 30-200 cm thick; T – temperature; S – salinity; Thick – thickness; * day 1 – 26 Oct 2007; ** measured in the top 100 cm of the 300 cm thick old ice core; $_{WAT}$ – under-ice sea water

Table 2.2 Mean α- and γ- HCH concentrations and sea ice salinities ± SE in different sea ice classes; lead data excluded

Ice type	Thickness (cm)	n	Mean α-HCH_{ICE} ± SE (ng/L)	Mean γ-HCH_{ICE} ± SE (ng/L)	Mean S_{ICE} ± SE (‰)
New & young ice	0-30	12	0.642 ± 0.046	0.066 ± 0.006	11.6 ± 1.2
First year ice	30-200	25	0.261 ± 0.015	0.040 ± 0.002	7.0 ± 0.3
Old ice	> 200	2	0.208 ± 0.045	0.040 ± 0.007	1.6 ± 1.1

S – salinity; SE – standard error; n – number of observations

2.4.3 *Importance of brine processes for the rejection of HCHs from the sea ice*

α-HCH and γ-HCH levels decreased exponentially with increasing sea ice thickness following the sea ice desalination curve (Figure 2.3) (Kovacs, 1997). The correlations between Log[HCH] and Log[salinity] and Log[HCH] and Log[thickness] in the sea ice were significant for the α- ($R^2 = 0.84$; $p < 0.01$ and $R^2 = 0.70$; $p < 0.01$, respectively) and γ-isomers ($R^2 = 0.39$; $p < 0.01$ and $R^2 = 0.40$; $p < 0.01$, respectively) (Figure 2.4). The correlations suggest that brine rejection is accompanied by HCH rejection. During the initial stage of ice formation, the growth velocity is relatively high and considerable amounts of brine are trapped in the sea ice. As the thickness of the ice increases, the growth velocity decreases and less brine is trapped (Cox and Weeks, 1975). Laboratory experiments suggest that gravity drainage is the main desalination mechanism for first year sea ice that is growing (Cox and Weeks, 1975), with the rate dependent on the temperature gradient within the ice. This could explain the gradual decrease in desalination amounts observed in thicker ice.

A multiple regression of HCH versus ice bulk salinity and ice thickness did not improve the predictability of α-HCH and γ-HCH rejection from the sea ice ($R^2 = 0.85$, $p = 0.000$ and $R^2 = 0.42$, $p = 0.000$, respectively) when compared to regression with ice thickness alone. Thus, the measurement of ice thickness is, by itself, a good predictor of HCH levels in the sea ice, particularly in the case of the α-isomer.

2.4.4 *α- and γ-HCH concentrations in the lead sea ice samples*

For α-HCH, different slopes in the trends of HCH with depth (Figure 2.4A,B) were observed for lead ice (L) and drifting/landfast ice (DF) with lower concentrations of α-HCH in the new and young lead ice samples (< 30 cm). γ-HCH concentrations in L and DF ice followed similar trends (Figure 2.4C,D).

Lead samples were sub-divided into new and young lead ice (< 30 cm) and first year ice (30-70 cm), and mean α- and γ-HCH levels in sea ice and under-ice water, and ice bulk salinity were compared to the DF ice samples of corresponding thicknesses. To ensure that the differences between L and DF groups were not influenced by differences in the mean ice thickness between groups, ANOVA (one-way, post-hoc test Tukey, $p = 0.05$) with ice thickness as a covariate was performed (Table 2.3).

In the < 30 cm ice category, L samples and under-ice water had significantly lower levels of α-HCH compared to the DF samples. In the 30-70 cm category, levels of α-HCH in the under-ice water were significantly lower for the L samples than for the DF samples but this difference was found not significant in the sea ice. There were no statistically significant differences in γ-HCH concentrations in the sea ice and under-ice sea water found between groups in both ice thickness categories. Furthermore, L samples did not differ significantly in bulk salinity from the DF samples. Thus, we attribute significantly lower concentrations of α-HCH in the L ice to the lower levels of this isomer in the under-ice water in the spring. Initial concentration of HCHs in sea water during entrapment are clearly important but for the ice samples between 30 and 70 cm thickness, smaller differences in the initial sea water concentrations are likely offset by the overriding effect of ice desalination.

Figure 2.3 Dependence of α-HCH and γ-HCH concentrations and salinity (S) on the sea ice thickness (Thick); mean concentrations of α-HCH (graph A), γ-HCH (graph B) and salinity (graph C) in the new and young ice, N&Y (0.5-30 cm), first year ice, FYI (30-200 cm) and old ice (> 200 cm) are also presented, SE – standard error; lead ice data excluded

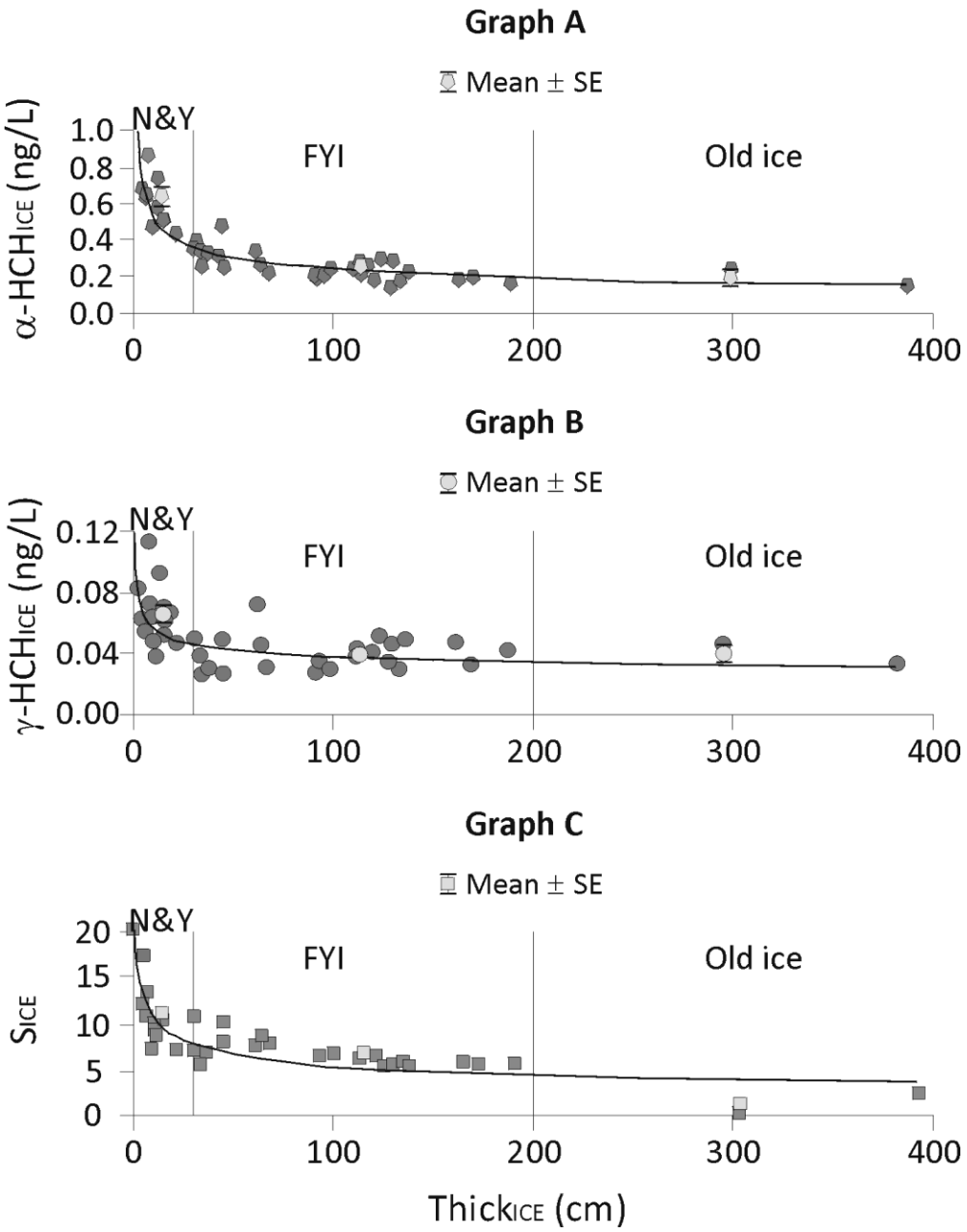

Figure 2.4 Relationship between α-HCH and γ-HCH concentration and sea ice thickness (Thick) and salinity (S) for drifting and landfast stations (DF), lead stations (L) and old ice stations (O); data log-transformed prior to analysis; regression lines do not include old ice and are performed separately for DF and L stations for the α isomer

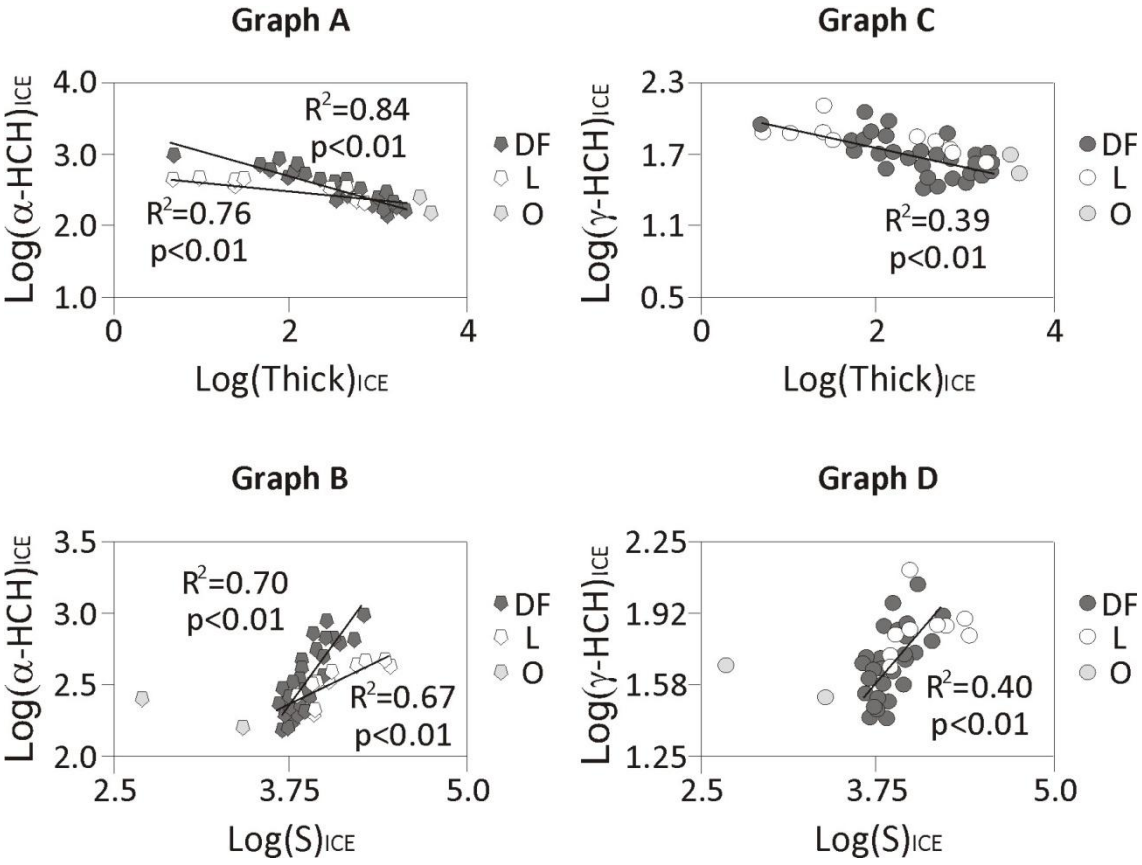

Table 2.3 Probability values (p) for rejecting the hypothesis that L samples do not differ from D&F samples for two thickness categories (< 30 cm and 30-70 cm); ANOVA with sea ice thickness as a covariate results; groups with statistically significant difference in mean values marked with brackets

	p-values	
	< 30 cm	30-70 cm
α-HCH_{ICE}	(0.000)	0.332
α-HCH_{WATER}	(0.000)	(0.001)
γ-HCH_{ICE}	0.406	0.288
γ-HCH_{WATER}	0.456	0.232
S_{ICE}	0.056	0.564

performed on log transformed data

2.4.5 *α- and γ-HCH concentrations in the old ice samples*

The brine drainage experiment was conducted to investigate the relation between salt and HCH rejection from the ice during the transition from the first year into the old ice. The temperature profile evolution during this experiment (Figure 2.5) closely followed the spring (May 5 – June 9 1998) temperature evolution measured *in situ* on first year fast ice in Kongsfjorden, Svalbard (Gerland *et al.*, 1999).

The experimental set up produced plausible natural spring melt conditions for the sea ice. Both HCH isomers exhibited profound decreases in melt water as the drainage progressed (Table 2.4, Figure 2.6) with the predominant decline occurring between the first and the second melt fraction, which also accounted for 73 % of salts lost from the sea ice. Rejection of 99 % of salts from the ice in the first three melt water fractions was accompanied by the loss of 78 % and 80 % of α- and γ-HCH, respectively. Thus, the first year to old ice spring transition, which exhibits pronounced desalination, should also result in pronounced decline of HCH in the ice.

Figure 2.5 Sea ice temperature profile as a function of time during the sea ice brine drainage experiment

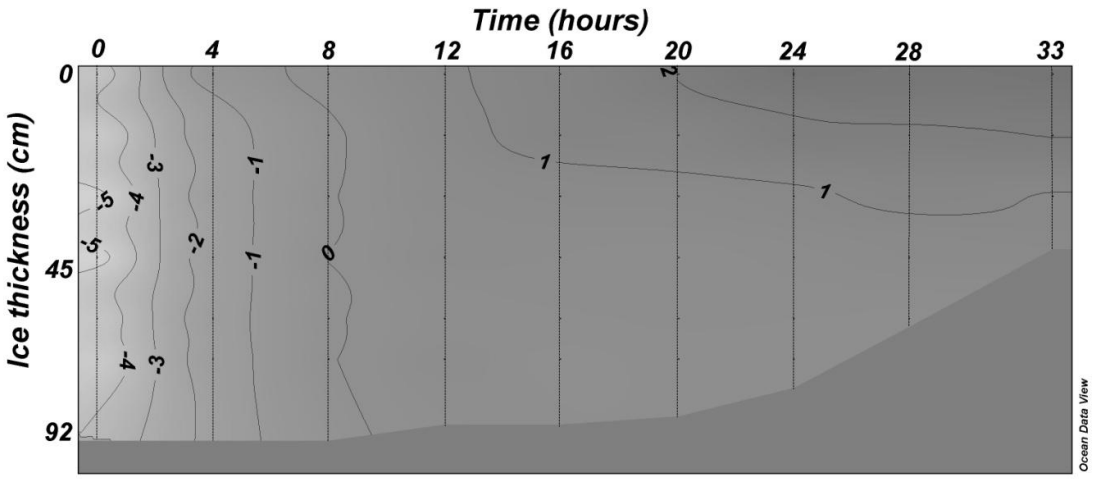

The two samples of old ice that were collected did not follow the α- and γ-HCH relationships observed for DF or L ice (Figure 2.4). Old ice had relatively high levels of both α- and γ-HCH considering the greater ice thickness and lower salinity. Although there was a statistically significant difference between the desalination in the two old ice samples compared to the first year ice samples, levels of HCHs were not significantly lower (ANOVA, one-way, Tukey test, $p = 0.05$) (Figure 2.3), suggesting that a secondary loading of HCHs into the ice must have occurred during the spring season.

Table 2.4 Sea ice brine drainage experiment results (24-26 Jan 08)

Time (hours)	Melt water fraction	$S_{MELT\ WATER}$ (‰)	$\alpha\text{-HCH}_{MELT\ WATER}$ (ng/L)	$\gamma\text{-HCH}_{MELT\ WATER}$ (ng/L)	S ($\%_{TOT}$)	α-HCH ($\%_{TOT}$)	γ-HCH ($\%_{TOT}$)
9	1 (23%)	20.1	0.391	0.040	73	42	44
14	2 (23%)	5.5	0.190	0.016	20	21	17
20	3 (24%)	1.6	0.132	0.017	6	15	19
28	4 (18%)	0.2	0.148	0.014	1	12	12
46	5 (12%)	0.0	0.174	0.013	0	10	8

S – salinity; EF – α-HCH enantiomer fraction; $\%_{TOT}$ – percent of the total core value

Figure 2.6 Salinity (graph A), α-HCH concentration (graph B) and γ-HCH concentration (graph C) in progressing melt water fractions in the sea ice brine drainage experiment

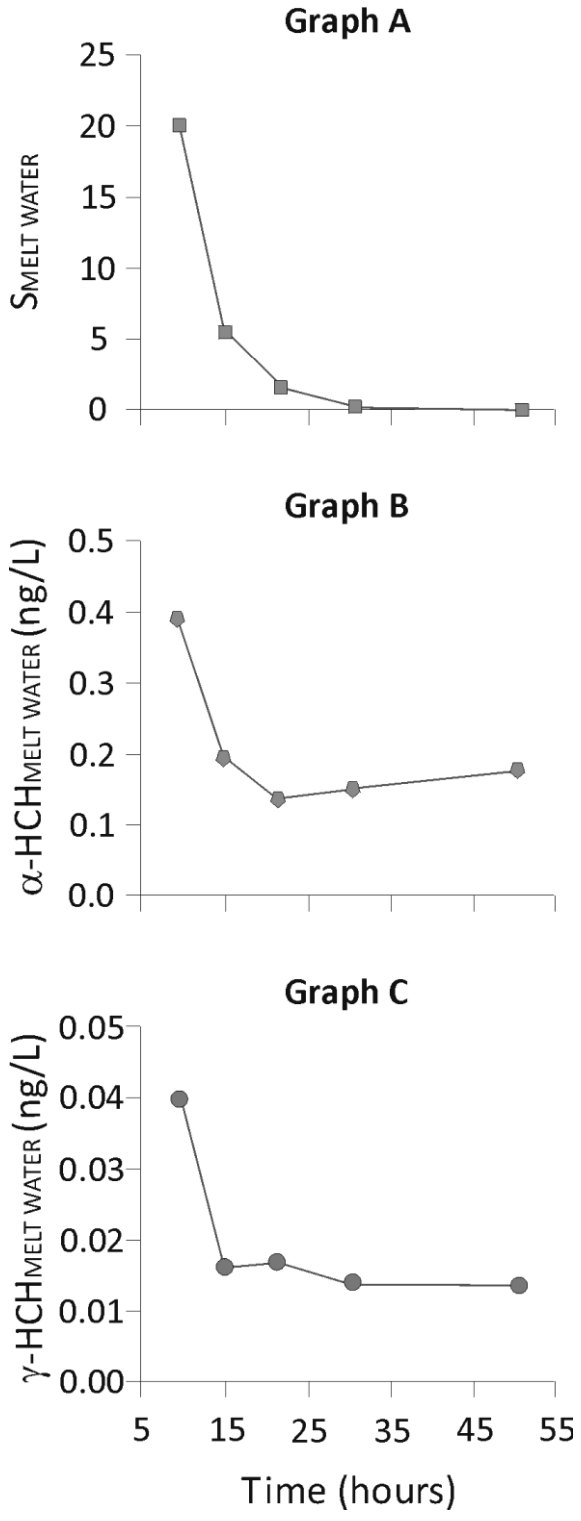

A profile of HCHs and α-HCH EFs in the old ice confirmed the above proposal of HCH deposition in late spring. The lowest concentrations of HCHs were measured in the middle of the core, which was also depleted in one of the enantiomers (EF of 0.27; Table 2.5, Figure 2.7). This part of the old ice core was isolated from potential secondary sources of HCHs from the atmosphere or sea water but could have been subjected to enantioselective bacterial degradation of α-HCH. Higher levels of HCHs at the top of the old ice could be produced by atmospheric wet deposition or air-water exchange with liquid water at the ice surface. Surface melt ponds, once fully formed in the Arctic in mid-July, can survive unfrozen until early August, refreeze again in mid-September (Eicken, 1994), and thus allow time for air-melt water gas exchange. This hypothesis is supported by significantly higher α-HCH EF, closer to racemic, in the top part of the core (cf. Jantunen *et al.*, 2008). The bottom most part of the old ice in May, which had higher bulk salinity, probably did not undergo summer desalination and enantioselective microbial breakdown, accounting for relatively high levels of HCHs and higher α-HCH EF.

Table 2.5 α-HCH and γ-HCH concentrations, α-HCH enantiomer fraction (EF_{ICE}) and ice bulk salinity (S_{ICE}) in the 3 layers of the old ice sample (O2, 25 May 2008)

Date	Station	$Layer_{ICE}$ (cm)	$\alpha\text{-}HCH_{ICE}$ (ng/L)	EF_{ICE}	$\gamma\text{-}HCH_{ICE}$ (ng/L)	S_{ICE} (‰)
25 May 08	O2	0-125	0.178	0.457	0.040	2.4
		125-250	0.122	0.268	0.027	2.4
		250-385	0.183	0.388	0.032	3.4

Figure 2.7 Vertical distribution of α-HCH (graph A), γ-HCH (graph B), bulk salinity (graph C) and α-HCH enantiomer fraction, EF (graph D) in the old ice sample (O2, 25 May 2008); S-salinity

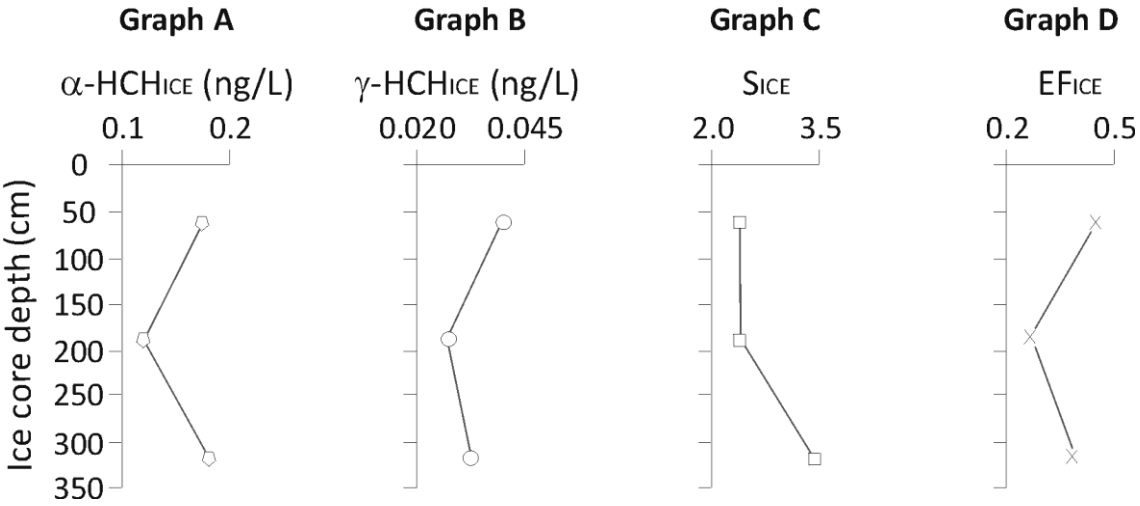

2.4.6 *Vertical distribution of HCHs in the first year ice as a function of ice thermodynamic state*

α- and γ-HCH concentrations, α-HCH EF and sea ice physical (bulk salinity and texture) and thermodynamic (temperature and brine volume) parameters were measured/calculated in 3-5 layers of the first year sea ice at twelve stations during the project from 25 December 2007, day 72, to 14 May 2008, day 173 (Table 2.6).

There were three main sea ice stages distinguishable in the sea ice annual cycle (Figure 2.8). The growth phase lasted from day 62 to day 126 (25 December 2007 – 28 March 2008) with strong temperature stratification in the ice column and relatively low brine volume fraction. The warming phase included profiles from days 136 and 140 (8 and 12 April 2008) with decreasing thermal stratification of the sea ice and relatively low brine volume fraction. Finally, the melting phase (day 157, 29 April 2008, and 173, 14 May 2008) was characterized by weak thermal stratification to isothermal sea ice

and high brine volume fractions exceeding the critical value of 5 % over the entire ice column.

α-HCH concentrations in growing ice were significantly related to all of the geophysical parameters measured in the study. α-HCH concentration depended strongly on the depth in the ice core and bulk salinity, and moderately on ice texture (Figure 2.9A). Granular ice pores are significantly larger than columnar ice pores (Bock and Eicken, 2005), and the amount of brine entrapped in sea ice depends proportionally on the growth velocities, which are approximately twice as fast in granular ice (Cox and Weeks, 1975; Weeks and Ackley, 1986). These considerations explain the observed initial dependence of α-HCH concentration on the sea ice texture and sea ice bulk salinity for growing ice. In warming ice, the vertical distribution of α-HCH becomes independent of sea ice texture, proportional to bulk salinity, and negatively correlated with depth in the ice (Figure 2.9B). Later in the season, desalination is the main mechanism governing the α-HCH distribution in the ice column, and the sea ice stratigraphy loses its importance for α-HCH entrapment. For melting sea ice, α-HCH levels could not be predicted by any of the sea ice geophysical variables (Figure 2.9C). Vertical distribution of α-HCH became roughly uniform with higher values in the bottom most part of the two profiles (presented as larger points in Figure 2.9C).

γ-HCH distribution in first year sea ice was independent of the ice geophysical variables throughout the sea ice annual cycle with the exception of a weak dependence on depth in growing ice and moderate for melting ice (Figure 2.10). However, the latter correlation was caused mainly by the substantial decrease of γ-HCH in the bottom most layers of the last two sampled ice cores.

Table 2.6 α-HCH and γ-HCH concentrations, α-HCH enantiomer fraction (EF_{ICE}) and α-HCH/γ-HCH ratio in different layers of the sea ice along with sea ice physical parameters (texture, salinity [S], temperature [T] and brine volume fraction [υ_b]) at different first year ice stations throughout the project (from Dec 2007 to May 2008)

Date [coded*]	Station	$Layer_{ICE}$ (cm)	Texture [coded**]	S_{ICE} (‰)	T_{ICE} (deg C)	υ_b (%)	$\alpha\text{-HCH}_{ICE}$ (ng/L)	EF_{ICE}	$\gamma\text{-HCH}_{ICE}$ (ng/L)	α/γ_{ICE}
25Dec 07 [62]	D11	0-11	1	13.3	-13.5	5.6	0.435	n/a	0.053	8.2
		11-22	1.75	9.7	-8.2	6.3	0.334	0.473	0.044	7.6
		22-30.5	2	9.1	-3.7	12.6	0.265	0.459	0.048	5.5
26Dec 07 [63]	D12	0-13	1	13.0	-18.5	4.1	0.423	0.455	0.049	8.6
		13-27	1.75	8.2	-12.6	3.6	0.262	0.452	0.043	6.1
		27-41	2	7.8	-8.7	4.8	0.218	0.439	0.056	3.9
		41-53	2	6.4	-7.4	4.6	0.207	0.443	0.043	4.8
		53-64.5	1.42	7.0	n/a	n/a	0.276	0.445	0.033	8.4
01Jan 08 [69]	D13	0-7.5	1	11.5	-20.7	3.3	0.403	0.448	0.030	13.4
		7.5-32.5	1.75	9.1	-15.3	3.4	0.315	0.454	0.038	8.3
		32.5-56	2	6.5	-11.3	3.2	0.218	0.459	0.034	6.4
		56-70	1.91	5.8	-7.9	3.9	0.204	0.447	0.029	7.0
		70-99.5	2	5.1	-4.9	5.4	0.191	0.448	0.026	7.3
18Jan 08 [86]	D17C	0-19	1	10.8	-20.8	3.1	0.325	0.453	0.044	7.4
		19-33.5	1.25	6.8	-19.2	2.1	0.219	0.440	0.035	6.3
		33.5-57	2	6.0	-15.9	2.2	0.201	0.446	0.029	6.9
		57-72	1.25	5.8	-10.1	3.1	0.179	0.445	0.035	5.1
		72-95	2	5.0	-5.2	5.0	0.161	0.474	0.027	6.0
20Jan 08 [88]	D17D	0-17	1	10.8	-17.7	3.6	0.285	0.437	0.035	8.1
		17-33	1.25	6.8	-15.5	2.5	0.221	0.436	0.030	7.4
		33-56.5	2	6.0	-13.2	2.6	0.205	0.436	0.024	8.5
		56.5-75.5	1.25	5.8	-8.1	3.8	0.184	0.433	0.027	6.8
		75.5-91	2	5.0	-3.9	6.6	0.177	0.476	0.025	7.1
24Jan 08 [92]	D19	0-11	1.2	9.9	-15.5	3.7	0.242	0.457	0.041	5.9
		11-32	2	7.1	-11.4	3.4	0.242	0.453	0.031	7.8
		32-55	1.8	5.9	-8.6	3.7	0.186	0.457	0.029	6.4

		55-73	1.8	5.2	-5.3	5.1	0.178	0.476	0.027	6.6
		73-92	1.9	5.0	-3.1	8.2	0.152	0.472	0.025	6.1
25Mar 08	D33	0-16	1.25	9.1	-20.2	2.7	0.307	0.485	0.051	6.0
[123]		16-40	1.75	5.8	-16.1	2.1	0.275	0.482	0.060	4.6
		40-70	2	4.7	-15.0	1.8	0.255	0.488	0.051	5.0
		70-100	2	4.3	-11.3	2.1	0.202	0.489	0.037	5.5
		100-138	2	4.5	-6.1	3.9	0.180	0.478	0.045	4.0
28Mar 08	F1	0-50	1.6	7.2	n/a	n/a	0.194	0.545	0.046	4.2
[126]		50-100	1.75	5.3	n/a	n/a	0.170	0.517	0.039	4.4
		100-150	2	5.6	n/a	n/a	0.146	0.487	0.031	4.7
		150-189	2	5.1	n/a	n/a	0.178	0.465	0.050	3.6
08Apr 08	D36C	0-23	1	8.2	-13.9	3.3	0.213	0.471	0.068	3.1
[136]		23-54	1.25	6.8	-11.3	3.3	0.234	0.429	0.044	5.3
		54-84	1.4	5.5	-9.8	3.1	0.202	0.417	0.044	4.6
		84-128	2	5.7	-6.8	4.4	0.182	0.453	0.044	4.1
		128-164	1.6	5.3	-3.2	8.4	0.146	0.430	0.044	3.3
12Apr 08	D38B	0-15	1.5	9.8	-9.8	5.4	0.222	0.463	0.037	6.0
[140]		15-32.5	1.8	8.3	-8.8	5.1	0.232	0.452	0.047	4.9
		32.5-65	2	5.3	-7.7	3.7	0.160	0.450	0.036	4.4
		65-93.5	1.6	5.7	-5.3	5.6	0.170	0.452	0.037	4.6
		93.5-121	2	5.6	-2.5	11.3	0.179	0.393	0.053	3.4
29Apr 08	D43	0-15	1.25	11.6	-9.1	6.9	0.187	0.470	0.047	4.0
[157]		15-30	1.25	6.2	-9.0	3.7	0.167	0.458	0.035	4.8
		30-65	1.9	5.7	-7.4	4.1	0.179	0.466	0.041	4.4
		65-100	1.9	4.8	-4.2	5.9	0.134	0.423	0.030	4.5
		100-134	2	5.5	-1.9	14.5	0.248	0.263	0.017	14.6
14May 08	F3	0-48	1.2	5.3	-0.8	32.9	0.196	0.443	0.040	4.9
[173]		48-80	2	5.2	-1.9	13.7	0.204	0.464	0.039	5.2
		80-122	2	5.6	-1.8	15.6	0.184	0.467	0.038	4.8
		122-171	2	6.4	-1.0	31.8	0.232	0.308	0.020	11.6

D – drift ice station; F – landfast ice station; S – salinity; T – temperature; * day 1 – 26 Oct 2007; ** 1 – g – granular, 1.25 – tg – transitional granular, 1.75 – tc – transitional columnar, 2 – c – columnar; υ_b – brine volume fraction; n/a – not available

Figure 2.8 Temperature (T) and brine volume fraction vertical profiles in the first year sea ice (30-200 cm) as a function of time, 25 December 2007 (day 62) to 14 May 2008 (day 173); three thermodynamic sea ice states are indicated

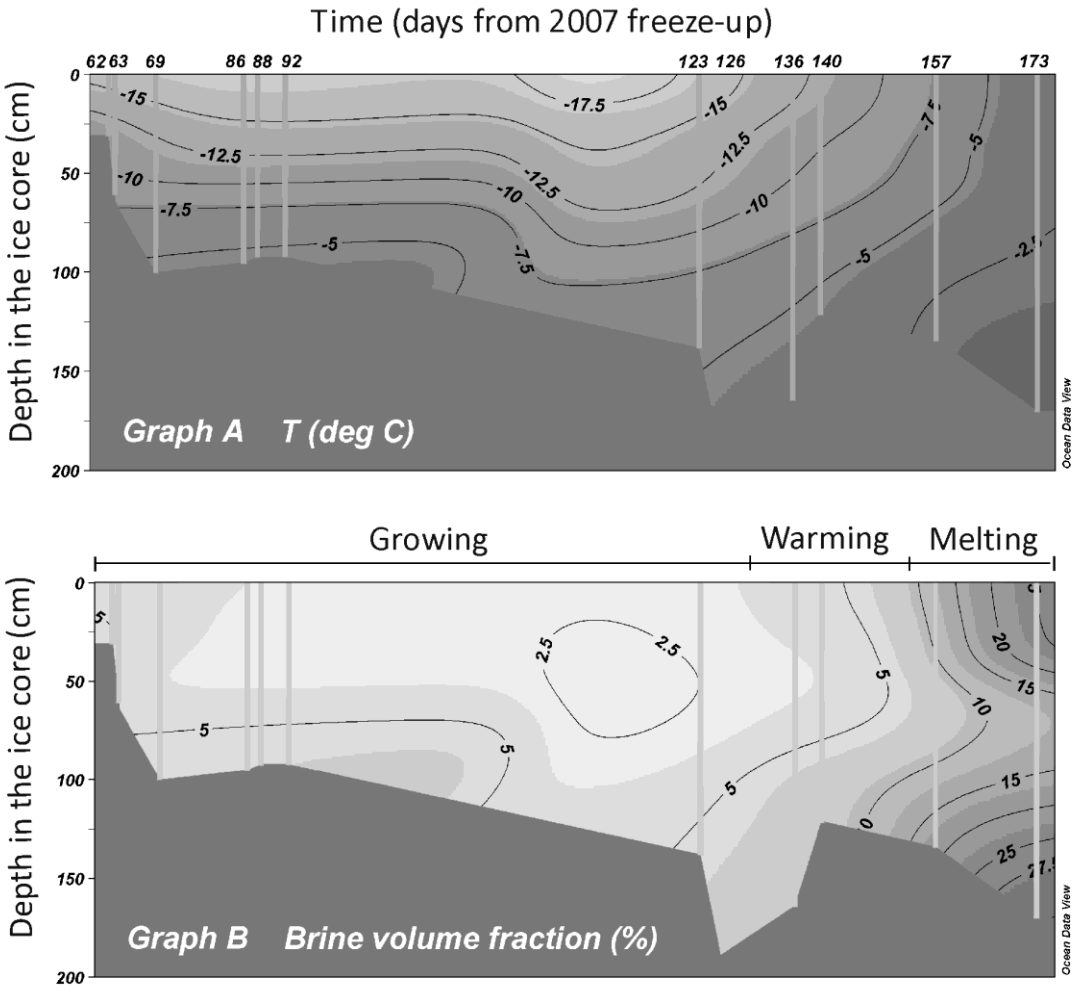

Figure 2.9 Relationship between levels of α-HCH in different layers of the first year sea ice and depth in the ice core (Depth), bulk salinity (S) and texture for growing ice (graph A), warming ice (graph B) and melting ice (graph C); data log-transformed prior to analysis; two large points in the melting ice represent bottom most layers of ice cores

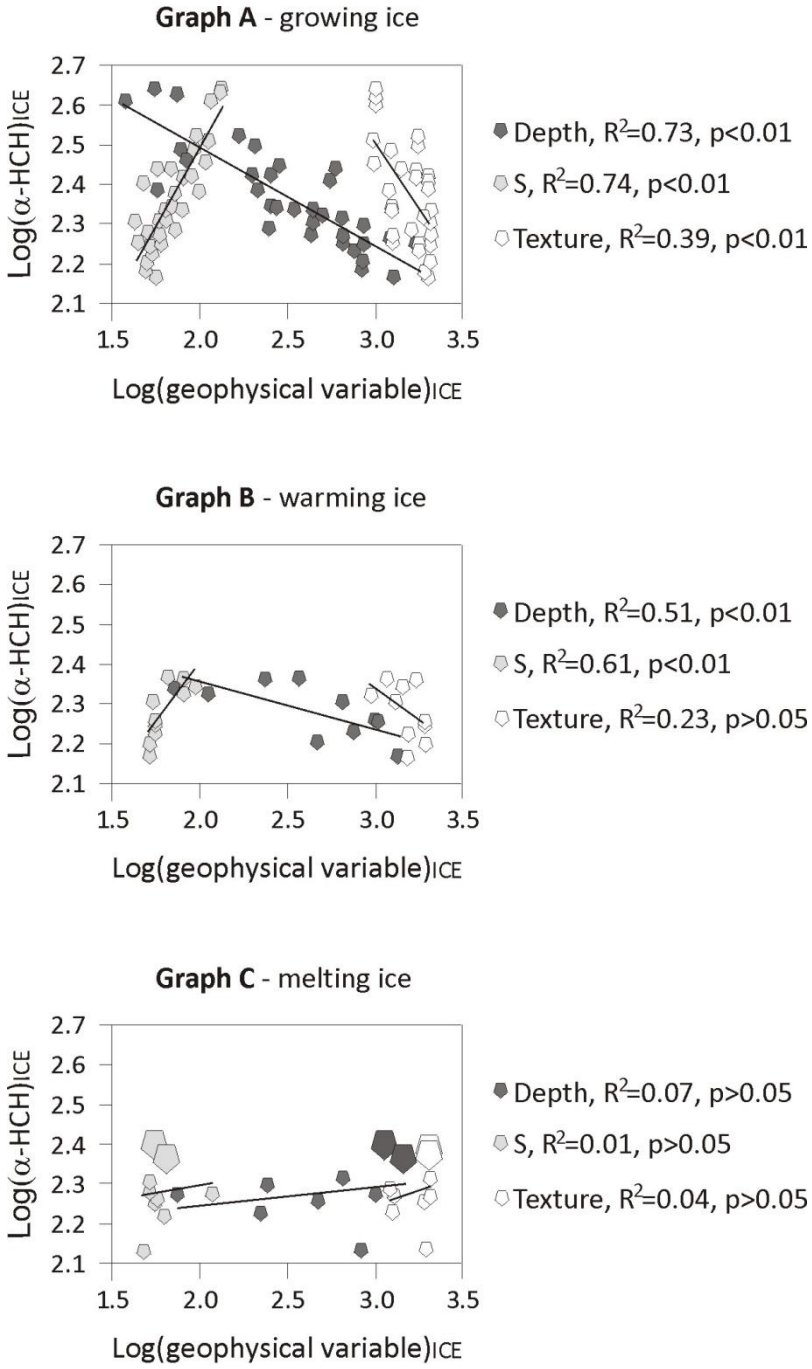

2.4.7 *Role of biological processes for HCHs in the melting ice regime*

There was a pronounced increase of the α/γ-HCH ratio in both ice cores undergoing melting (Figure 2.11A). This increase was caused primarily by a substantial decrease in the γ-isomer (Figure 2.10C) accompanied by only a minor decrease in the α-isomer (Figure 2.9C). Vertical movement of brine within the ice could not account for increase in the α/γ ratio as the two points were outliers from the trend lines with salinity, particularly in the case of γ-HCH. Furthermore, the change in the α/γ ratio was noticeable only for the bottom most part of ice cores. Under-ice water penetrating into the bottom of the ice would not be capable of producing the increasing in α/γ-HCH given that the α/γ ratio in this water was below the ratio observed in the bottom of the ice (Table 2.1). For these reasons, it appears clear that the α/γ distribution must be a product of processes occurring at the bottom of the ice exclusively in spring. This period coincides with ice algal blooms observed between 3 April and 18 May 2008, and increases in bacterial numbers between 14 April and 18 May 2008 in the bottom 10 cm of the ice (Rodd Laing, personal communication).

Figure 2.10 Relationship between levels of γ-HCH in different layers of the first year sea ice and depth in the ice core (Depth), bulk salinity (S) and texture for growing ice (graph A), warming ice (graph B) and melting ice (graph C); data log-transformed prior to analysis; two large points in the melting ice represent bottom most layers of ice cores

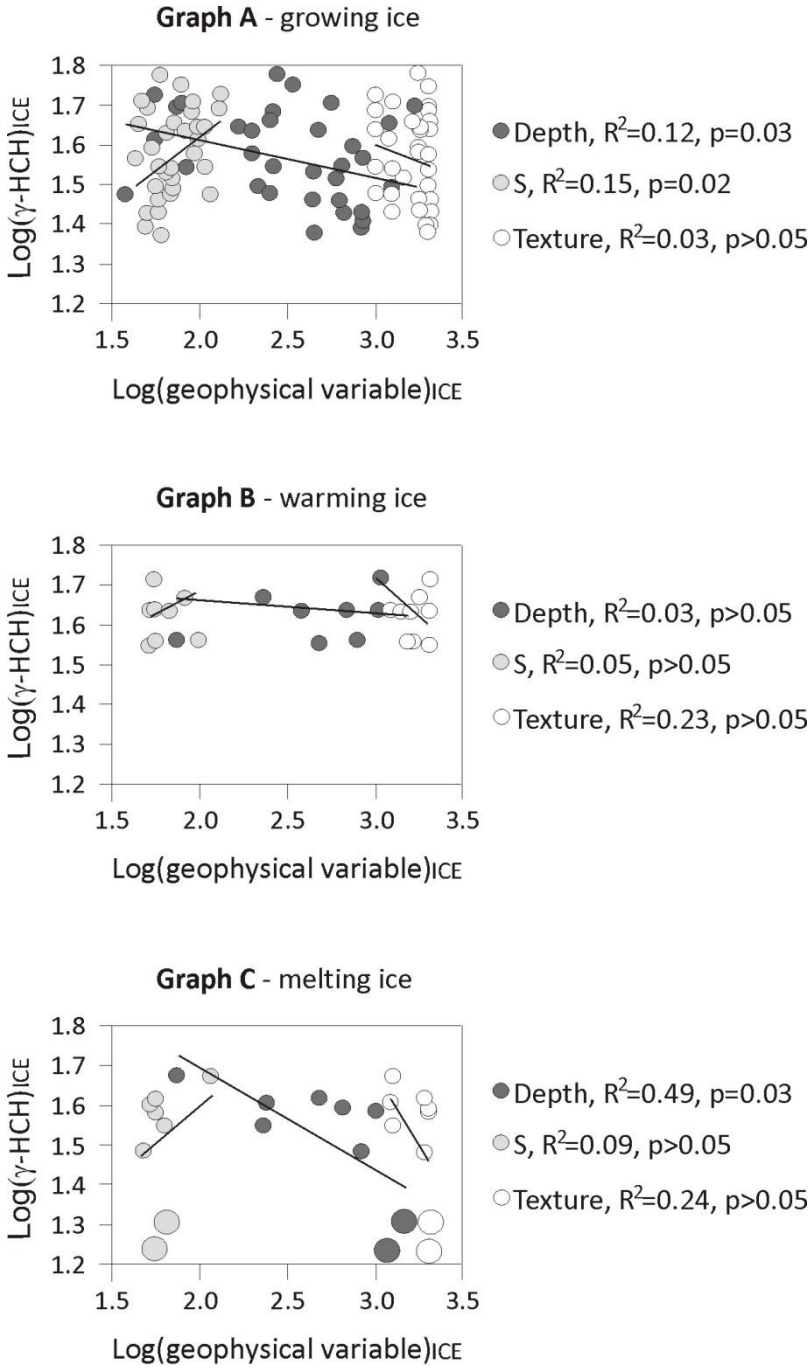

Figure 2.11 Vertical profiles of α/γ-HCH (graph A), α-HCH EF (graph B) and γ-HCH concentration (graph C) in the first year sea ice (30-200 cm thick) as a function of time, 25 December 2007 (day 62) to 14 May 2008 (day 173)

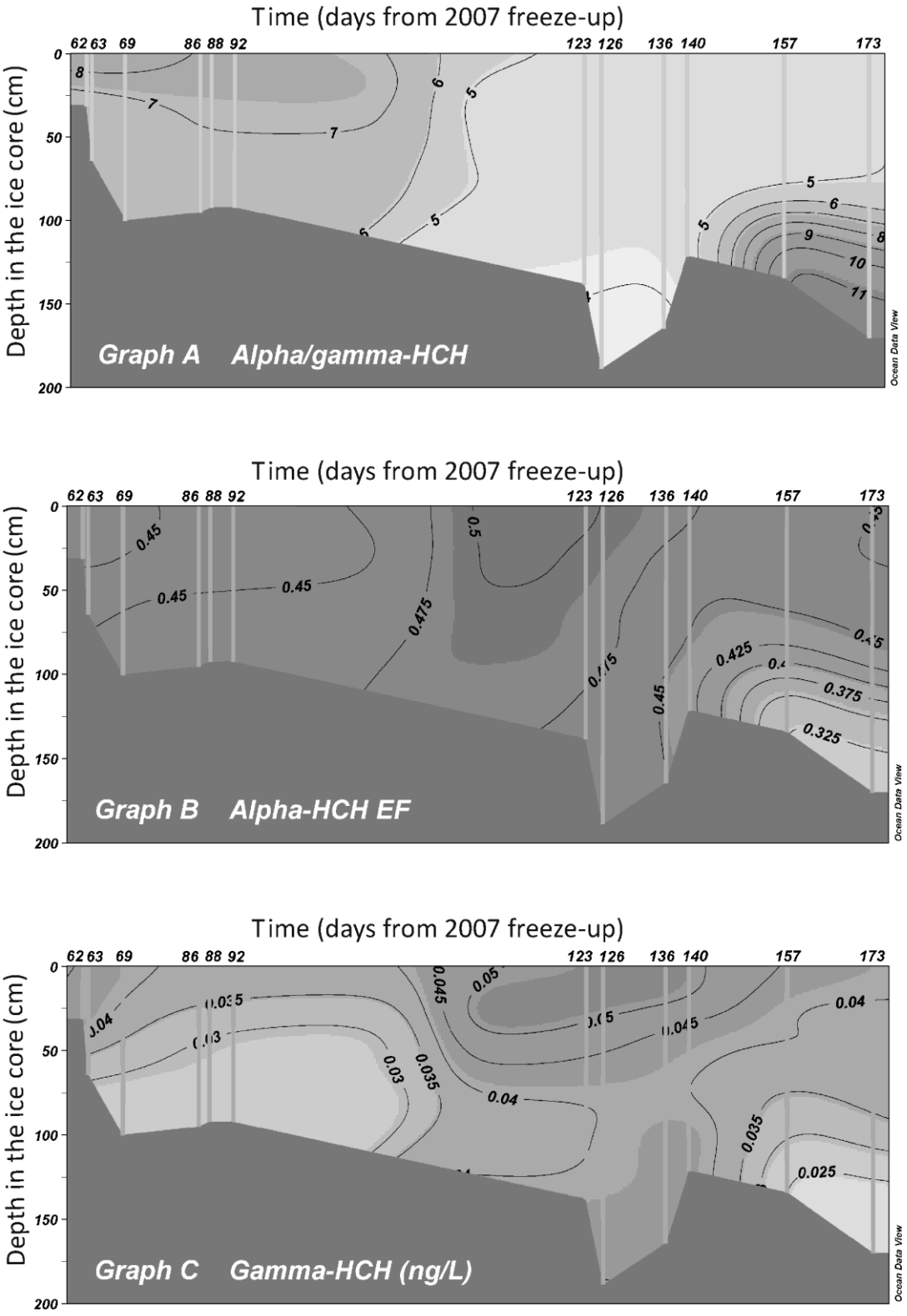

Redundancy Analysis, a multivariate technique, was applied to examine the extent to which the axes previously constrained by ice physical variables accounted for α- and γ-HCH levels in the entire ice column (average values from all layers), top most core layer and bottom most core layer (Figure 2.12). Similar Redundancy Analysis ordination triplots were produced for the average values for the ice core and only the top most layers of the ice core (Figure 2.12A,B). Sea ice physical parameters and one of the predicted variables, α-HCH concentration, trended with the first axis. γ-HCH concentration in the sea ice (the second predicted variable) was independent of the sea ice physical variables and trended with the second axis. Values of α-HCH in the sea ice (both average and top most layer) decreased over time in response to changing sea ice physical state. The largest component of HCH variability was explained by the two RDA axes previously constrained by sea ice physical variables in the top most layer of the ice core (43 %) and average value for the ice core (36 %). Only 21 % of the HCH variability was explained by the first two RDA axes constrained by sea ice physical variables for the bottom ice layer values. The distribution of values of HCHs changed on the RDA ordination triplot for the bottom most parts of the ice cores (Figure 2.12C), though relations between the variables remained similar to the other RDA triplots. Initially, the points were distributed along the first axis but bottom core slices 7-11 (25 March 2008 – 14 May 2008) trended strongly with the second axis, independently of the sea ice physical variables. The change in the trend direction was not observed for the average values for the ice core and the top most layers of the ice core supporting the conclusion from univariate analysis that there is an additional factor determining HCH levels in the bottom of the ice coinciding with the spring algal bloom.

Mean α-HCH concentration in sea ice algae was 1.198 ± 0.219 and 0.807 ± 0.222 ng/g dry weight for α- and γ-HCH, respectively (Table 2.7). The ratio of α/γ-

HCH was 1.9 ± 0.7 and the α-HCH EF was above detection limit in only 3 samples (0.460 ± 0.004; n=3). This evidence suggests algal growth as a mechanism for the rapid increase of α/γ-HCH in the bottom most part of the ice caused by algae favoring bioaccumulation of the γ-isomer. The α/γ ratio found here agrees with one reported for the ice algae from under continuous ice cover of up to 1.5 m thick in May and June 1993 in Resolute Bay, Canadian High Arctic which reached 3 ± 0.9 in three analyzed samples (Hargrave *et al.*, 2000).

There was also a profound decrease in α-HCH EF in the bottom part of melting ice (Figure 2.11B). Under-ice water penetrating into the bottom of the ice could not cause the decline of EF, as the EF in the under-ice water was between 0.416 and 0.433 from 29 April 2008, day 157, to 14 May 2008, day 173 (Table 2.1). Furthermore, algal activity was unlikely to cause the observed decline in EF as the α-HCH EF in the ice algae was comparable to that from the ice where the algae grew. Thus, enantioselective microbial degradation provides the most plausible explanation for the observed decrease (cf. Falconer *et al.*, 1995).

Figure 2.12 Redundancy Analysis (RDA) ordination triplots for average values in the ice core (graph A), top ice layer values (graph B) and bottom ice layer values (graph C); Redundancy = 35.86 %, 43.07 % and 21.33 %, respectively; T – ice temperature, Text – ice texture, υ_b – brine volume fraction, S – ice salinity; predicted variables marked with circles (α-HCH_{ICE} and γ-HCH_{ICE}); numbers of samples start from 1 (25 December 2007) and follow in a time-wise order to 11 (14 May 2008) according to Table 2.6

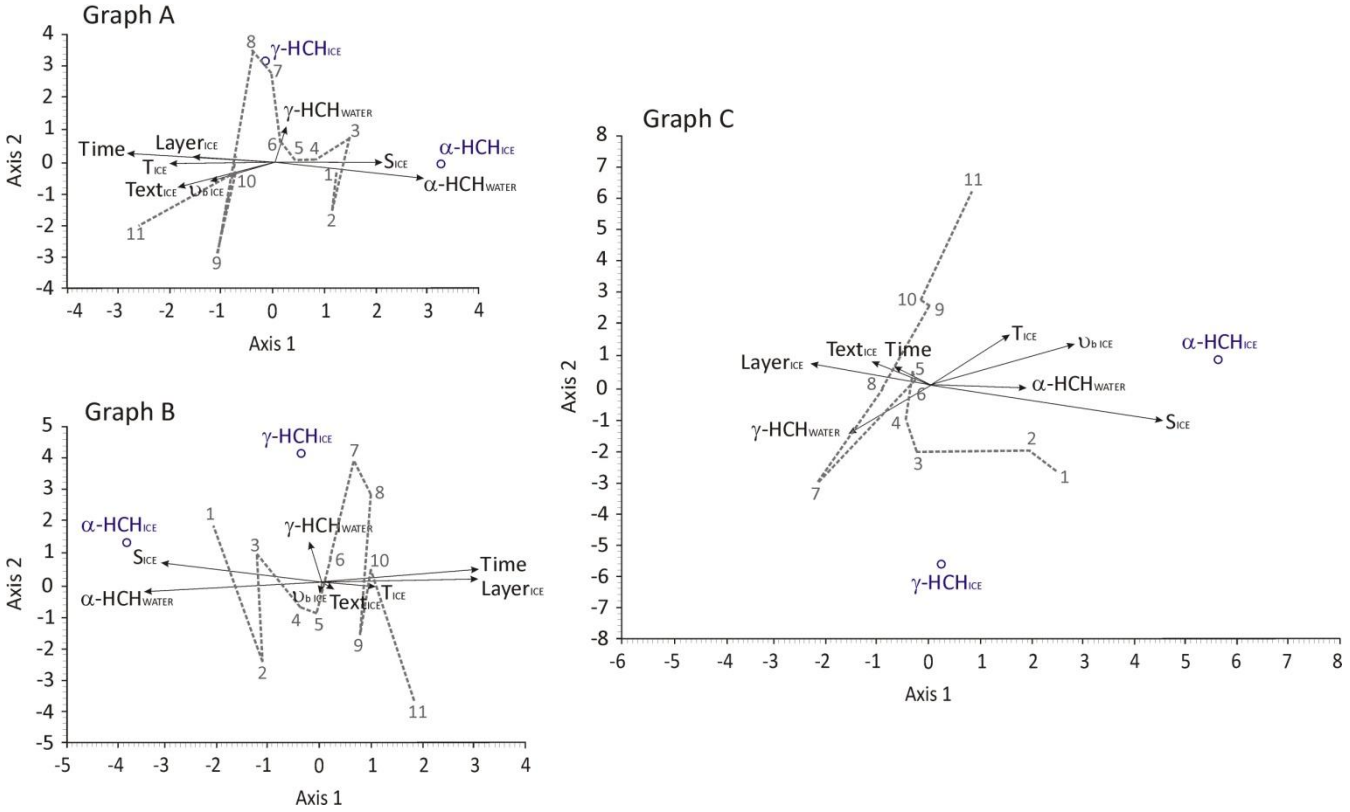

Table 2.7 α- and γ- HCH concentrations, α/γ HCH and α-HCH enantiomer fraction (EF_{ALGAE}) in the sea ice algae samples

Date [coded*]	Station	Method of collection	α-HCH_{ALGAE} (ng/g dry weight)	γ-HCH_{ALGAE} (ng/g dry weight)	α/γ_{ALGAE}	EF_{ALGAE}
11Apr 08 [139]	D38B	Under-ice slurping	1.496	0.375	4.0	0.463
20Apr 08 [148]	D41	Ice core extraction	1.403	1.872	0.7	< LOD
17Apr 08 [145]	D41	Under-ice slurping	1.498	0.535	2.8	0.465
17Apr 08 [145]	D41	Under-ice scraping	1.252	0.679	1.8	0.451
09May 08 [168]	F2	Ice core extraction	< LOD	0.549	n/a	< LOD
14May 08 [173]	F3	Ice core extraction	0.342	0.833	0.4	< LOD

* day 1 – 26 Oct 2007; < LOD – below Limit of Detection; n/a – not available

2.4.8 *The discrepancy between the predictability of the two HCH isomers levels*

A discrepancy occurs between the predictability of the two HCH isomers in the ice using relationships between the average values of HCHs and geophysical variables in the ice column, and the vertical distribution of HCHs and the sea ice geophysical variables. To exclude the potential importance of spatial variability in the dataset, residuals from the linear regression of α-HCH and γ-HCH concentrations in the sea ice with ice thickness expressing the sea ice annual cycle progression, were regressed with the geographical position of sampling (based on the average values for the ice column, Table 2.1). This relationship proved to be weak and statistically insignificant for both α-HCH ($R^2 = 0.13$, $p = 0.213$) and γ-HCH ($R^2 = 0.12$, $p = 0.253$). The absence of large-scale geographical trends in the distribution of HCHs has previously been reported for sea ice from the Ob-Yenisey River watershed (Melnikov *et al.*, 2003). Proximity to the limit of quantification also could not account for the observed discrepancy between the two isomers as all the results were at least twice the LOQ. Wet deposition in the winter could be a contributing factor as scavenging rates for γ-HCH are considerably higher for γ- than α-HCH (Macdonald *et al.*, 2000). A noticeable increase in γ-HCH concentrations in the ice corresponded to the increase in α-HCH EF from roughly 0.45 to about 0.50 in cores 123-136 with the most pronounced increase in the top parts of the ice (Figure 2.11B,C), again pointing to the importance of atmospheric deposition. Finally, spatial variability of the γ-isomer levels could explain the observed discrepancy, something that can only be properly addressed through further studies.

2.5 Acknowledgements

We would like to thank the crew of CCGS *Amundsen* for the field work assistance without which this study could not be accomplished. We also thank CFL

team 2 and team 8 members as well as Wojciech Walkusz, Eric Collins, Jason Pavlich, Rodd Laing and the divers (John Jorgenson and Jeremy Stewart) for sharing their knowledge and time in the field collecting samples and in the laboratory processing them. We give special credit to Dr. Norman Kenkel (University of Manitoba) for his time and effort in helping to interpret the results. Finally, we thank the Canadian program office of the International Polar Year, the Natural Sciences and Engineering Research Council (NSERC), Canada Foundation for Innovation (CFI), and the Canada Research Chairs (CRC) for funding.

2.6 References

Barber, D. G.; S. P. Reddan, and E. F. LeDrew. 1995. Statistical Characterization of the Geophysical and Electrical Properties of Snow on Landfast First-Year Sea Ice. *J. Geophys. Res*. **100:** 2673-2686.

Bock, C. and H. Eicken. 2005. A magnetic resonance study of temperature-dependent microstructural evolution and self-diffusion of water in Arctic first-year sea ice. *Ann. Glaciol.* **40:** 179-184.

Cox, G. F. N. and W. F. Weeks. 1975. Brine drainage and initial salt entrapment in sodium chloride ice., CRREL Res Rep 345, Cold Reg Res Eng Lab, Hanover. 88 pages.

Eicken, H. 1994. Structure of under-ice melt ponds in the central Arctic and their effect on the sea-ice cover. *Limnol. Oceanogr*. **39:** 683-694.

Eicken, H. 2004. The Role of Arctic Sea Ice in Transporting and Cycling Terrestrial Organic Matter. In: Stein R., and R. W. Macdonald (eds) The Organic Carbon Cycle in the Arctic Ocean. Springer. Germany. 7 pages.

Eicken, H. and M. A. Lange. 1989. Development and properties of sea ice in the coastal regime of the southeastern Weddell Sea. *J. Geophys. Res.* **94:** 8193-8206.

Eide, I. E. and S. Martin. 1975. The formation of brine drainage features in young sea ice. *J. Glaciol.* **14:** 137-154.

Falconer, R. L.; T. F. Bidleman, D. J. Gregor, R. Semkin and C. Teixeira. 1995. Enantioselective Breakdown of α-Hexachlorocyclohexane in a Small Arctic Lake and Its Watershed. *Environ. Sci. Technol.* **29:** 1297-1302.

Faller, J.; H. Hühnerfuss, W. A. König, R. Krebber and P. Ludwig. 1991. Do Marine Bacteria Degrade α-Hexachlorocyclohexane Stereoselectively? *Environ. Sci. Technol.* **25:** 676-678.

Frankenstein, G. E. and R. Garner. 1967. Equations for Determining the Brine Volume of Sea Ice from -0.5 to -22.9 C. *J. Glaciol.* **6:** 943-944.

Gaul, H. 1989. Organochlorine compounds in water and sea ice of the European Arctic Sea. The 8th International Conference of Comite Arctique International. Oslo. 18-22 September 1989. 10 pages.

Gerland, S.; J.-G. Winther, J. B. Ørbæk and V. Ivanov. 1999. Physical properties, spectral reflectance and thickness development of first year fast ice in Kongsfjorden, Svalbard. *Polar Res.* **18:** 275-282.

Golden, K. M.; S. F. Ackley and V. I. Lytle. 1998. The Percolation Phase Transition in Sea Ice. *Science.* **282:** 2238-2241.

Golden, K. M; A. L. Heaton, H. Eicken and V. I. Lytle. 2006. Void bounds for fluid transport in sea ice. *Mech. Mater.* **38:** 801-817.

Hargrave, B. T.; P. Vass, P. E. Erickson and B. R. Fowler. 1988. Atmospheric transport of organochlorines to the Arctic Ocean. *Tellus.* **40:** 480-493.

Hargrave, B. T.; G. A. Phillips, W. P. Vass, P. Bruecker, H. E. Welch and T. D. Siferd. 2000. Seasonality in Bioaccumulation of Organochlorines in Lower Trophic Level Arctic Marine Biota. *Environ. Sci. Technol.* **34:** 980-987.

Harner, T.; H. Kylin, T. F. Bidleman and W. M. J. Strachan. 1999. Removal of α- and γ-Hexachlorocyclohexane and Enantiomers of α-Hexachlorocyclohexane in the Eastern Arctic Ocean. *Environ. Sci. Technol.* **33:** 1157-1164.

Hühnerfuss, H.; J. Faller, W. A. König and P. Ludwig. 1992. Gas Chromatographic Separation of the Enantiomers of Marine Pollutants. 4. Fate of Hexachlorocyclohexane Isomers in the Baltic and North Sea. *Environ. Sci. Technol.* **26:** 2127-2133.

Iwata, H.; S. Tanabe, N. Sakal and R. Tatsukawa. 1993. Distribution of Persistent Organochlorines in the Oceanic Air and Surface Seawater and the Role of Ocean on Their Global Transport and Fate. *Environ. Sci. Technol.* **27:** 1080-1098.

Jantunen, L. M.; P. A. Helm, H. Kylin and T. F. Bidleman. 2008. Hexachlorocyclohexanes (HCHs) In the Canadian Archipelago. 2. Air-Water Gas Exchange of α- and γ-HCH. *Environ. Sci. Technol.* **42:** 465-470.

Kovacs, A. 1997. The bulk salinity of Arctic and Antarctic sea ice versus thickness. Proceedings of the International Conference on Offshore Mechanics and Arctic Engineering – OMAE. **4:** 271-281.

Krembs, C.; R. Gradinger and M. Spindler. 2000. Implications of brine channel geometry and surface area for the interaction of sympagic organisms in Arctic sea ice. *J. Exp. Mar. Biol. Ecol.* **243:** 55-80.

Macdonald, R. W.; A. L. Barrie, T. F. Bidleman, M. L. Diamond, D. J. Gregor, R. G. Semkin, W. M. J. Strachan, Y.-F. Li, F. Wania, M. Alaee, L. B. Alexeeva, S. M. Backus, R. Bailey, J. M. Bewers, C. Gobeil, C. J. Halsall, T. Harner, J. T. Hoff, L.

M. M. Jantunen, W. L. Lockhart, D. Mackay, D. C. G. Muir, J. Pudykiewicz, K. J. Reimer, J. N. Smith, G. A. Stern, W. H. Schroeder, R. Wagemann and M. B. Yunker. 2000. Contaminants in the Canadian Arctic: Five years of progress in understanding sources, occurrence and pathways. *Sci. Total Environ.* **254:** 93-236.

Magnusson, K.; R. Ekelund, G. Dave, Å. Granmo, L. Förlin, L. Wennberg, M.-O. Samuelsson, M. Berggren and E. Brorström-Lunden. 1996. Contamination and correlation with toxicity of sediment samples from the Skagerrak and Kattegat. *J. Sea Res.* **35:** 223-234.

Melnikov, S.; J. Carroll, A. Gorshkov, S. Vlasov and S. Dahle. 2003. Snow and ice concentrations of selected persistent pollutants in the Ob-Yenisey River watershed. *Sci. Total Environ.* **306:** 27-37.

Möller, K.; H. Hühnerfuss and D. Wölfle. 1996. Differential Effects on the Enantiomers of α-Hexachlorocyclohexane (α-HCH) on Cytotoxicity and Growth Stimulation in Primary Rat Hepatocytes. *Organohalogen Compd.* **29:** 357-360.

Mukherjee, I. and M. Gopal. 1996. Chromatographic techniques in the analysis of organochlorine pesticide residues. *J. Chromatogr. A.* **754:** 33-42.

Müller, T. A. and H.-P. E. Kohler. 2004. Chirality of pollutants – effects on metabolism and fate. *Appl. Microbiol. Biotechnol.* **64:** 300-316.

Mundy, C. J.; D. G. Barber and C. Michel. 2005. Variability of snow and ice thermal, physical and optical properties pertinent to sea ice algae biomass during spring. *J. Mar. Syst.* **58:** 107-120.

Nakawo, M. and N. K. Sinha. 1984. A Note on Brine Layer Spacing of First-Year Sea Ice. *Atmos. Ocean.* **22:** 193-206.

Perovich, D. K. and A. J. Gow. 1996. A quantitative description of sea ice inclusions. *J. Geophys. Res.* **101:** 18,327-18,343.

Prasad, A. K.; N. Pant, S. C. Srivastava, R. Kumar and S. P. Srivastava. 1995. Effect of dermal application of hexachlorocyclohexane (HCH) on male reproductive system in rat. *Hum. Exp. Toxicol.* **14:** 484-488.

Schlitzer, R. 2002. Ocean Data View, http://www.awi-bremerhaven.de/GEO/ODV.

Sinha, N. K. 1977. Technique for studying structure of sea ice. *J. Glaciol.* **18:** 315-323.

Weeks, W. F. 1994. Possible roles of sea ice in the transport of hazardous material. In: Proc. Workshop on Arctic Contamination. Interagency Arctic Research Policy Committee. Anchorage. Alaska. 1993. *Arctic Res. US.* **8:** 34-52.

Weeks, W. F. and S. F. Ackley. 1986. The growth, structure and properties of sea ice. In: Untersteiner, N. (ed) The geophysics of sea ice. Matrinus Nijhoff, Dordrecht (NATO ASI B146): 9-164.

Weissenberger, J.; G. Dieckmann, R. Gradinger and M. Spindler. 1992. Sea ice: A cast technique to examine and analyze brine pockets and channel structure. *Limnol. Oceanogr*. **37:** 179-183.

Wiberg, K.; R. J. Letcher, C. D. Sandau, R. J. Norstrom, M. Tysklind and T. F. Bidleman. 2000. The Enantioselective Bioaccumulation of Chiral Chlordane and α-HCH Contaminants in the Polar Bear Food Chain. *Environ. Sci. Technol.* **34:** 2668-2674.

World Meteorological Organization. 1970. WMO Sea-Ice Nomenclature. Volume 1: Terminology and Codes. Part I and II. Report 259. Geneva. Switzerland. 14 pages.

Chapter 3

α- and γ-hexachlorocyclohexane (HCH) measurements in the brine fraction of sea ice in the Canadian High Arctic using a sump-hole technique

3.1 Abstract

Holes augered partially into first-year sea ice (sumps) were used to determine α- and γ-HCH concentrations in sea-ice brine. The overwintering of the CCGS *Amundsen* in the Canadian western Arctic, as part of the Circumpolar Flaw Lead (CFL) System Study, provided the circumstances to allow brine to accumulate in sumps sufficiently to test the methodology. As much as 50 % of total HCHs in sea water can become entrapped within the ice crystal matrix. On average, in the winter first-year sea ice HCH brine concentrations reached 4.013 ± 0.307 ng/L and 0.423 ± 0.013 ng/L for the α- and γ-isomer, respectively. In the spring, HCHs decreased gradually with time, with increasing brine volume fraction and decreasing brine salinity. These decreasing concentrations could be accounted for by both the dilution with the ice crystal matrix and under-ice sea water. The former process probably plays a more significant role considering brine volume fractions calculated in this study were below 20 %. Levels of HCHs in the brine exceed under-ice water concentrations by approximately a factor of 3, a circumstance suggesting that the brine ecosystem has been, and continues to be, the most exposed to HCHs.

3.2 Introduction

Hexachlorocyclohexane (HCH) was used as an insecticide between 1950 and 2000 in two main formulations: lindane (pure γ isomer) and technical HCH (α isomer 60-70 %, β isomer 5-12 %, and γ isomer 10-15 %). HCHs are transported to Arctic regions by winds and ocean currents and can be removed from the marine systems by bacterial degradation, outgassing and Arctic Ocean outflow (Jantunen and Bidleman, 1995; Harner *et al.*, 1999; Bidleman *et al.*, 2007; Jantunen *et al.*, 2008). Although levels of HCHs in the Arctic declined rapidly over the last 20 years (Li *et al.*, 2004), they

remain high enough to make HCH a 'contaminant of concern' (Macdonald *et al.*, 2000). HCH high concentrations and isomeric differences in physical and chemical properties (Xiao *et al.*, 2004) provide unique opportunities to develop insight into contaminant pathways in Arctic ecosystems (Li and Macdonald, 2005).

There is a large body of research and modeling available on the accumulation of HCHs in the Arctic Ocean (Jantunen and Bidleman, 1995; Harner *et al.*, 1999; Macdonald *et al.*, 2000; Li *et al.*, 2004; Xiao *et al.*, 2004; Bidleman *et al.*, 2007; Jantunen *et al.*, 2008). In contrast, almost nothing is known about the accumulation of HCHs in sea ice. Sea ice has an intricate and highly variable internal structure consisting of ice crystals and inclusions of brine and air, often referred to as total porosity (Perovich and Gow, 1996). Brine pockets, with mean major axis lengths 100s of microns, are much smaller than air bubbles (millimeters). Brine inclusions are sandwiched between the ice crystals, and their size and degree of connectivity are strongly associated with temperature at the time of ice formation. As ice warms and its brine volume increases, the size distribution shifts toward larger brine pockets. As sea ice passes a critical brine volume fraction of 5 %, a marked transition occurs (Golden *et al.*, 1998). Above 5 %, brine can move through the ice, individual brine pockets may coalesce, and gravity drainage and replenishment of brine with sea water becomes possible. The relatively small air volume typical of first-year sea ice that has not experienced any significant periods of warming, is usually negligible compared to brine volume (Richter-Menge and Jones, 1993). As sea ice warms to about -3 °C in the spring, air volume may account for approximately 20 % of the total porosity (Richter-Menge and Jones, 1993).

In general, salts become entrapped in the brine fraction of sea ice as the ice forms (Weeks and Ackley, 1986), however almost nothing is known about concurrent

partitioning of HCHs. There has been only one study of these contaminants in Arctic sea ice that we are aware of (Pućko *et al.*, 2010). The authors emphasized the importance of brine processes for accumulation/rejection of HCHs during ice formation. They showed that HCH is generally associated with the brine fraction of sea ice; however, they also noted that as much as 40 % of total HCH inventory can remain within the ice crystal matrix, which contains only 7 % of the total salts, until the final stages of melt. However, no direct measurements of HCHs in the brine have ever been published.

Here, the concentrations of α- and γ-HCH measured directly in the brine using an ice sump are reported. Reliability of this sampling technique for HCHs under winter and spring ice conditions is discussed. Based on total ice measurements, the partitioning of HCHs between the brine and ice crystal matrix is also estimated. Finally, the potential for ice crystal melting and sea water replenishment to dilute the HCH in brine during spring is described with respect to the measured decrease of HCH brine concentrations.

3.3 Materials and methods

Samples were collected from the CCGS *Amundsen* as a part of the International Polar Year (IPY) Circumpolar Flaw Lead (CFL) System Study in the Canadian High Arctic (Beaufort Sea) between the 6th and 11th of January (winter, one station) and the 21st of April and 14th of May (spring, 4 stations), 2008 (Figure 3.1). Winter samples consisted of a set of 10 measurements taken every 12 hours for 5 days. Brine samples were measured for α- and γ-HCH and salinity (90 cm depth); bulk ice samples were measured for α- and γ-HCH concentration (0-10 cm and 70-108 cm depth), ice bulk salinity and temperature; sea water beneath the ice was measured for α- and γ-HCH

concentration and salinity and; air was measured for α- and γ-HCH concentration (Figure 3.1). Spring measurements included α- and γ-HCH brine concentration (80 cm and 100 cm depth) and corresponding brine salinity, ice bulk salinity and temperature, and under-ice sea water α- and γ-HCH concentration (Figure 3.1).

Figure 3.1 Sampling locations in the winter (D14) and spring (D41, D43, F2, F3) 2008 (A) and scheme of sampling at winter and spring stations (B)

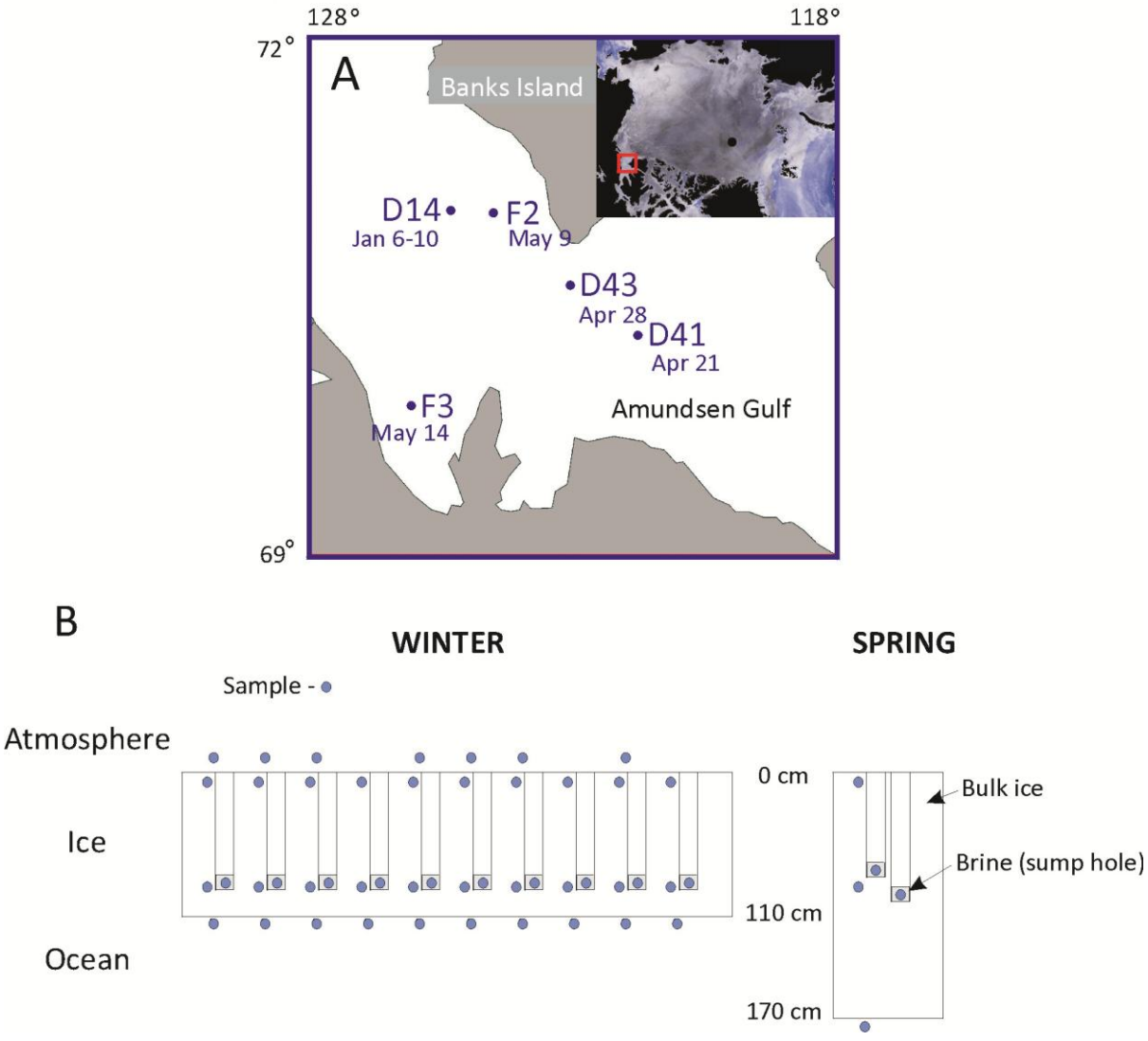

3.3.1 *Field sampling*

Sea ice samples were obtained with a 9 cm i.d., Mark II coring system (Kovacs Enterprises, Lebanon, USA). After collection, ice cores were cut into 4 layers (0-10 cm, 10-40 cm, 40-70 cm and 70-108 cm based on differences in vertical ice texture) using a metal saw, placed in tightly closed containers, and melted. Ice cores were stored at -23 °C in horizontal position before cutting to minimize artifacts related to vertical brine movement. Brine samples were obtained by coring a hole in the ice to a prescribed depth, closing it tightly with a styrofoam cap, and pumping the brine out of it after 2-12 hours using a syringe and 100 cm of Teflon tubing. Sea water was collected from beneath the ice using a Wildco Kemmerer water sampler (Ben Meadows Company, Yulee, USA), through the hole immediately after ice core extraction. Sea ice temperature profiles were measured immediately after extracting the ice core by placing a Traceable digital thermometer (model 4000, Control Company, Friendswood, USA (± 0.05 °C)), in 5 mm diameter holes drilled at 5-10 cm intervals starting from the bottom of the ice core. Air was sampled by drawing about 2500 m^3 (sampling duration of about 7 hours, flow rate of about 7 m^3/min) through a Whatman EPM 2000 glass fiber (GF) filter followed by polyurethane foam (PUF) plugs of 7.5 cm i.d. and 6.5 cm in length (Tish Environmental) using the Gast Regenair Blower (Cole-Parmer, Vernon Hills, USA). The pump was mounted on the bow of the ship at deck level (~ 10 m above the sea level). The blower was calibrated using the Sierra 620 Mass Flow Meter (Sierra Instruments, Monterey, USA).

3.3.2 *Laboratory analysis*

Salinity was calculated from conductivity and temperature using a HACH SENSION5 portable conductivity meter (Hach, Loveland, USA, ± 0.01). Melted sea ice

samples, under-ice sea water samples (4 L) and brine samples (2-4 L) were spiked with d_6-α-HCH surrogate, pumped through 0.7 μm GFF filters (Whatman) to remove particulate matter, and filtered through solid-phase extraction (SPE) cartridges (Oasis) at a flow rate < 20 mL/min. Extraction of HCHs was done by elution of SPE cartridges with acetone. Subsequently, they were transferred into iso-octane. Finally, the solution was cleaned-up with concentrated sulphuric acid (Mukherjee and Gopal, 1996).

In the case of air samples, PUF filters were spiked with recovery standard (PCB 30 congener), extracted using ASE 2000 Accelerated Solvent Extractor (Dionex) with hexane, reduced to 1 mL volume by rotoevaporation and cleaned-up and fractionated on Florisil column chromatography.

Quantitative analysis of α- and γ-HCH was performed using a Varian 3800 Gas Chromatograph-Electron Capture (GC-ECD) equipped with a 60 m, JW DB5 column (0.25 mm i.d., 0.25 μm film thickness). For details see description in (Pućko *et al.*, 2010).

α- and γ-HCH concentrations presented in this study were corrected for percent recovery but not for mean blank. Average recovery was 80 % for brine, 83 % for the sea water, 73 % for ice, and 73 % for air. Limits of detection (LOD), defined as 3 standard deviations of the mean field blank, were 0.019 ng/L and 0.007 ng/L for α- and γ-HCH, respectively. Limits of quantification (LOQ), defined as 10 standard deviations of the mean field blank value, were estimated at 0.047 ng/L and 0.011 ng/L for α- and γ-HCH, respectively.

3.3.3 *Calculations and data analysis*

Brine volume fraction, υ_{BRINE}, was calculated as follows (Frankenstein and Garner, 1967):

$$\upsilon_{BRINE} = S_{ICE} (49.185/ \left| T_{ICE} \right| + 0.532) \cdot 0.1 \quad (-0.5\ °C \geq T_{ICE} \geq -22.9\ °C) \quad \text{(eq. 3.1)}$$

where υ_{BRINE} is brine volume fraction (%) (± 0.06 %), S_{ICE} is ice salinity, and T_{ICE} is ice temperature (°C).

Mixing ratios (V_2/ V_1) of brine and sea water, or brine and melting ice crystal matrix, of salinity S_2 and salinity S_1, required to produce the volume of liquid (V_1+V_2) of salinity S_3, were calculated as follows:

$$V_2/V_1 = (S_1-S_3)/ (S_3-S_2) \quad \text{(eq. 3.2)}$$

Concentrations of HCHs in the brine (C_{BRINE1}) resulting from previously calculated mixing ratios of brine (V_{BRINE0}) and sea water (V_{SW}) or melting ice crystal matrix (V_{IM}) accounting for the observed decrease in salinity between the sampling periods were calculated as follows:

$$C_{BRINE1} = (V_{BRINE0}\, C_{BRINE0} + V_{IM/SW}\, C_{IM/SW})/ (V_{BRINE0} + V_{IM/SW}) \quad \text{(eq. 3.3)}$$

where C_{BRINE0} is the HCH concentration in the brine measured in the previous sampling period, C_{IM} is the HCH concentration in the ice crystal matrix calculated in this paper (0.162 ng/L and 0.017 ng/L for α-HCH and γ-HCH, respectively), and C_{SW} is the HCH concentration in the under-ice sea water measured in the previous sampling period.

Relative brine-water to air concentrations at equilibrium partitioning (fugacity ratio, $f_w/ f_a = 1$) in the sump were calculated for both HCH isomers (Jantunen and Bidleman, 1995):

$$C_w/ C_a = R\ T/ HLC \quad \text{(eq. 3.4)}$$

where C_w and C_a are the concentrations of dissolved and gaseous HCHs in the brine water and air, respectively, R is the gas constant (8.314 Pa m^3/deg mol), T is the air temperature (249 K), and HLC is the Henry's Law Constant at the closest available temperature and salinity (0.104 and 0.0627 Pa m^3/mol for 0.5 °C sea water for α- and γ-HCH, respectively) (Kuklick *et al.*, 1991).

Coefficient of variation (CV) was used as a measure of HCH variability in the brine (Sokal and Rohlf, 1980):

$$CV\ (\%) = 100\ SD/\ Mean \qquad \text{(eq. 3.5)}$$

where SD is the standard deviation.

Statistical analyses include Pearson's correlation matrix with Bonferroni probability test, and two-sample t-Test (SYSTAT 11, Systat Software Inc.). Prior to statistical analyses, α- and γ-HCH concentrations, ice bulk salinity, ice temperature, brine salinity and brine volume fraction were log-transformed to meet the normal distribution criterion.

3.4 Results and discussion

3.4.1 *Reliability of the sumps for HCH sampling*

Sumps have not previously been used to measure HCH concentrations directly in sea-ice brine. The sump technique allows for the collection of sufficient volumes of brine such that LOQs for HCH are exceeded. However, the method might be vulnerable to seepage of brine from upper layers of ice or from the underlying sea water, to melting of the ice crystal matrix in direct contact with the brine in the sump hole, and to air-brine gas exchange (Figure 3.2).

Figure 3.2 Schematic diagram of potent methodological issues associated with a sump-hole technique in the case of HCH measurements

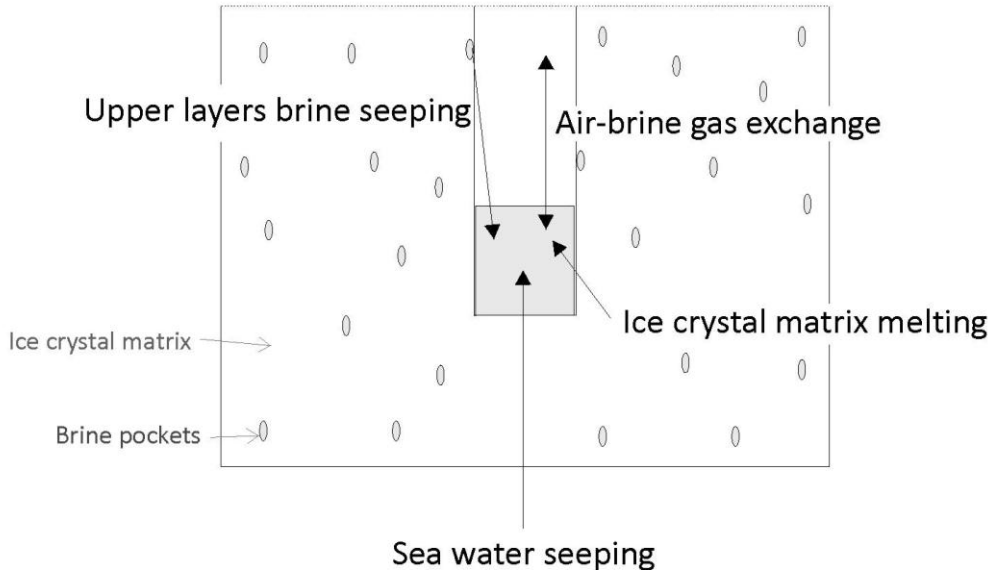

In the winter, the mean brine volume fraction for the bulk sea ice layer corresponding to the depth of sump holes was 4.3 %. Thus, based on conservative partitioning of salts between brine and the ice crystal matrix, salinity measured in the sump holes should be roughly 23 times more concentrated than that of the corresponding bulk ice samples (Weeks and Ackley, 1986). Our samples exhibited a ratio of 29, implying that the brine from a 90 cm deep hole contained a portion of more concentrated brine from the upper core layers. Considering the most extreme mixing scenario, brine from the top 10 cm of ice with salinity of 293.6 (based on a mean ice bulk salinity and brine volume fraction of 8.5 and 3.0, respectively), and the requirement to increase the brine salinity from 101.6 (23-fold increase) to 128.1 (29-fold increase), equation 3.2 implies that 0.16 parts of brine from top 10 cm would have to mix with one part of brine from the 90 cm sump hole. For HCHs, this would result in a maximum increase of 13 % and 8 % for the α- and γ-isomers, respectively. Seeping of underlying sea water, with average salinity of 28.8 (Table 3.1), or the melting of the ice

crystal matrix into the sump hole, would result in a significant decline in brine salinity and therefore need not be considered further. Using equation 3.4, and an average air temperature of -24 °C during the sampling period, the sump-hole ratios of HCH concentrations in the brine-water to air are estimated to be approximately $20 \cdot 10^3$ and $33 \cdot 10^3$ for the α- and γ-isomers at equilibrium, respectively. Assuming a rough air/brine volume ratio in the sump hole of 11.5, brine-air gas exchange could not decrease brine HCH concentrations by more than 0.1 %.

In the spring, average brine salinity was 16 times greater than in the corresponding bulk ice sample compared to the expected ratio of 10 based on an average brine volume fraction of 9.7 % (Table 3.1). In this case, we calculated that 0.35 parts of brine from the top 10 cm, with salinity of 168.1, would need to have mixed with one part of brine from the 90 cm sump hole to increase the final salinity from 50.9 (expected) to 81.5 (measured). As in the winter season, this would not be expected to have any significant impact on HCH brine concentrations.

These calculations suggest, therefore, that the sump technique provides a reliable method to measure HCH concentrations in the brine under both winter and spring ice conditions.

Table 3.1 Values, means, standard errors (SEs), and coefficients of variability (CVs) for α- and γ-HCH concentration and corresponding physical variables in the brine, bulk ice, under-ice sea water, and air in the winter 2007/2008 and spring 2008

WINTER 2007/2008													
Date (Station) → Variable ↓	6Jan (D14)	6Jan (D14)	7Jan (D14)	7Jan (D14)	8Jan (D14)	8Jan (D14)	9Jan (D14)	9Jan (D14)	10Jan (D14)	10Jan (D14)	Mean	SE	CV (%)
α-$HCH_{BRINE\ 90cm}$ (ng/L)	4.715	5.322	3.343	5.165	4.637	4.473	2.433	3.169	3.303	3.572	4.013	0.307	24
γ-$HCH_{BRINE\ 90cm}$ (ng/L)	0.398	0.469	0.421	0.456	0.381	0.491	0.427	0.391	0.435	0.364	0.423	0.013	10
$S_{BRINE\ 90cm}$	132.5	124.0	122.0	126.5	131.0	118.0	154.0	125.0	117.5	130.0	128.1	3.3	8
α-$HCH_{ICE\ 90cm}$ (ng/L)	0.275	0.325	0.413	0.285	0.420	n/a	0.254	0.220	0.287	0.267	0.305	0.023	23
γ-$HCH_{ICE\ 90cm}$ (ng/L)	0.032	0.033	0.034	0.034	0.030	0.038	0.029	0.029	0.045	0.032	0.034	0.002	14
$S_{ICE\ 90cm}$	4.2	4.2	4.6	4.1	5.6	4.2	4.2	4.1	4.2	4.2	4.4	0.1	11
$T_{ICE\ 90cm}$ (°C)	-4.4	-5.8	-6.1	-6.4	-5.2	-4.9	-5.5	-5.0	-5.3	-4.8	-5.3	0.2	12
$\upsilon_{BRINE\ 90cm}$ (%)	4.9	3.8	3.9	3.3	5.6	4.4	3.9	4.3	4.1	4.5	4.3	0.2	15
α-$HCH_{ICE\ 5cm}$ (ng/L)	0.288	0.299	0.416	0.377	0.284	0.334	0.314	0.298	n/a	0.253	0.318	0.017	16
γ-$HCH_{ICE\ 5cm}$ (ng/L)	0.037	0.040	0.057	0.043	0.038	0.047	0.039	0.047	0.046	0.046	0.044	0.002	14
$S_{ICE\ 5cm}$	9.5	8.7	9.0	8.3	8.7	8.6	7.6	8.1	8.5	8.1	8.5	0.2	6
$T_{ICE\ 5cm}$ (°C)	-11.2	-18.0	-17.7	-17.3	-17.3	-18.9	n/a	-19.1	-18.0	-18.7	-17.4	0.8	14
$\upsilon_{BRINE\ 5cm}$ (%)	4.7	2.8	3.0	2.8	2.9	2.7	n/a	2.5	2.8	2.6	3.0	0.2	22
α-HCH_{WATER} (ng/L)	1.144	1.084	1.091	1.033	1.092	0.917	1.047	0.950	0.927	0.955	1.024	0.026	8
γ-HCH_{WATER} (ng/L)	0.101	0.106	0.112	0.096	0.089	0.104	0.115	0.099	0.117	0.113	0.105	0.003	9
S_{WATER}	31.7	29.1	20.9	29.0	27.5	29.0	30.0	31.5	30.8	28.7	28.8	1.0	11
α-HCH_{AIR} (pg/m^3)	10.726	10.855	9.875	n/a	6.775	6.755	5.657	n/a	9.128	n/a	8.539	0.800	25
γ-HCH_{AIR} (pg/m^3)	9.362	6.851	9.759	n/a	6.760	3.194	n/a	n/a	7.459	n/a	7.231	0.960	33

SPRING 2008											
Date (Station) → Variable ↓	21Apr ($D41_{80cm}$)	21Apr ($D41_{100cm}$)	28Apr ($D43_{80cm}$)	28Apr ($D43_{100cm}$)	9May ($F2_{80cm}$)	9May ($F2_{100cm}$)	14May ($F3_{80cm}$)	14May ($F3_{100cm}$)	Mean	SE	CV (%)
α-HCH_{BRINE} (ng/L)	3.190	3.624	2.809	3.027	2.095	2.012	1.848	1.827	2.554	0.245	27
γ-HCH_{BRINE} (ng/L)	0.478	0.570	0.411	0.349	0.271	0.257	0.223	0.215	0.347	0.046	37
S_{BRINE}	105.0	92.5	93.5	93.0	73.5	71.5	60.0	63.0	81.5	5.8	20

S_{ICE}	5.3	3.7	4.7	4.7	5.9	5.6	5.1	5.9	5.1	0.3	15
T_{ICE} (°C)	-5.4	-3.7	-4.5	-3.1	-3.0	-1.9	-2.2	-1.7	-3.2	0.5	41
υ_{BRINE} (%)	5.0	5.1	5.3	7.7	10.1	14.7	11.8	17.6	9.7	1.7	49
α-HCH_{WATER} (ng/L)	0.885		0.912		0.877		0.883		0.889	0.008	2
γ-HCH_{WATER} (ng/L)	0.122		0.126		0.107		0.104		0.115	0.005	10

n/a-not available; S-salinity; T-temperature; υ_{BRINE}-brine volume fraction

3.4.2 *Distribution of HCHs between the brine fraction and ice crystal matrix*

HCH levels in the brine in the winter were approximately 13 times higher than in bulk ice (Table 3.1), reaching 4.013 ± 0.307 (SE) ng/L for α-HCH, and 0.423 ± 0.013 (SE) ng/L for γ-HCH. Assuming conservative partitioning of HCHs between the ice crystal structure and brine, and 1 to 0.16 volume mixing of brine from 90 cm and the top 10 cm of ice, HCH brine concentrations should equal 7.660 ng/L and 0.882 ng/L for the α- and γ-isomers, respectively. Accordingly, up to 48 % of α-HCH and 52 % of γ-HCH must be entrapped within the ice crystal matrix. If we neglect the air volume (Richter-Menge and Jones, 1993), attribute 95.7 % of the total ice volume to the ice crystal matrix, and apply a 10 % correction for ice matrix versus brine density (Timcorint and Frederking, 1996), the associated α-HCH and γ-HCH concentrations are calculated to be 0.162 ng/L and 0.017 ng/L, respectively. This result compares very well with those of an independent brine drainage experiment (Pućko *et al.*, 2010), where the authors simulated the spring ice melt conditions by gradual warming of the ice cores, and determined HCH levels and salinity in the progressing melt-water fractions. In this experiment, roughly 40 % of the total HCH inventory was associated with the last three melt-water fractions containing only 7 % of the total salts. The α- and γ-HCH concentrations measured in each of these melt water-fractions averaged 0.151 ng/L and 0.015 ng/L, respectively.

3.4.3 *Gradual decrease of HCH brine concentrations in the spring*

In winter, HCH brine concentrations were not significantly correlated with ice and brine physical characteristics including brine and bulk ice salinity, ice temperature, and brine volume fraction (Pearson's correlations, data log-transformed prior to analysis, $p > 0.05$). The mean coefficients of variability (CVs) were estimated at 24 %

for α-HCH, and 10 % for γ-HCH (Table 3.1), which was most probably associated with the small-scale randomness of distribution in the environment. However, in spring ice, which becomes permeable to liquid transport, as its mean brine volume fraction approached 9.7 % ± 4.7 % (SD), both α- and γ-HCH concentrations gradually decreased as a function of increasing brine volume fraction and decreasing brine salinity (Figure 3.3). Both of these ice physical parameters could independently explain over 80 % of HCH variability in the brine in the spring ($R^2 > 0.80$, $p < 0.05$). Spring sea-ice processes that could potentially be responsible for gradual dilution of brine HCH include melting of the ice crystal matrix and replenishment of brine with sea water.

Figure 3.3 Pearson's correlations between HCH concentrations and brine volume fraction, and brine salinity in the spring; results log-transformed prior to analysis

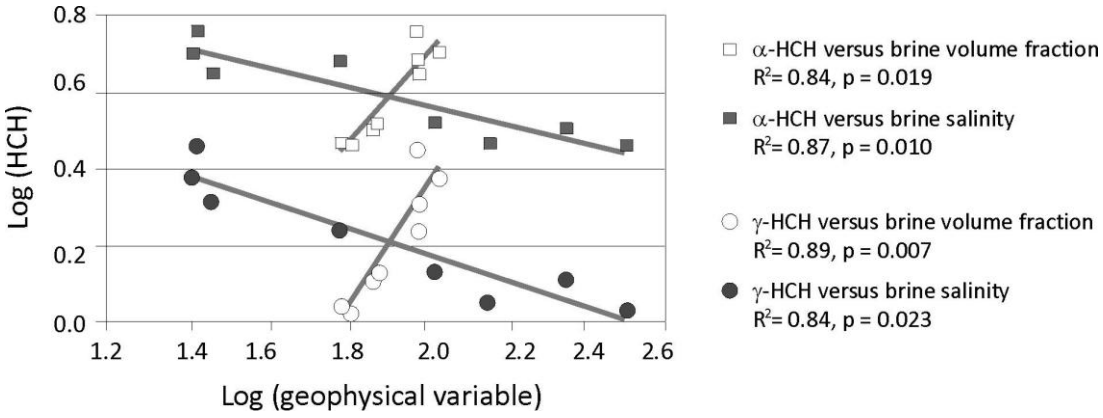

To quantify how much each of these processes could contribute to the dilution of HCH, we calculated the volumes in which the brine would have to mix with sea water or the ice matrix to re-produce the salinity observations using equation 3.2. The calculations were made for the period transitions between each of the 4 sampling stations characterized by a progressive increase in brine volume fraction, and decrease in brine salinity (Table 3.2; 1-2, 2-3, 3-4). For example, the observed decrease in brine

salinity of 32 between periods 1 and 2 could be accounted for by mixing 1 part of brine with 0.48 parts of sea water or with 0.33 parts of the melting ice crystal matrix. The resulting calculated concentrations of α-HCH and γ-HCH in the brine (equation 3.3) are presented in Table 3.2 and range between 3-19 % and 2-31 % of their measured values, respectively. Thus, both dilution with the ice crystal matrix and replenishment of brine with sea water could account for the gradual decrease of HCH concentrations as the season progressed (Figure 3.4). Although the relative importance of these two diluting mechanisms cannot be established with the present data, it is most likely that ice crystal matrix melting is primarily responsible for the decrease in the HCH brine concentrations until brine pockets grow large enough to coalesce. Once coalescence has occurred, the elongated brine channels from the bottom of the ice to the depth of brine sampling would provide a plausible means to permit brine replenishment with sea water. However, replenishment by sea water has been shown to occur only when brine volume fractions exceed 20 % (Perovich and Gow, 1996), a threshold not reached in the current study.

3.4.4 *γ-HCH levels in the brine at the beginning of the spring*

In the early spring (stations D41 and D43, 21-28 Apr, 2008) the levels of γ-HCH in the brine did not decrease compared to the winter sampling period as might have been predicted from brine salinity (Figure 3.4B). Average γ-HCH brine concentration in the early spring, 0.452 ± 0.047 ng/L (SE), was not significantly different from the winter value of 0.423 ± 0.013 ng/L (t-Test, p = 0.60). A similar phenomenon was observed to occur for γ-HCH concentrations in ice samples collected from the same sampling locations (Pućko *et al.*, 2010). The authors reported that relative to the α-HCH concentrations, the γ-HCH levels in the bulk sea ice samples were harder to predict

based on the long-term dependence on sea ice salinity (R^2 = 0.70, $p < 0.01$, and R^2 = 0.40, $p < 0.01$, respectively). This discrepancy was ascribed to differences in atmosphere-snow processes in the spring and/or spatial variability. Correcting for this discrepancy (as estimated based on the differences in HCH concentrations in the ice samples between the α- and γ-isomers, 36 %), the γ-HCH brine concentration for the early spring period was calculated to be 0.377 ng/L, which is much closer to the value calculated assuming dilution with the melting ice crystal matrix (Figure 3.4B).

Figure 3.4. Measured versus calculated brine α-HCH (A) and γ-HCH (B) concentrations as a function of decreasing brine salinity and progressing sampling season; *1 – 6-10 Jan, 2008, 2 – 21-28 Apr, 2008, 3 – 9 May, 2008, 4 – 14 May, 2008

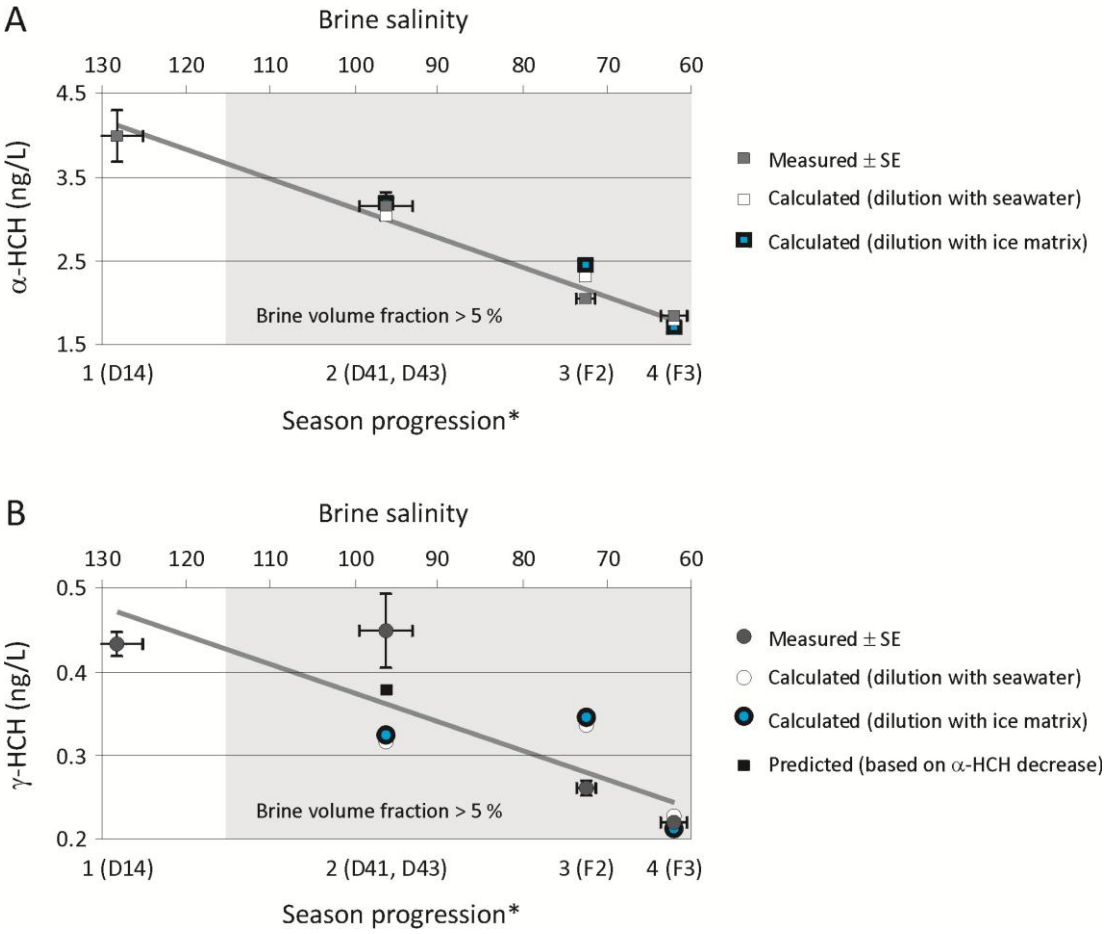

Table 3.2 Brine/sea water and brine/ice matrix mixing ratios that would account for the decrease in the brine salinity, and measured brine HCH concentrations versus calculated ones based on the brine dilution with sea water or ice crystal matrix as the sampling season progressed*

Season progression* → Variable ↓	1 (D14)	2 (D41-D43)	3 (F2)	4 (F3)
Number of samples	10	4	2	2
Average brine volume fraction (%)	4.3	5.8	12.4	14.7
Average brine salinity	128.1	96.0	72.5	61.5
Brine/sea water mixing ratio		1/0.48	1/0.57	1/0.34
Brine/ice matrix mixing ratio		1/0.33	1/0.32	1/0.18
Measured α-HCH concentration (ng/L)	4.013	3.163	2.054	1.838
Calculated α-HCH concentration (brine dilution with sea water) (ng/L)		3.044	2.341	1.753
Calculated α-HCH concentration (brine dilution with ice matrix) (ng/L)		3.057	2.435	1.765
Measured γ-HCH concentration (ng/L)	0.423	0.452	0.264	0.219
Calculated γ-HCH concentration (brine dilution with sea water) (ng/L)		0.320	0.333	0.224
Calculated γ-HCH concentration (brine dilution with ice matrix) (ng/L)		0.322	0.346	0.226

*1 (D14)- Jan 6-10, 2008; 2 (D41 and D43), Apr 21-28, 2008; 3 (F2), May 9, 2008; 4 (F3), May 14, 2008

3.4.5 *Implications for biological exposures*

Brine contained within sea ice currently exhibits the highest HCH concentrations in any abiotic Arctic environment, exceeding under-ice water concentrations by a factor of approximately 3 in the spring (Table 3.1). Sea-ice brine pockets comprise an extreme-environment habitat, the function of which in polar marine environments remains unclear (Deming, 2004). The present high levels in brine, which imply former concentrations during the period of peak loading (1980-1990) of perhaps 10 times greater (Macdonald *et al.*, 2000; Li *et al.*, 2004), therefore pose a risk to the sea ice biota inhabiting the bottom of the ice in spring, or living within brine channels throughout winter (Horner *et al.*, 1992). In the central Arctic, ice algae are thought to contribute up to 57 % of the primary production (water column + sea ice) (Gosselin *et al.*, 1997), again emphasizing the potential importance of the brine-concentration process in amplifying lower food web exposure, which then translates into higher biological exposures all the way up through the Arctic marine food web.

We expect that observed and projected change in Arctic sea-ice climate will make the brine concentration pathway more widespread in the future Arctic Ocean. Recent observations show that multiyear ice area in the Arctic Ocean is dwindling, with seasonal ice expanding to fill the space. This shift will also affect the structure of the Arctic marine food web (Gradinger, 1995). Open water regions of enhanced primary productivity (polynyas and marginal ice zones, MIZ) will occur in areas that until now have been characterized by a perennial ice cover and an extremely low biological productivity. This shift will most likely decrease the annual percentage contribution to the food web by sea-ice primary producers in favor of pelagic producers. Taken together, we could see a more widespread late winter-early spring exposure to brine

contaminant amplification followed by a late-spring pelagic dilution within the food web.

3.5 Acknowledgements

We would like to thank the crew of CCGS *Amundsen* for the field work assistance without which this study could never be accomplished. Also, we express our gratitude to CFL participants - Debbie Armstrong, Amanda Chaulk, Elizabeth Shadwick and Laura Simms - for sharing their time and knowledge in the field. Our special thanks goes to Jason Pavlich and Wojciech Walkusz for the unbelievable amount of hard physical field work they put in ice sampling for this study, without which the samples collection for this experiment would never be possible. We also thank Bruno Rosenberg for help and advice regarding laboratory analysis. Finally, we thank the Canadian program office of the International Polar Year, the Natural Sciences and Engineering Research Council (NSERC), Canada Foundation for Innovation (CFI), Canada Research Chairs (CRC), the Department of Fisheries and Oceans Canada, and ArcticNet for funding.

3.6 References

Bidleman, T. F.; H. Kylin; L. M. Jantunen; P. A. Helm, and R. W. Macdonald. 2007. Hexachlorocyclohexanes in the Canadian Archipelago. 1. Spatial Distribution and Pathways of α- β- and γ-HCHs in Surface Water. *Environ. Sci. Technol.* **41:** 2688-2695.

Deming, J. 2004. Psychrophiles and polar regions. *Curr. Opin. Microbiol.* **5:** 310-309.

Frankenstein, G. E. and R. Garner. 1967. Equations for Determining the Brine Volume of Sea Ice from -0.5 to -22.9 C. *J. Glaciol.* **6:** 943-944.

Golden, K. M.; S. F. Ackley, and V. I. Lytle. 1998. The Percolation Phase Transition in Sea Ice. *Science.* **282:** 2238-2241.

Gosselin, M.; M. Levasseur; P. A. Wheeler; R. A. Horner, and B. C. Booth. 1997. New measurements of phytoplankton and ice algal production in the Arctic Ocean. *Deep-Sea Res. II.* **44:** 1623-1644.

Gradinger, R. 1995. Climate change and biological oceanography of the Arctic Ocean. *Philos. Trans. R. Soc. London, Ser. A.* **352:** 277-286.

Harner, T.; H. Kylin; T. F. Bidleman, and W. M. J. Strachan. 1999. Removal of α- and γ-Hexachlorocyclohexane and Enantiomers of α-Hexachlorocyclohexane in the Eastern Arctic Ocean. *Environ. Sci. Technol***. 33:** 1157-1164.

Horner, R.; S. F. Ackley; G. S. Dieckmann; B. Gulliksen; T. Hoshiai; L. Legendre; I. A. Melnikov; W. S. Reeburgh; M. Spindler, and C. W. Sullivan. 1992. Ecology of sea ice biota. 1. Habitat, terminology, and methodology. *Pol. Biol.* **12:** 417-427.

Jantunen, L. M. and T. F. Bidleman. 1995. Reversal of the Air-Water Gas Exchange Direction of Hexachlorocyclohexanes in the Bering and Chukchi Seas: 1993 versus 1988. *Environ. Sci. Technol.* **29:** 1081-1088.

Jantunen, L. M.; P. A. Helm; H. Kylin, and T. F. Bidleman. 2008. Hexachlorocyclohexanes (HCHs) In the Canadian Archipelago. 2. Air-Water Gas Exchange of α- and γ-HCH. *Environ. Sci. Technol.* **42:** 465-470.

Kucklick, J. R.; D. A. Hinckley, and T. F. Bidleman. 1991. Determination of Henry's law constants for hexachlorocyclohexanes in distilled water and artificial seawater as a function of temperature. *Mar. Chem.* **34:** 197-209.

Li, Y. F. and R. W. Macdonald. 2005. Sources and pathways of selected organochlorine pesticides to the Arctic and the effect of pathway divergence on HCH trends in biota: a review. *Sci. Total Environ.* **342:** 87-106.

Li, Y.-F.; R. W. Macdonald; J. M. Ma; H. Hung, and S. Venkatesh. 2004. Historical alpha-HCH budget in the Arctic Ocean: the Arctic Mass Balance Box Model (AMBBM). *Sci. Total. Environ.* **324:** 115-139.

Macdonald, R. W.; A. L. Barrie; T. F. Bidleman; M. L. Diamond; D. J. Gregor; R. G. Semkin; W. M. J. Strachan; Y.-F. Li; F. Wania; M. Alaee; L. B. Alexeeva; S. M. Backus; R. Bailey; J. M. Bewers; C. Gobeil; C. J. Halsall; T. Harner; J. T. Hoff; L. M. M. Jantunen; W. L. Lockhart; D. Mackay; D. C. G. Muir; J. Pudykiewicz; K. J. Reimer; J. N. Smith; G. A. Stern; W. H. Schroeder; R. Wagemann, and M. B. Yunker. 2000. Contaminants in the Canadian Arctic: Five years of progress in understanding sources, occurrence and pathways. *Sci. Total Environ.* **254:** 93-236.

Mukherjee, I. and M. Gopal. 1996. Chromatographic techniques in the analysis of organochlorine pesticide residues. *J. Chromatogr. A.* **754:** 33-42.

Perovich, D. K. and A. J. Gow. 1996. A quantitative description of sea ice inclusions. *J. Geophys. Res.* **101 (C8):** 18,327-18,343.

Pućko, M.; G. A. Stern; D. G. Barber; R. W. Macdonald, and B. Rosenberg. 2010. The International Polar Year (IPY) Circumpolar Flaw Lead (CFL) System Study: the importance of brine processes for α- and γ-hexachlorocyclohexane (HCH) accumulation or rejection in sea ice. *Atmos.-Ocean.* **48:** 244-262.

Richter-Menge, J. A. and K. F. Jones. 1993. The tensile strength of first-year sea ice. *J. Glaciol.* **39:** 609-618.

Sokal, R. R. and F. J. Rohlf. 1980. *Biometry;* 2nd, ed.; W.H. Freeman and Company: New York, pp 860.

Timco, G. W. and R. M. W. Frederking. 1996. A review of sea ice density. *Cold Reg. Sci. Technol.* **24:** 1-6.

Weeks, W. F. and S. F. Ackley.1986. The growth, structure and properties of sea ice. In *The geophysics of sea ice*; Untersteiner, N., Ed.; Matrinus Nijhoff: Dordrecht (NATO ASI B146); pp 164.

Xiao, H.; N. Li, and F. Wania. 2004. Compilation, Evaluation, and Selection of Physical-Chemical Property Data for α-, β-, and γ-Hexachlorocyclohexane. *J. Chem. Eng. Data.* **49:** 173-185.

Chapter 4

The influence of the atmosphere-snow-ice-ocean interactions on the levels of hexachlorocyclohexanes (HCHs) in the Arctic cryosphere

4.1 Abstract

α- and γ-HCHs are being scavenged from the atmosphere by falling snow, with the average total scavenging ratios (W_T) of $3.8 \cdot 10^4$ and $9.6 \cdot 10^3$, respectively. After deposition, HCH snow concentrations can decrease by 40 % due to snow pack ventilation and increase by 50 % due to upward migration of brine from the ice. HCH vertical distribution in sufficiently cold winter sea ice, which maintains brine volume fractions < 5 %, reflects the ice growth history. Initially, the entrapment of brine (and HCHs) in ice depends on the rates of ice growth and desalination. However, after approximately the first week of ice formation, ice growth rate becomes dominant. Deviations of HCH concentrations from the values predicted by the ice bulk salinity (rate of brine entrapment) can be explained by spatial variability of HCHs in surface water. HCH burden in the majority of the ice column remains locked throughout most of the season until the early spring when snow melt water percolates into the ice, delivering HCHs to the upper ocean via desalination by flushing. Percolation can lead to an increase in α- and γ-HCH in the sea ice by up to 2 %-18 % and 4 %-32 %, respectively.

4.2 Introduction

Hexachlorocyclohexane (HCH) is an organochlorine insecticide used between 1970 and 2000 in two main isomeric formulations: lindane (pure γ isomer) and technical HCH (α isomer 60-70 %, β isomer 5-12 %, and γ isomer 10-15 %) (Macdonald *et al.*, 2000). Although HCHs in the Arctic have declined rapidly over the last 20 years after banning their use (Li *et al.*, 2004), their concentrations remain high enough to make HCH a 'contaminant of concern' (Macdonald *et al.*, 2000). The standing stock of HCHs in the upper 200 m of the Arctic Ocean was estimated at 2910

tonnes in 2000 (Macdonald *et al.*, 2000). The major routes of entry to the Arctic Ocean include ocean currents, atmospheric deposition, and rivers. HCH removal occurs by water outflow, degradation, volatilization, and ice export. α-HCH consists of two stereoisomers (enantiomers), termed (+) and (-), which are released to the environment from original sources as a racemic mixture (1:1). Once in the environment, the enantiomers behave differently when taken up by organisms or degraded by microbes, as enzymes exhibit stereo selectivity (Müller and Kohler, 2004). Differences in enantiomer fraction (EF), where;

$$EF = (+)\alpha\text{-HCH}/[(+)\alpha\text{-HCH}+(-)\alpha\text{-HCH}] \qquad \text{(eq. 4.1)}$$

therefore, indicate biological processes (Kallenborn and Hühnerfuss, 2001), and regional variability in these process provide opportunities to use enantiomeric composition as a tracer of air-water exchange (Ridal *et al.*, 1997).

Sea ice has a complex internal structure consisting of ice crystals and inclusions of liquid brine and air (Perovich and Gow, 1996). As the sea ice forms, only a portion of the salt in sea water is entrapped in the liquid brine fraction, and the rest is expelled at the ice-ocean interface. The efficiency of salt rejection depends primarily on the ice growth rate (Nakawo and Sinha, 1981); however, desalination by gravity drainage plays a significant role during the initial week of the ice sheet formation (Notz and Worster, 2009). When the ice reaches a thickness of a few centimeters and cools, some of the trapped brine freezes decreasing its volume and causing a high-salinity 1-5 mm skim surface layer to be created (Perovich and Richter-Menge, 1994; Martin *et al.*, 1995). Once the ice temperature cools enough for the brine volume fraction to drop below 5 %, the ice becomes impermeable to liquid transport (Golden *et al.*, 1998). Thus, ice desalination will not occur in the majority of the ice column throughout the winter season. In spring, when the ice warms and the brine volume fraction increases above 5

%, the percolation of the snow melt water into the ice can then take place leading to a flushing of brine from the ice (Golden *et al.*, 1998; Notz and Worster, 2009). Early season brine drainage also occurs when the basal snow layer, which contains brine, preferentially drains due to elevated spring temperatures (Barber *et al.*, 1995).

To date there have been only two detailed studies of HCHs in Arctic sea ice (Pućko *et al.*, 2010a, 2010b). In these studies, brine processes were shown to be crucial in the accumulation/rejection of HCHs in Arctic sea ice, and as much as 50 % of the total HCH burden in the sea ice can be entrapped within the ice crystal matrix itself. Although there are several studies of HCH dynamics in snow packs after snowfall (Wania, 1997; Halsall, 2004; Herbert *et al.*, 2006), and the release of HCH from melting snow (Meyer and Wania, 2008; Meyer *et al.*, 2009a, 2009b), none of these studies consider the ice beneath the snow. Here, we examine the interaction between snow and sea ice in the Arctic Ocean, in particular focusing on how the exchange of salt and HCH are affected during early growth (brine rejection) and mid-season temperature minimums (isolation of brine channels).

4.3 Materials and methods

This study is a component of the 2007/2008 Circumpolar Flaw Lead (CFL) System Study, a multidisciplinary International Polar Year (IPY) project conducted in the Canadian High Arctic from the CCGS *Amundsen*. Ice and surface water samples were collected from the beginning of the 2007 freeze-up until the ice reached a thickness of about 100 cm (January 2008) at varied locations in the Beaufort Sea (Figure 4.1A). Sampling ended with a local-scale sampling experiment performed between the 6th and 11th of January, 2008 (polar night). At the time of the experiment the ship was anchored at a typical drift ice station - D14 (Figure 4.1A). Also, air

samples were collected in the study region between 27th of December, 2007 and 23rd of January, 2008.

Figure 4.1 Location of the local-scale winter experiment and distributed ice sampling between 26th of October, 2007 and 11th of January, 2008 (A), and the scheme of the local-scale winter sampling experiment (B)

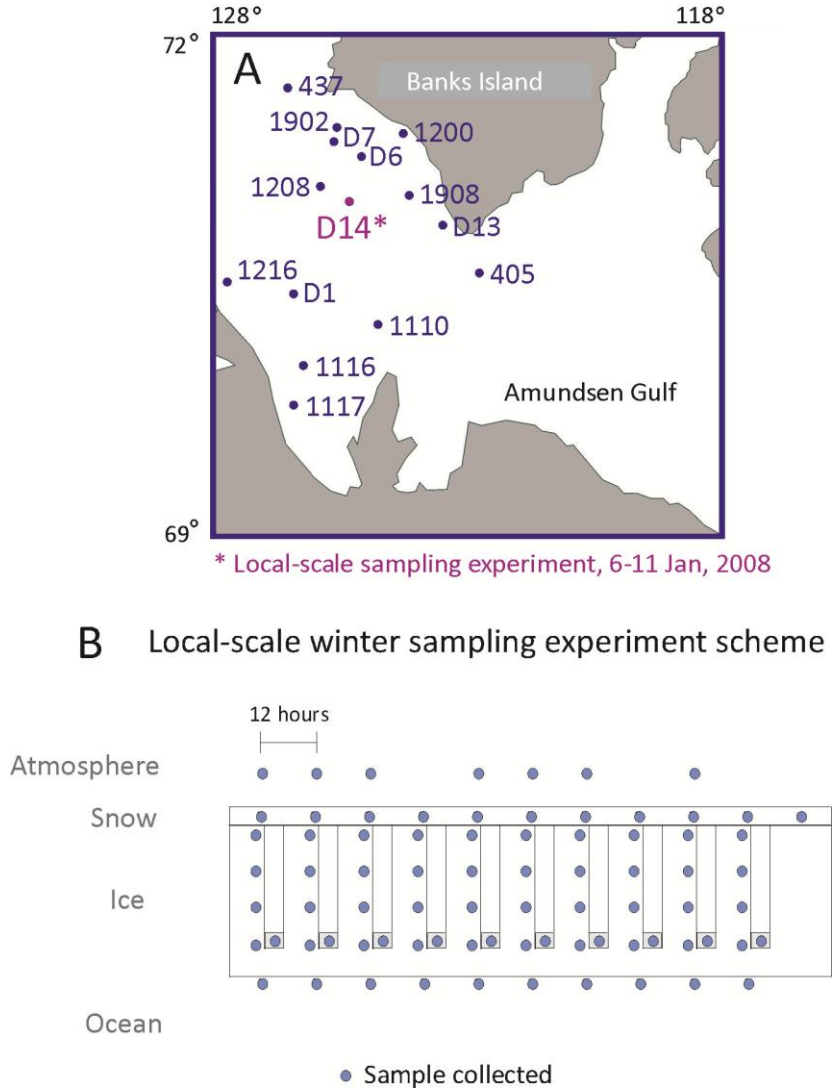

4.3.1 *Winter local-scale sampling experiment*

Snow, four layers of ice, brine, under-ice sea water, and air samples were collected every 12 hours, at 8 am and 8 pm, over the period of 5 days from the same

location (within 10 meters) (Figure 4.1B). The first set of samples was taken about 12 hours after the first major snow event in the area (2 cm). Snow fell two more times over the course of sampling, on days 2-3 (1.5 cm) and 5 (0.5 cm). Atmospheric conditions were calm for the first 4 days and there was heavy blowing snow on the last two days of the experiment, with winds exceeding 10 m/s.

4.3.2. *Field sampling*

All snow samples were collected with a 2500 cm^2 stainless steel pan. To ensure not to include any ice in the snow sample, about 0.5 cm of snow was left on the ice surface which was then brushed off using a semi-hard metal brush, making sure to include only the snow hoar layer (bottom layer of the snow pack, relatively hard and saline). After collection, the snow samples (4 L) were melted in tightly sealed plastic containers at room temperature. Sea ice samples were obtained with a 9 cm (i.d.) ice corer (Mark II coring system, Kovacs Enterprises, Lebanon, USA). After extraction, ice cores were cut into 4 layers (0-10 cm, 10-40 cm, 40-70 cm and 70-108 cm), placed in tightly closed containers, and melted at room temperature. Brine samples were obtained by drilling a sump hole in the ice to the depth of about 80-90 cm with the ice corer, closing it tightly with a styrofoam cap, and pumping the brine out of it after about 12 hours (Pućko *et al.*, 2010b). Sea water was collected from beneath the ice by deploying a Wildco Kemmerer water sampler (Ben Meadows Company, Yulee, USA) through the hole immediately after ice core extraction. Sea ice temperature profiles were measured immediately after extracting the ice core by placing a Traceable digital thermometer (model 4000, Control Company, Friendswood, USA (± 0.05 °C)), in 5 mm diameter holes drilled at 5-10 cm intervals starting from the bottom of the ice core. Air samples were collected by pulling about 2500 m^3 of air through a Whatman EPM 2000 glass

fiber (GF) filter followed by polyurethane foam (PUF) plugs of 7.5 cm i.d. and 6.5 cm in length (Tish Environmental) using a Gast Regenair Blower (Cole-Parmer, Vernon Hills, USA). The flow rate used was 7 m^3/min with an average sampling time of 7 hours. The blower was calibrated using the Sierra 620 Mass Flow Meter (Sierra Instruments, Monterey, USA).

4.3.3 *Laboratory analysis*

Salinity of sea ice, snow, and brine samples was calculated from conductivity and temperature using a HACH SENSION5 portable conductivity meter (Hach, Loveland, USA (± 0.01)). Melted sea ice and snow samples (4 L), under-ice sea water samples (4 L) and brine samples (2-4 L) were spiked with d_6-α-HCH surrogate. Subsequently, spiked samples were pumped through a 0.7 μm GFF filter (Whatman, 42.5 mm i.d.) which was contained in a 47 mm in-line pre-assembled single stage filter holder (Savillex, Minnetonka, USA), followed by Oasis solid-phase extraction (SPE) cartridges with HLB 20cc, 1g (Waters, Mississauga, Canada). A Masterflex peristaltic pump (Cole-Parmer, Vernon Hills, USA) was used for filtration at a flow rate < 20 mL/min. Cartridges were tested for recoveries using d_6-α-HCH surrogate (> 97 %), activated with 20 mL of methanol prior filtration, and stored at -20 °C after filtration. The main steps of the subsequent laboratory procedure included elution of SPE cartridges with ~40 mL of acetone, transfer into iso-octane by adding 1 mL of this solvent to the acetone extract previously rotoevaporated to 3 mL, vortexing and transferring the more non-polar phase (top phase) into the new test tube, rinsing the acetone phase with n-hexane three times, reducing the volume of the solvents mixture to 1 mL under nitrogen flow, and cleaning-up the solution with 0.5 mL of concentrated sulphuric acid (Mukherjee and Gopal, 1996). In the case of air samples, PUF filters

were spiked with recovery standard (PCB 30 congener), extracted using ASE 300 Accelerated Solvent Extractor (Dionex, Sunnyvale, USA) with n-hexane, reduced to 1 mL volume by rotoevaporation and cleaned-up and fractionated on Florisil column chromatography (Mukherjee and Gopal, 1996). All organic solvents used in the laboratory were distilled in glass (trace organic analysis quality, Caledon Laboratories, Georgetown, Canada).

Quantitative analysis of α- and γ-HCH was performed using a Varian 3800 Gas Chromatograph-Electron Capture (GC-ECD) equipped with a 60 m, JW DB5 column (0.25 mm i.d., 0.25 μm film thickness). Chiral composition of α-HCH was determined by GC-negative ion mass spectrometry on an Agilent 5890 GC coupled to a 5973 Mass Selective Detector (MSD) operated in Single Ion Monitoring (SIM) mode equipped with a 30 m Supelco BetaDex 120 (0.25 mm i.d., 0.25 μm film thickness) column. External calibration standards, obtained from Cerilliant (Round Rock, USA), were run after every 5^{th} sample. Details of quantitative methods are described in (Pućko *et al.*, 2010a).

The average ± standard deviation (SD) of EFs for a racemic α-HCH standard was 0.501 ± 0.005. α- and γ-HCH concentrations presented in this study were corrected for percent recovery. Average recovery was 80 % for brine, 83 % for sea water, 73 % for ice, 73 % for air, and 99 % for snow samples. The Limits of Detection (LODs), calculated as the 3 standard deviation of the mean field blank, were 0.019 ng/L and 0.007 ng/L for α- and γ-HCH, respectively. All laboratory blanks were below LOD.

4.3.4. *Calculations and data analysis*

Brine volume fraction, υ_{BRINE}, was calculated as follows (Frankenstein and Garner, 1967):

$$\upsilon_{BRINE} = S_{ICE} (49.185/ \left| T_{ICE} \right| + 0.532) \cdot 0.1 \quad (-0.5\ °C \geq T_{ICE} \geq -22.9\ °C) \qquad \text{(eq. 4.2)}$$

where υ_{BRINE} is the brine volume fraction (%) (± 0.06 %), S_{ICE} is ice salinity, and T_{ICE} is ice temperature (°C).

To quantify snow scavenging of HCHs from the atmosphere, the total scavenging ratio, W_T, conventionally applied to rain scavenging, was adopted (Wania *et al.*, 1998):

$$W_T = C_s / C_a \qquad \text{(eq. 4.3)}$$

where C_s is the total mass of HCH per volume of melt water, and C_a is the total mass of HCH per volume of air.

Coefficient of variation, CV (%), was used as a measure of HCH variability (Sokal and Rohlf, 1980):

$$CV = 100\ SD / Mean \qquad \text{(eq. 4.4)}$$

The amount of HCHs (ng) that would have to be transferred over the area of 1 m^2 of sea ice to account for the observed increase in the HCH concentrations in the snow layer over the same area during the sampling period ($\Delta HCH/m^2_{ICE}$) was calculated as follows:

$$\Delta HCH/m^2_{ICE} = \Delta HCH/m^3_{SNOW}\ \upsilon_{SNOW} \qquad \text{(eq. 4.5)}$$

where $\Delta HCH/m^3_{SNOW}$ is the increase in the concentration of HCHs in the snow over the duration of sampling (ng/m^3), and υ_{SNOW} is the snow volume over the area of 1 m^2 (m^3).

The amount of HCHs that could be delivered to the sea ice from the melting snow in the early spring relative to the amount entrapped within the ice, $\Delta HCH/m^2_{SNOW}$ (%), was estimated as follows:

$$\Delta HCH/m^2_{SNOW} = (100\ HCH_{SNOW}\ \upsilon_{SNOW}) / (HCH_{ICE}\ \upsilon_{ICE}) \qquad \text{(eq. 4.6)}$$

where HCH_{SNOW} and HCH_{ICE} are the average HCH concentrations in the snow and ice column (ng/m^3) in the winter, and υ_{SNOW} and υ_{ICE} are the volumes of snow and ice under the same area (m^3).

Statistical analyses include Pearson's correlation matrix with Bonferroni probability test, and two-sample t-Test (SYSTAT 11, Systat Software Inc.). Prior to statistical analyses, α- and γ-HCH concentrations, α-HCH EF, ice and snow bulk salinity, ice temperature, brine salinity and brine volume fraction were log-transformed to meet the normal distribution criterion. Plots of vertical distribution of variables in the ice core as a function of time were graphed using Ocean Data View 4 software (R. Schlitzer, 2009) available from the Alfred-Wegener Institute for Polar and Marine Research, Bremerhaven, Germany (http://odv.awi.de).

4.4 Results and discussion

4.4.1 *Levels of HCHs in the sea ice, fresh snow and the atmosphere*

Mean HCH concentrations in 1 m thick first-year sea ice sampled in this study reached 0.349 ± 0.011 (SE) ng/L and 0.041 ± 0.001 (SE) ng/L for the α- and γ-isomer, respectively (Table 4.1). These levels were in good agreement with those reported previously by Pućko *et al.* (2010a). Levels of α-HCH in the fresh snow averaged 0.306 ± 0.031 (SE) ng/L, 3-fold lower than reported 3 decades ago (Gregor and Gummer, 1989), and were similar to those measured in sea ice (t-Test, $p = 0.210$). In contrast, γ-HCH concentration in the snow was significantly higher than in the sea ice (t-Test, $p = 0.003$) with a mean value of 0.064 ± 0.006 (SE) ng/L (Table 4.1). Mean air HCH concentrations reached 8.048 ± 0.755 pg/m^3 and 6.690 ± 0.749 pg/m^3 for α- and γ-

isomer, respectively (Table 4.2), and are similar to the concentrations reported in other regions of the Arctic (Jantunen *et al.*, 2008; Hung *et al.*, 2010; Wong *et al.*, 2011).

Average total scavenging ratio (W_T) of cold winter snow (at air temperature about -24 °C) was calculated to be $3.8 \cdot 10^4$ and $9.6 \cdot 10^3$ for α-HCH and γ-HCH, respectively (equation 4.3). Thus, for a given amount of snowfall, the scavenging of α-HCH was approximately 4-fold faster than that of the γ-isomer. Typically, measured snow scavenging ratios for semi-volatile organic compounds range from 10^5-10^7, but are greatly influenced by temperature (Wania *et al.*, 1998).

4.4.2 *HCH vertical distribution in winter ice as a record of history*

It was previously found that HCH concentrations decreased downwards in the ice column as ice salinity declined (Pućko *et al.*, 2010a). In this study, however, HCHs exhibited relatively high values at intermediate depths (10-40 cm) of the sea ice (Figure 4.2, 4.3A).

Salinity decreased significantly from 0-10 cm to 10-40 cm to 40-70 cm to 70-106 cm by 18 %, 18 %, and 8 %, respectively, compared to a layer directly above (t-Test, $p < 0.001$, $p < 0.001$, and $p = 0.021$, respectively; Table 4.3). α-HCH concentrations increased significantly by 30 % in the second ice layer compared to the top layer, and then decreased downwards by 15 % and 13 % (t-Test, $p = 0.001$, $p = 0.006$, and $p = 0.120$, respectively; Table 4.3). γ-HCH concentrations did not differ significantly between the first and the second ice layer (2 %), and decreased in the lower layers by 11 % and 15 % (t-Test, $p = 0.777$, $p = 0.051$, and $p = 0.011$, respectively; Table 4.3). Vertical distribution of α-HCH EF remained relatively stable throughout the ice column (Figure 4.2C, Table 4.1).

Table 4.1 Values, means, standard errors (SEs), and coefficients of variation (CVs) for ice physical parameters (S - salinity, T – temperature, and υ_{BRINE} – brine volume fraction), α- and γ-HCH concentration and α-HCH enantiomer fraction (EF) in 4 layers of sea ice melt water, snow melt water, brine and under-ice sea water during the winter sampling experiment

	Date (08) → Layer (cm) ↓	6Jan am	6Jan pm	7Jan am	7Jan pm	8Jan am	8Jan pm	9Jan am	9Jan pm	10Jan am	10Jan pm	11 Jan am	Mean	SE	CV (%)
S_{ICE}	0-10	9.5	8.7	9	8.3	8.7	8.6	7.6	8.1	8.5	8.1	n/a	8.5	0.2	6
	10-40	7.2	7.2	7.1	7	7	7.1	7.2	7.2	6.5	6.6	n/a	7.0	0.1	4
	40-70	5.5	6	6.5	5.7	5.5	5.4	5.6	5.3	5.9	5.9	n/a	5.7	0.1	6
	70-106	5.2	5.6	4.9	5.1	5.1	4.9	5.1	4.7	5.8	6.2	n/a	5.3	0.1	9
T_{ICE} (°C)	0-10	-12.4	-18.0	-17.9	-17.7	-17.1	-18.8	-20.9	-18.9	-18.0	-18.4	n/a	-17.8	0.7	12
	10-40	-9.1	-13.6	-15.1	-14.9	-12.1	-15.9	-16.3	-17.2	-15.8	-15.5	n/a	-14.6	0.8	16
	40-70	-7.4	-8.9	-11.9	-11.5	-8.8	-11.4	-9.8	-12.3	-9.9	-11.3	n/a	-10.3	0.5	16
	70-106	-4.9	-5.5	-6.0	-6.2	-5.2	-5.3	-5.7	-5.4	-4.7	-5.1	n/a	-5.4	0.1	9
υ_{BRINE} (%)	0-10	4.4	2.8	3.0	2.8	3.0	2.7	2.2	2.5	2.8	2.6	n/a	2.9	0.2	20
	10-40	4.3	3.1	2.7	2.7	3.3	2.6	2.7	2.4	2.4	2.5	n/a	2.9	0.2	20
	40-70	4.0	3.7	3.1	2.8	3.4	2.6	3.1	2.4	3.4	3.0	n/a	3.2	0.2	16
	70-106	5.9	5.9	5.5	5.2	5.9	5.8	5.0	5.3	7.2	7.0	n/a	5.9	0.2	12
$\alpha\text{-HCH}_{ICE}$ (ng/dm^3)	0-10	0.288	0.299	0.416	0.377	0.284	0.334	0.314	0.298	n/a	0.253	n/a	0.318	0.017	16
	10-40	0.381	0.403	0.488	0.428	0.414	0.435	0.455	0.424	0.396	0.312	n/a	0.414	0.015	11
	40-70	0.352	0.353	0.380	0.362	0.335	0.347	0.332	0.432	0.351	0.254	n/a	0.350	0.014	13
	70-106	0.275	0.325	0.413	0.285	0.420	n/a	0.254	0.220	0.287	0.267	n/a	0.305	0.023	23
$\gamma\text{-HCH}_{ICE}$ (ng/dm^3)	0-10	0.037	0.040	0.057	0.043	0.038	0.047	0.039	0.047	0.046	0.046	n/a	0.044	0.002	14
	10-40	0.043	0.049	0.055	0.043	0.044	0.041	0.043	0.041	0.049	0.039	n/a	0.045	0.002	11
	40-70	0.047	0.051	0.039	0.036	0.036	0.042	0.039	0.036	0.036	0.038	n/a	0.040	0.002	13
	70-106	0.032	0.033	0.034	0.034	0.030	0.038	0.029	0.029	0.045	0.032	n/a	0.034	0.002	14
EF_{ICE}	0-10	0.485	0.495	0.480	0.461	0.504	0.488	0.482	0.484	0.470	0.478	n/a	0.483	0.004	2
	10-40	0.481	0.490	0.464	0.469	0.499	0.496	0.480	0.473	0.484	0.473	n/a	0.481	0.004	2
	40-70	0.461	0.470	0.468	0.466	0.486	0.506	0.467	0.474	0.465	0.472	n/a	0.474	0.004	3
	70-106	0.469	0.469	0.499	0.469	0.480	0.475	0.499	0.472	0.468	0.473	n/a	0.477	0.004	3
$\alpha\text{-HCH}_{SNOW}$ (ng/L)		0.424	0.422	0.498	0.313	0.330	0.243	0.265	0.254	0.199	0.213	0.202	0.306	0.031	33
$\gamma\text{-HCH}_{SNOW}$ (ng/L)		0.085	0.090	0.104	0.057	0.064	0.055	0.062	0.049	0.040	0.048	0.051	0.064	0.006	32
EF_{SNOW}		0.517	0.494	0.462	0.489	0.509	0.524	0.519	0.491	0.477	0.477	0.457	0.492	0.007	5

α-HCH_{BRINE} (ng/L)	4.715	5.322	3.343	5.165	4.637	4.473	2.433	3.169	3.303	3.572	n/a	4.013	0.307	24
γ-HCH_{BRINE} (ng/L)	0.398	0.469	0.421	0.456	0.381	0.491	0.427	0.391	0.435	0.364	n/a	0.423	0.013	10
EF_{BRINE}	0.463	0.467	0.462	0.454	0.459	0.455	0.455	0.449	0.456	0.462	n/a	0.458	0.002	1
α-HCH_{WATER} (ng/L)	1.144	1.084	1.091	1.033	1.092	0.917	1.047	0.950	0.927	0.955	n/a	1.024	0.026	8
γ-HCH_{WATER} (ng/L)	0.101	0.106	0.112	0.096	0.089	0.104	0.115	0.099	0.117	0.113	n/a	0.105	0.003	9
EF_{WATER}	0.455	0.453	0.456	0.452	0.450	0.456	0.459	0.457	0.462	0.463	n/a	0.456	0.001	1

n/a – not available

Table 4.2 Values, means, and standard errors (SEs) for α- and γ-HCH concentration and α-HCH enantiomer fraction (EF) in the air between December 27, 2007 and January 23, 2008

	27Dec	1Jan	6Jan am	6Jan pm	7Jan am	8Jan am	8Jan pm	9Jan am	10Jan am	15Jan	18Jan	22Jan	23Jan	Mean	SE
α-HCH_{AIR} (pg/m^3)	5.504	3.509	10.726	10.855	9.875	6.775	6.755	5.657	9.128	5.924	6.836	10.348	12.738	8.048	0.755
γ-HCH_{AIR} (pg/m^3)	3.200	3.031	9.362	6.851	9.759	6.760	3.194	n/a	7.459	6.771	5.400	7.770	10.726	6.690	0.749
EF_{AIR}	0.508	n/a	0.504	n/a	n/a	n/a	n/a	n/a	0.502	0.500	0.493	0.510	0.506	0.503	0.002

n/a – not available

Table 4.3 Ice growth rate in 4 layers of sea ice from the winter sampling experiment extrapolated from Figure 4, along with relative change of mean salinity (S_{ICE}), and α- and γ-HCH concentrations between ice layers

Ice layer (cm)	$Form_{START}$ (days from freeze-up)[a]	$Form_{END}$ (days from freeze-up)[a]	Total $Form_{DAYS}$[b]	Growth rate (cm/day)[c]	Relative S_{ICE} change (%)	Relative α-HCH change (%)	Relative γ-HCH change (%)
0-10	0	3	3	3.3			
10-40	3	15	12	2.5	↓ 18	↑ 30	↑ 2
40-70	15	38	23	1.3	↓ 18	↓ 15	↓ 11
70-106	38	74	36	1.0	↓ 8	↓ 13	↓ 15

$Form_{START}$ – start of formation; $Form_{END}$ – end of formation; Total $Form_{DAYS}$ – total number of days of formation; [a] Values extrapolated from Figure 4; [b] Total $Form_{DAYS}$ = $Form_{END}$ – $Form_{START}$;

[c] Growth rate = ice layer thickness (cm) / Total $Form_{DAYS}$

Figure 4.2 α-HCH concentration (A), γ-HCH concentration (B), and α-HCH EF (C) in sea ice melt water during the local-scale sampling experiment with the brine volume fraction (υ_{BRINE}) of 5 % marked

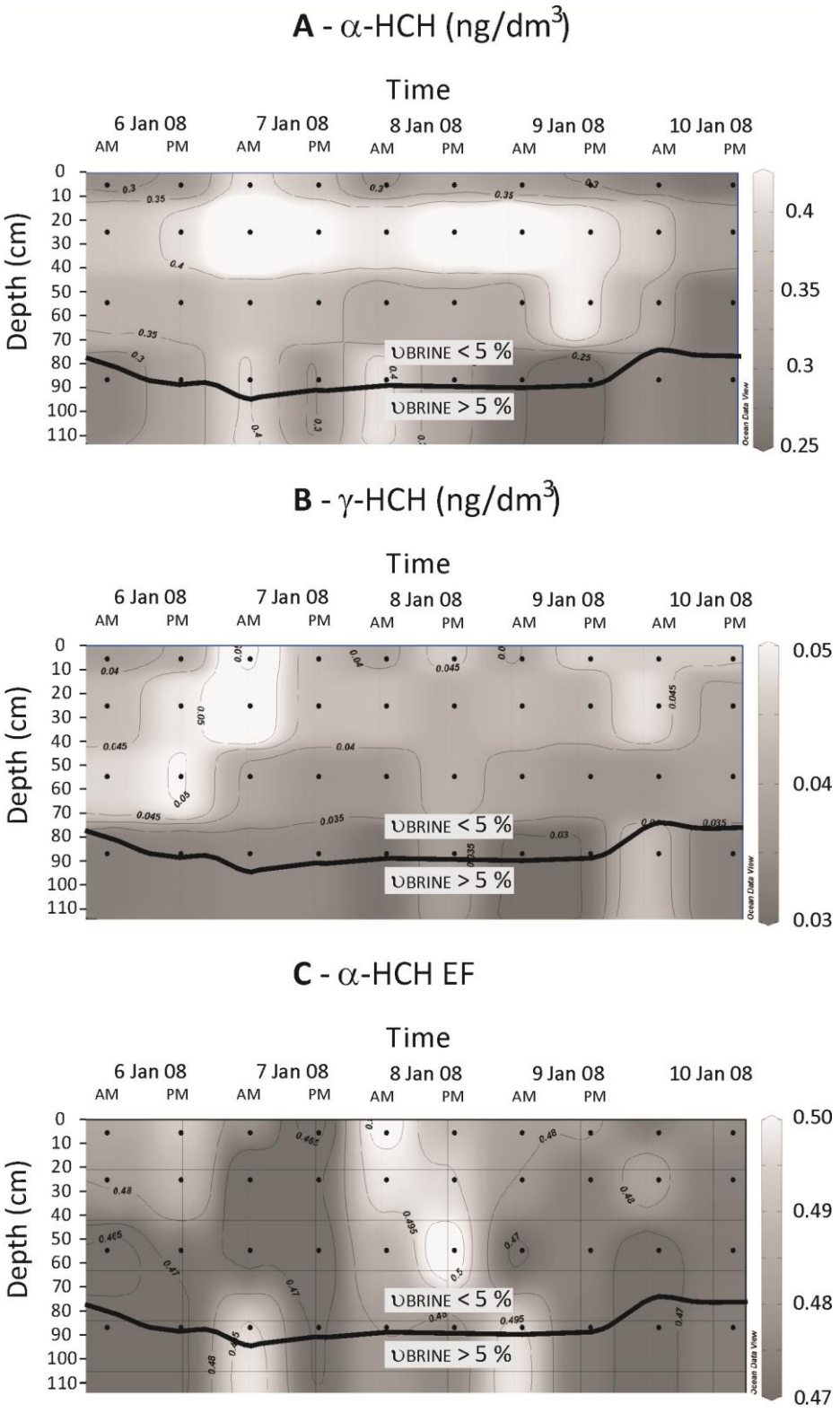

Figure 4.3 Relative change in average ice salinity (S_{ICE}), and α- and γ-HCH concentrations between layers in sea ice collected during the winter sampling experiment (A), and ice growth rate for those ice layers extrapolated from data in the Table 4.4 and Figure 4.4 (B)

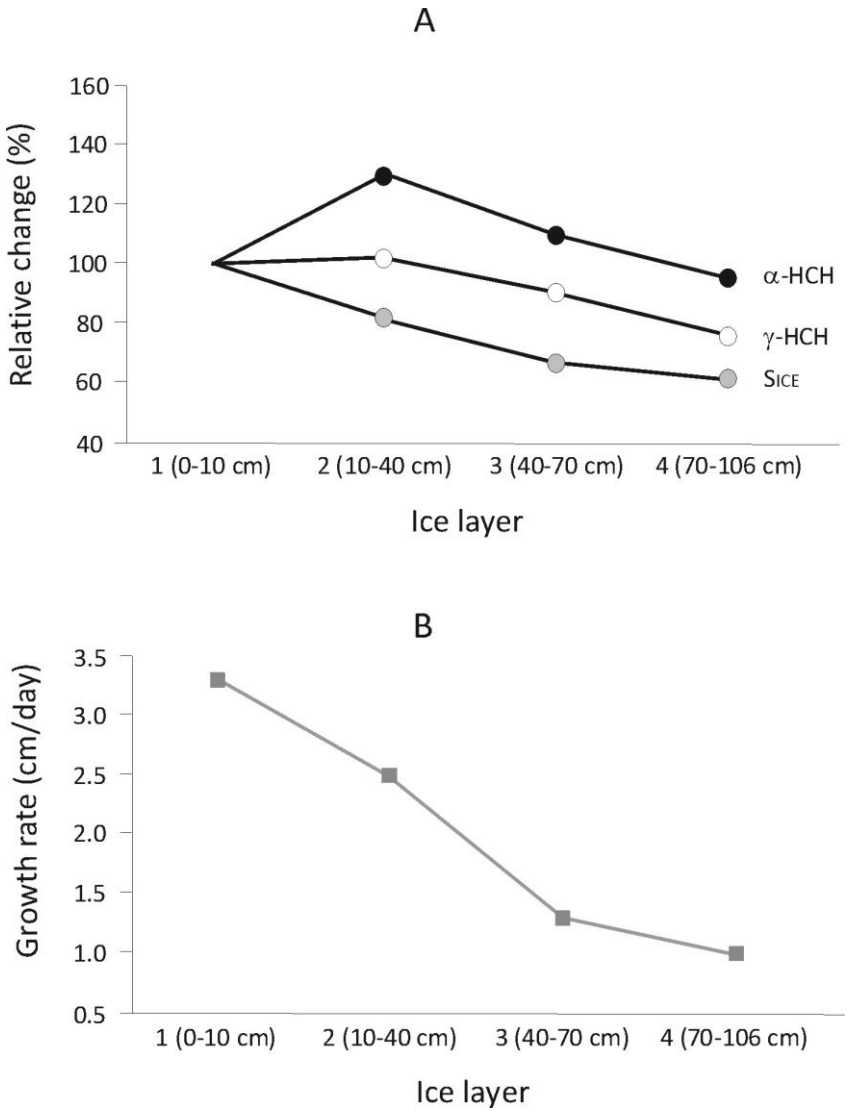

Ice salinity is determined by the rate of brine entrapment during ice formation, and brine rejection during ice desalination (Nakawo and Sinha, 1981; Notz and Worster, 2009). Based on the ice samples from the study region collected from the 2007 freeze-up (26 Oct, 2007) until the winter local-scale sampling experiment (Table 4.4), we estimated the evolution of the brine volume fraction in the region (Figure 4.4) and

ice growth rate for each layer (Table 4.3; Figure 4.3B). After the brine volume fraction in most of the ice layer drops below 5 % (about a month after the ice formation starts), brine and HCH burden become locked and reflect the growth history of this layer until it warms enough in the early spring for the brine (and HCHs) to start moving again (Golden *et al.*, 1998). Since ice desalination can play a significant role in brine rejection from the sea ice for only about a week after freeze-up and in the spring when the sea ice brine volume fractions exceed 5 % (Nakawo and Sinha, 1981; Golden *et al.*, 1998), decreasing growth rate was probably the main reason for decreasing ice salinities, and could explain corresponding decrease in HCH concentrations between layers 2 and 4 (Figure 4.3B). However, the relative difference in the HCH concentrations between the top two layers not corresponding to the change in salinity must be a reflection of the sea ice early growth conditions, not connected to the brine processes. We propose that ice advection during early ice growth period, and spatial variability of HCHs in the under-ice sea water described by CVs of 15 % for α-HCH and 10 % for γ-HCH (Table 4.4), could be responsible for the relatively high HCH concentrations in the second ice layer.

Figure 4.4 Sea ice brine volume fraction (υ_{BRINE}) evolution from the 2007 freeze-up date (26 Oct) until the ice reached 100 cm thickness (2 Jan 08)

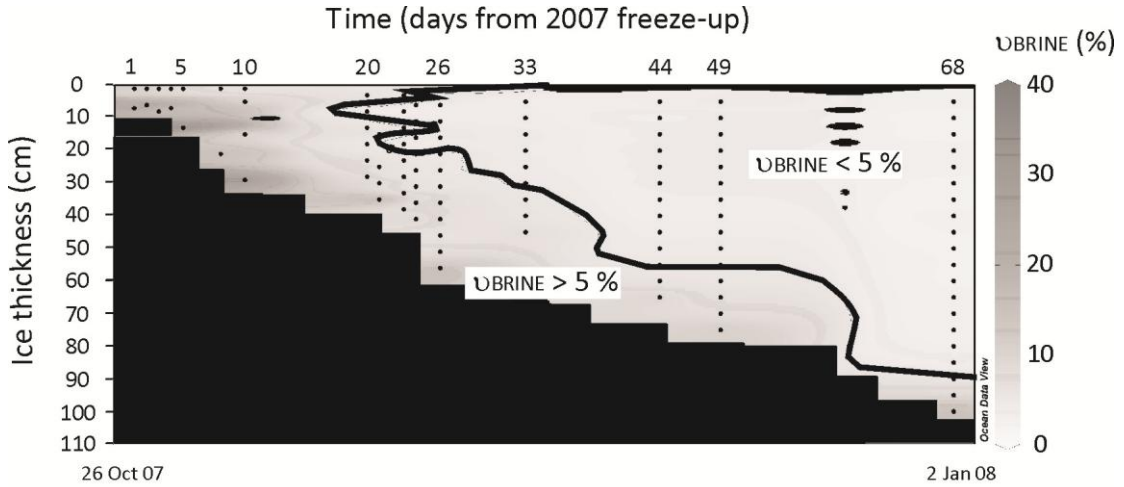

Table 4.4 Ice physical parameters (S - salinity, T – temperature, and υ_{BRINE} – brine volume fraction) and α- and γ-HCH under-ice sea water concentrations at different stations of increasing ice thickness from the 2007 freeze-up (26Oct07) to 100 cm (02Jan08)

Date [a]	St.	Lat (degN)	Long (degW)	$Thick_{ICE}$ (cm)	$Depth_{ICE}$ (cm)	S_{ICE}	T_{ICE} (°C)	υ_{BRINE} (%)	$\alpha\text{-}HCH_{WAT}$ (ng/L)	$\gamma\text{-}HCH_{WAT}$ (ng/L)
27Oct07 [1]	1110	70.322	124.936	8	1 7	14.6 11.6	-4.6 -2.0	16.4 29.1	1.356	0.126
28Oct07 [2]	1116	70.043	126.279	7	1 6	14.2 10.5	-6.0 -2.0	12.4 26.4	1.831	0.141
29Oct07 [3]	1216	70.597	127.704	10	1 8	12.6 6.2	-6.8 -2.0	9.8 15.6	1.168	0.105
30Oct07 [4]	1208	71.065	126.047	8	1 7	8.7 4	-7.7 -2.0	6.0 10.0	n/a	n/a
31Oct07 [5]	1200	71.544	124.461	14	1 13	5.8 13.8	-9.9 -2.0	3.2 34.7	1.573	0.118
03Nov07 [8]	1902	71.546	125.799	22	1 21	11.9 6	-13.4 -2.0	5.0 15.1	1.665	0.136
05Nov07 [10]	1908	71.144	124.353	30	1 5 15 29	9.3 6.8 5.4 11.7	-8.8 -4.3 -3.6 -2.0	5.7 8.1 7.7 29.4	1.272	0.116
15Nov07 [20]	1117	69.868	126.500	33	3 8 13 18 23 28	10.4 5.4 7.3 4.9 5.4 5.0	-8.5 -7.2 -5.6 -4.4 -3.3 -2.9	6.6 4.0 6.8 5.7 8.3 8.7	1.493	0.109
16Nov07 [21]	1117	69.897	126.514	35	5 10 15 25 30 34	10.2 5.9 7.4 6.3 6.4 11.5	-6 -5.6 -5.1 -3.9 -2.8 -2.2	8.8 5.4 7.5 8.3 11.5 26.3	1.463	0.127
18Nov07 [23]	405	70.637	122.963	43	3	11.9	-14.2	4.7	1.676	0.133

					8	6.7	-11.7	3.2		
					13	8.0	-10.2	4.3		
					18	6.7	-9.8	3.7		
					23	6.0	-8.7	3.7		
					28	5.3	-7.7	3.7		
					33	5.1	-5.6	4.8		
					38	4.3	-3.8	5.8		
19Nov07 [24]	405	70.665	122.993	46	3	10.4	-15.5	3.9	n/a	n/a
					6	7.5	-12.5	3.4		
					11	7.2	-11	3.6		
					16	6.2	-10.1	3.3		
					21	7.0	-9	4.2		
					26	5.6	-7.2	4.1		
					31	5.3	-6.4	4.3		
					36	4.7	-5.1	4.8		
					41	7.5	-3.2	12.0		
21Nov07 [26]	437	71.739	126.647	56	1	14.0	-12.5	6.3	1.699	0.121
					6	8.1	-10.0	4.4		
					11	7.6	-9.2	4.5		
					16	8.3	-8.2	5.4		
					21	7.6	-7.2	5.6		
					26	6.5	-7.2	4.8		
					31	5.9	-6.5	4.8		
					36	6.0	-5.4	5.8		
					41	5.4	-6.5	4.4		
					46	5.5	-5.4	5.3		
					51	6.3	-4.3	7.6		
					55	6.9	-2.6	13.5		
28Nov07 [33]	D1	70.432	126.470	50	5	6.5	-9.2	3.8	n/a	n/a
					10	5.6	-7.2	4.1		
					15	5.3	-6.3	4.4		
					20	5.0	-6.2	4.2		
					25	4.5	-5.4	4.3		
					30	4.5	-5.0	4.6		
					35	4.2	-4.3	5.0		
					40	3.6	-3.4	5.4		

					45	3.8	-2.7	7.1		
9Dec07 [44]	D6	71.335	125.199	69	5	7.6	-10.8	3.9	n/a	n/a
					10	6.4	-11.7	3.0		
					15	5.9	-9.0	3.5		
					20	5.8	-8.9	3.5		
					25	5.4	-8.2	3.5		
					30	5.3	-8.0	3.5		
					35	5.0	-7.5	3.5		
					40	4.8	-7.0	3.6		
					45	4.5	-5.8	4.1		
					50	4.1	-4.9	4.4		
					55	3.7	-4.0	4.7		
					60	3.6	-3.2	5.7		
					65	4.8	-2.2	11.0		
14Dec07 [49]	D7	71.436	125.886	78	5	10.0	-11.5	4.8	n/a	n/a
					10	6.6	-10.2	3.5		
					15	6.6	-9.8	3.7		
					20	5.7	-9.5	3.3		
					25	5.7	-9.0	3.4		
					30	5.3	-8.5	3.3		
					35	5.4	-7.7	3.7		
					40	5.5	-7.3	4.0		
					45	5.6	-6.7	4.4		
					50	5.4	-6.1	4.7		
					55	5.2	-5.4	5.0		
					60	4.3	-4.7	4.7		
					65	4.4	-4.0	5.7		
					70	4.1	-2.9	7.3		
					75	4.7	-2.0	11.8		
02 Jan08 [68]	D13	70.978	123.480	100	5	9.0	-20.5	2.6	1.799	0.139
					10	8.1	-20.0	2.4		
					15	8.1	-19.7	2.4		
					20	8.5	-18.7	2.7		
					25	8.0	-17.8	2.6		
					30	7.7	-17.8	2.5		
					35	6.9	-16.8	2.4		

	40	5.9	-16.7	2.0		
	45	5.2	-13.6	2.1		
	50	4.9	-10.5	2.5		
	55	5.0	-10.8	2.5		
	60	4.3	-9.5	2.5		
	65	4.2	-8.5	2.6		
	70	4.3	-8.7	2.7		
	75	3.8	-8.0	2.5		
	80	3.8	-7.6	2.7		
	85	4.0	-6.8	3.1		
	90	3.8	-5.0	4.0		
	95	5.6	-3.9	7.3		
	100	7.5	-2.0	19.2		
				Mean (ng/L)	1.545	0.125
				CV (%)	14	10

St. – station; Lat – latitude; Long – longitude; S – salinity; T – temperature; υ_{BRINE} – brine volume fraction; Thick – thickness; [a]days from 2007 freeze-up: day 0 – 26 Oct 2007; $_{WAT}$ – under-ice sea water; n/a – not available

4.4.3 *Upward migration of brine to the snow*

α-HCH EFs measured in fresh snow (0.517 ± 0.004 (SE)) and the atmosphere (0.503 ± 0.002 (SE)) after major snowfall events (1.5-2 cm of snow), were not significantly different (t-Test, p = 0.069). However, the mean α-HCH EF in the snow 12 or more hours after the precipitation event, decreased by almost 8 % to 0.478 ± 0.005 (SE) (Figure 4.5A). α-HCH EF was significantly (negatively) correlated with snow conductivity, implying that an upward migration of the α-HCH with lower EF from the brine (0.458 ± 0.002 (SE)) may be responsible for this phenomenon (Figure 4.5B, 4.6; Table 4.1). During calm atmospheric conditions (wind < 5 m/s), both the α- and γ-HCH levels in the snow melt water were significantly and positively correlated with snow conductivity as well as highly inter-correlated (Pearson's R^2 = 0.91, p = 0.000) (Figure 4.6). These results suggest that both isomers migrated upward from the ice in conjunction with the brine, which resulted in approximately 0.255 ng/L (51 %) and 0.049 ng/L (47 %) increase in the concentrations of α- and γ-HCH in the snow melt water, respectively. Based on an average density of cold winter snow of 0.275 kg/dm^3 (Langois *et al.*, 2007), the observed increase in HCH concentrations in the snow would equal 0.070 ng/dm^3 for α-HCH and 0.013 ng/dm^3 for γ-HCH. Applying a volume of snow over 1 m^2 of ice of 0.035 m^3 (based on the measured maximum snow thickness for the sampling period of 0.035 m) to equation 4.5, the amounts of HCHs required to be transferred over an area of 1 m^2 are 2.5 ng and 0.5 ng for the α- and γ-HCH, respectively.

Field and laboratory observations consistently indicate that during the initial hours of new sea ice growth, a liquid-like skim, also referred to as a slush layer, develops on the surface of the ice (Perovich and Richter-Menge, 1994). This high-salinity (80-100) 1-5 mm thick layer is generated by the upward expulsion of brine from

the ice interior associated with the cooling of the ice (Perovich and Richter-Menge, 1994; Martin *et al.*, 1995). This process results in significantly higher salinities found in the surface few millimeters of the ice compared to salinities measured in the top few centimeters. In our study, salinity of the surface 5-10 mm of ice, measured on the 8th of Jan, 2008, reached 32.3 or 3.8-fold higher than the average salinity of the top 10 cm of ice (8.5, Table 4.1). Ice samples collected in this study likely lacked most of this high-salinity layer as the ice sampling was performed after removal of the snow along with the surface few millimeters of the ice. Although HCH concentrations in the surface 10 mm of sea ice were impossible to measure directly due to the limited sample volume, HCH concentrations in Arctic sea ice can be predicted based on the ice salinity (Pućko *et al.*, 2010a) applying a 50 % correction for the discrepancy in salts and HCHs partitioning between the brine and ice crystal matrix (Pućko *et al.*, 2010b). Based only on these considerations, HCHs in the top 5-10 mm of ice should have been about 1.9 times concentrated compared to the top 10 cm ice layer, which would result in values of 0.604 ng/L and 0.084 ng/L for the α- and γ-isomers, respectively. The amount of HCHs that would have to be transferred over the area of 1 m^2 of sea ice to account for the observed increase in HCH concentrations in the snow layer over the same area (calculated above; 2.5 ng and 0.5 ng for the α- and γ-HCH, respectively) would have been available in the surface 6 mm of this high-salinity surface ice layer, with the assumption of the average first-year sea ice density above the waterline of 0.875 kg/dm^3 (Timco and Frederking, 1996).

Figure 4.5 Concentrations of α- and γ-HCH, and α-HCH EF in the snow melt water, and snow conductivity (Snow cond.) (A), and concentrations of α- and γ-HCH, and α-HCH EF in the brine, and brine salinity (B) during the winter sampling experiment with falling and blowing snow events marked

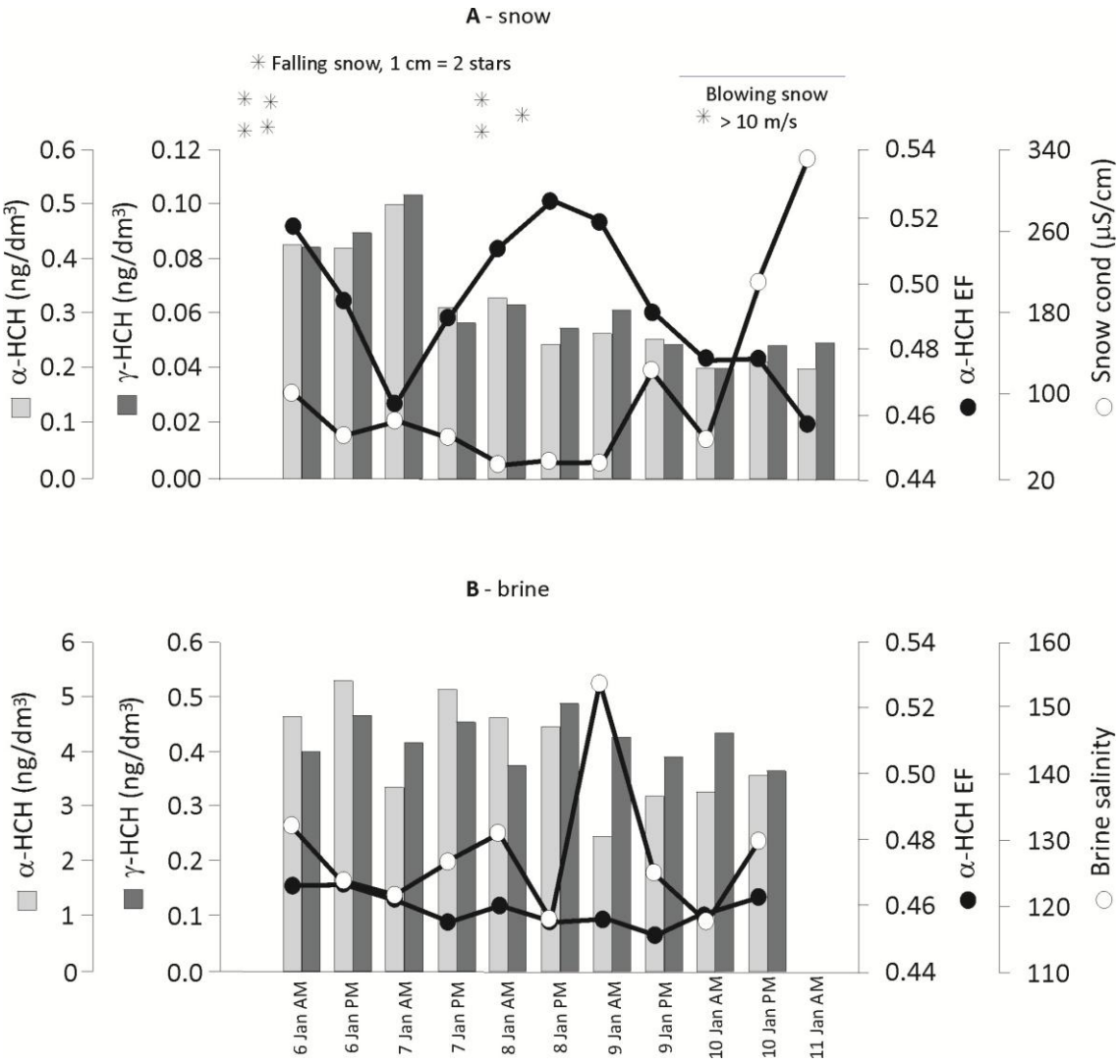

Figure 4.6 Relationships between snow conductivity and α-HCH concentration, γ-HCH concentration and α-HCH EF in the snow melt water; data log-transformed prior to analysis; bolder marker line indicates wind speed > 10 m/s, and these points were excluded from the correlation analysis in the case of concentrations

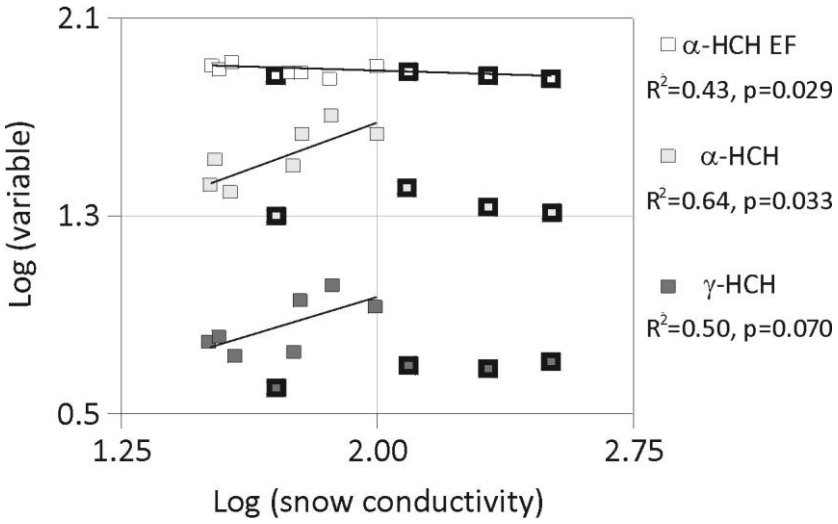

Upward migration of salts by as much as 17 cm in the winter snow has been shown in both the Canadian and European High Arctic (Dominé *et al.*, 2004), provided brine volume fractions in the sea ice exceed 5 %, which permits vertical movement of brine (Golden *et al.*, 1998). Brine volume fraction of the surface 10 mm of ice in our study was estimated at 10.6 % using equation 4.2, a measured salinity of 32.3, and a measured average temperature for the top of the sea ice of -17.8 °C (Table 4.1). Under these circumstances, the upward migration of brine was indeed possible within the surface 10 mm of ice.

4.4.4 *Snow pack ventilation*

Meteorological conditions are known to have major impact on the dynamics of HCHs in the snow pack after snowfall (Cabanes *et al.*, 2002; Halsall, 2004). For

example, in windy conditions (~ 10 m/s over 24 hours), as much as 75 % of a semi-volatile organic contaminant can be lost from the fresh snow pack, compared to only 5 % under calm atmospheric conditions. The rapid loss is caused by the reduction of snow specific surface area (SSA) during ventilation, which then leads to increased snow density and reduced snow capacity to hold sorbed chemicals effectively (i.e., sintering) (Burniston *et al.*, 2007). As a result, chemicals re-partition back into the interstitial pore spaces and are subsequently out-gassed back into the atmosphere. This explains significantly lower levels (by about 40 %) of both α- and γ-HCH in the snow during the blowing snow event (wind > 10 m/s) that occurred during the last 2 days of sampling (Figure 4.5A; t-Test, p = 0.007 and 0.009 for α- and γ-HCH, respectively). Also, those values did not follow the correlation line for HCH concentration in the snow melt water and snow conductivity for calm atmospheric conditions (Figure 4.6).

4.4.5 *Snow melt*

Snow may influence the ice HCH levels only after the brine volume fractions in the entire ice column exceed the threshold of 5 %, enabling snow melt water to percolate into the ice and the underlying aquatic environment (Golden *et al.*, 1998). This was shown to occur in late April 2008 in the Beaufort Sea, when sea ice thickness was approximately 150 cm (Pućko *et al.*, 2010a). During spring warming, some of the HCH burden from the snow will be out-gassed back into the atmosphere before the onset of melt (Meyer and Wania, 2008; Meyer *et al.*, 2009a, 2009b). Neglecting this process, and assuming that all of the HCHs in the snow are delivered to the ice with the melt water, we can estimate the maximum effect that snow melt might have on the ice. Using average snow and ice HCH concentrations measured here in the melt water in the winter season (Table 4.1) together with average snow and ice densities in spring (0.350

kg/dm^3 (Langois *et al.*, 2007) and 0.920 kg/dm^3 (Timco and Frederking, 1996)), and snow thicknesses reported for the Beaufort Sea region in May of 10-80 cm (Langois *et al.*, 2007), equation 4.6 implies that snow could potentially contribute 2 %-18 % of α-HCH, and 4 %-32 % of γ-HCH to the sea ice.

4.5 Acknowledgements

We would like to thank the crew of CCGS *Amundsen* for the field work assistance without which this study could never be accomplished. Also, we express our gratitude to CFL participants - Debbie Armstrong, Amanda Chaulk, Elizabeth Shadwick and Laura Simms - for sharing their time and knowledge in the field. Our special thanks goes to Jason Pavlich and Wojciech Walkusz for the unbelievable amount of hard physical field work they put in ice sampling for this study, without which the samples collection for this experiment would never be possible. We also thank CFL Team 2 members – Phil Hwang, Matthew Asplin, Dustin Isleifson, and Mukesh Gupta - for some of the ice physical measurements used in this study. Finally, we thank the Canadian program office of the International Polar Year, the Natural Sciences and Engineering Research Council (NSERC), Canada Foundation for Innovation (CFI), Canada Research Chairs (CRC), the Department of Fisheries and Oceans Canada, and ArcticNet for funding.

4.6 References

Barber, D. G.; S. P. Reddan, and E. F. LeDrew. 1995. Statistical Characterization of the Geophysical and Electrical Properties of Snow on Landfast First-Year Sea Ice. *J. Geophys. Res.* **100(C2):** 2673-2686.

Burniston, D. A.; W. J. M. Strachan; J. T. Hoff, and F. Wania. 2007. Changes in Surface Area and Concentrations of Semivolatile Organic Contaminants in Aging Snow. *Environ. Sci. Technol.* **41:** 4932-4937.

Cabanes, A.; L. Legagneux, and F. Dominé. 2002. Evolution of the specific surface area and morphology of Arctic fresh snow during the ALERT 2000 campaign. *Atmos. Environ.* **36:** 2767-2777.

Dominé, F.; R. Sparapani; A. Ianniello, and H. J. Beine. 2004. The origin of sea salt in snow on Arctic sea ice and in coastal regions. *Atmos. Chem. Phys.* **4:** 2259-2271.

Frankenstein, G. E. and R. Garner. 1967. Equations for Determining the Brine Volume of Sea Ice from -0.5 to -22.9 C. *J. Glaciol.* **6:** 943-944.

Golden, K. M.; S. F. Ackley, and V. I. Lytle. 1998. The Percolation Phase Transition in Sea Ice. *Science*. **282:** 2238-2241.

Gregor, D. J. and W. D. Gummer. 1989. Evidence of Atmospheric Transport and Deposition of Organochlorine Pesticides and Polychlorinated Biphenyls in Canadian Arctic Snow. *Environ. Sci. Technol.* **23:** 561-565.

Halsall, C. J. 2004. Investigating the occurrence of persistent organic pollutants (POPs) in the arctic: their atmospheric behavior and interaction with the seasonal snow pack. *Environ. Pollut.* **128:** 163-175.

Herbert, B. M. J.; S. Villa, and C. J. Halsall. 2006. Chemical interactions with snow: Understanding the behavior and fate of semi-volatile organic compounds in snow. *Ecotox. Environ. Safe.* **63:** 3-16.

Hung, H.; R. Kallenborn; K. Breivik; Y. Su; E. Brorström-Lundén; K. Olafsdottir; J. M. Thorlacius; S. Leppänen; R. Bossi; H. Skov; S. Manø; G. W. Patton; G. Stern; E. Sverko, and P. Fellin. 2010. Atmospheric monitoring of organic pollutants in the

Arctic under the Arctic Monitoring and Assessment Programme (AMAP): 1993–2006. *Sci. Total Environ.* doi:10.1016/j.scitotenv.2009.10.044.

Jantunen, L. M.; P. A. Helm; H. Kylin, and T. F. Bidleman. 2008. Hexachlorocyclohexanes (HCHs) In the Canadian Archipelago. 2. Air-Water Gas Exchange of α- and γ-HCH, *Environ. Sci. Technol.* **42:** 465-470.

Kallenborn, R. and H. Hühnerfuss. 2001. *Chiral Environmental Pollutants: Trace Analysis and Ecotoxicology*, Sringer-Verlag, Berlin, Germany, pp. 245.

Langois, A.; C. J. Mundy, and D. G. Barber. 2007. On the winter evolution of snow thermophysical properties over land-fast first-year sea ice. *Hydrol. Process.* **21:** 705-716.

Li, Y.-F.; R. W. Macdonald; J. M. Ma; H. Hung, and S. Venkatesh. 2004. Historical alpha-HCH budget in the Arctic Ocean: the Arctic Mass Balance Box Model (AMBBM). *Sci. Total. Environ.* **324:** 115-139.

Macdonald, R. W.; A. L. Barrie; T. F. Bidleman; M. L. Diamond; D. J. Gregor; R. G. Semkin; W. M. J. Strachan; Y.-F. Li; F. Wania; M. Alaee; L. B. Alexeeva; S. M. Backus; R. Bailey; J. M. Bewers; C. Gobeil; C. J. Halsall; T. Harner; J. T. Hoff; L. M. M. Jantunen; W. L. Lockhart; D. Mackay; D. C. G. Muir; J. Pudykiewicz; K. J. Reimer; J. N. Smith; G. A. Stern; W. H. Schroeder; R. Wagemann, and M. B. Yunker. 2000. Contaminants in the Canadian Arctic: Five years of progress in understanding sources, occurrence and pathways. *Sci. Total Environ.* **254:** 93-236.

Martin, S.; R. Drucker, and M. A. Fort. 1995. Laboratory study of frost flower growth on the surface of young sea ice. *J. Geophys. Res.* **100:** 7027-7036.

Meyer, T.; Y. D. Lei; I. Muradi, and F. Wania. 2009a. Organic Contaminant Release from Melting Snow. 1. Influence of Chemical Partitioning. *Environ. Sci. Technol.* **43:** 657-662.

Meyer, T.; Y. D. Lei; I. Muradi, and F. Wania. 2009b. Organic Contaminant Release from Melting Snow. 2. Influence of Snow Pack and Melt Characteristics. *Environ. Sci. Technol.* **43:** 663-668.

Meyer, T. and F. Wania. 2008. Organic contaminant amplification during snowmelt. *Water Res.* **42:** 1847-1865.

Mukherjee, I. and M. Gopal. 1996. Chromatographic techniques in the analysis of organochlorine pesticide residues. *J. Chromatogr. A.* **754:** 33-42.

Müller, T. A. and H.-P. E. Kohler. 2004. Chirality of pollutants – effects on metabolism and fate. *Appl. Microbiol. Biotechnol.* **64:** 300-316.

Nakawo, M. and N. K. Sinha. 1981. Growth rate and salinity profile of first-year sea ice in the High Arctic. *J. Glaciol.* **27:** 315-330.

Notz, D. and M. G. Worster. 2009. Desalination processes of sea ice revisited. *J. Geophys. Res.* **114(C05006):** doi:10.1029/2008JC004885.

Perovich, D. K. and A. J. Gow. 1996. A quantitative description of sea ice inclusions. *J. Geophys. Res.* **101(C8):** 18,327-18,343.

Perovich, D. K. and J. A. Richter-Menge. 1994. Surface characteristics of lead ice. *J. Geophys. Res.* **99:** 16,341-16,350.

Pućko, M.; G. A. Stern; D. G. Barber; R. W. Macdonald, and B. Rosenberg. 2010a. The International Polar Year (IPY) Circumpolar Flaw Lead (CFL) System Study: the importance of brine processes for α- and γ-hexachlorocyclohexane (HCH) accumulation or rejection in sea ice. *Atmosphere-Ocean*. **48:** 244-262.

Pućko, M.; G. A. Stern; R. W. Macdonald, and D. G. Barber. 2010b. α- and γ-hexachlorocyclohexane (HCH) measurements in the brine fraction of sea ice in the Canadian High Arctic using a sump-hole technique. *Environ. Sci. Technol.* **44:** 9258-9264.

Ridal, J. J.; T. F. Bidleman; B. R. Kerman; M. E. Fox, and W. M. J. Strachan. 1997. Enantiomers of α-Hexachlorocyclohexane as Tracers of Air-Water Gas Exchange in Lake Ontario. *Environ. Sci. Technol.* **31:** 1940-1945.

Sokal, R. R. and F. J. Rohlf. 1980. *Biometry 2nd edition*, W.H. Freeman and Company, New York, USA, pp. 347.

Timco, G. W. and R. M. W. Frederking. 1996. A review of sea ice density. *Cold Reg. Sci. Technol.* **24:** 1-6.

Wania, F. 1997. Modelling the fate of non-polar organic chemicals in an aging snow pack. *Chemosphere*. **35:** 2345-2363.

Wania, F.; J. T. Hoff; C. Q. Jia, and D. Mackay. 1998. The effects of snow and ice on the environmental behaviour of hydrophobic organic chemicals. *Environ. Pollut.* **102:** 25-41.

Wong, F; L. M. Jantunen; M. Pućko; T. Papakyriakou; G. A. Stern, and T. F. Bidleman. 2011. Air-Water Exchange of Anthropogenic and Natural Organohalogens on International Polar Year (IPY) Expeditions in the Canadian Arctic. *Environ. Sci. Technol*. doi:10.1021/es1018509.

Chapter 5

When will α-HCH disappear from the Arctic Ocean?

5.1 Abstract

Water column concentrations of α-HCH were measured in the southern Beaufort Sea as part of the Canadian Arctic Shelf Exchange Study (CASES; 2003-04), the Circumpolar Flaw Lead System Study (CFL; 2007-08), and in the Mackenzie River during the 2008 NAHIDIK program. Atmospheric α-HCH concentrations were measured during CASES program. Inventories of α-HCH in the Polar Mixed Layer (PML) and the Pacific Mode Layer (PL) of the Beaufort Sea were calculated between 1986 and 2007 based on the available data. Between 1986 and 1993, there was a significant loading of α-HCH to the Beaufort Sea *via* the ocean currents. About 12 % of the loading to the PML could be explained by the combined effect of the air-water gas exchange and river runoff. After 1993, α-HCH inventories started decreasing, and could be well predicted exclusively by degradation. Ice formation was shown to be a solvent depleting process leading to a significant increase in the α-HCH concentration in the water just beneath the ice. Associated low α-HCH concentrations in the ice and relatively low ice export from the Beaufort Sea resulted in negligible influence of this output route on the inventories in the PML. The majority of α-HCH in the Beaufort Sea could be eliminated due to degradation by 2020, with concentrations in 2040 dropping to < 0.006 ng/L and < 0.004 ng/L in the PML and PL, respectively. Elimination of α-HCH from sea water takes significantly longer than from the atmosphere, with a lag of about two decades.

5.2 Introduction

α-hexachlorocyclohexane (α-HCH) is the classical example of a volatile halogenated organic contaminant whose distribution in the world ocean is under the thermodynamic control of water temperature as reflected by Henry's Law (Li *et al.*,

2002). About 6 Mt of α-HCH was released to the environment in the mid-latitudes and tropics between the 1940s and 2000 as a major constituent of technical HCH (Li and Macdonald, 2005). Due to its high vapor pressure, α-HCH readily entered the atmosphere where it underwent long-range transport, partitioning favorably into cold surface water in the Arctic Ocean (Iwata *et al.*, 1993; Wania and Mackay, 1993; Oehme *et al.*, 1996). α-HCH poses a risk for the environment and living organisms because it is persistent, bioaccumulative and toxic (Prasad *et al.*, 1995; Willett *et al.*, 1998; Hargrave *et al.*, 2000). The total loading of α-HCH to the Arctic Ocean was estimated at ~27 700 tonnes between 1945 and 2000, approximately 0.4 % of the total released, with highest concentrations found in the surface water of the Beaufort Gyre and the central Canada Basin (Carmack *et al.*, 1997; Macdonald *et al.*, 1997; Macdonald *et al.*, 2000; Li *et al.*, 2004).

With the banning of technical HCH use during the 1980s, atmospheric concentrations of α-HCH declined such that in about 1990, the Arctic Ocean switched from being a sink for atmospheric HCH to a source. Furthermore, the buildup of HCH concentrations in the cold, ice-covered surface waters of the western Arctic Ocean prior to the 1990s produced a large inventory, which continues to supply HCH to out-flowing waters in the Canadian Archipelago (Bidleman *et al.*, 1995; Jantunen and Bidleman, 1995; Harner *et al.*, 1999; Wania and Mackay, 1999; Macdonald *et al.*, 2000; Li *et al.*, 2004; Shen *et al.*, 2004; Bidleman *et al.*, 2007). In this process, the Arctic Ocean became the last refuge of α-HCH (Macdonald *et al.*, 1997; Wania and Mackay, 1999).

Sea water in the southern Beaufort Sea exhibits strong layering reflecting density contrasts of source waters (riverine inflow, sea-ice melt, Pacific water, Atlantic water), which may be distinguished by chemical tracers like stable oxygen isotope composition ($\delta^{18}O$), salinity (S), temperature (T) and nutrients (Macdonald *et al.*, 1989).

The water mass in the top 30 m – 50 m, often referred to as the Polar Mixed Layer (PML) (Macdonald *et al.*, 1989), is re-formed annually in winter when cooling and brine rejection from ice formation lead to uniform mixing. In summer, this layer becomes strongly stratified by river inflow (predominantly the Mackenzie River) and sea-ice melt. Beneath the PML (40 m – 225 m) is a halocline containing Pacific Ocean water which has been strongly processed during passage across the Chukchi Shelf. This layer, referred to as the Pacific Mode Layer (PL), has a residence time of about 10 years (Macdonald *et al.*, 1989). Deeper still, the water masses originate in the Atlantic Ocean with the water undergoing processing during its long (~15 – 20 year) passage from Fram Strait and the Barents Sea (Macdonald *et al.*, 1989). Sea-ice cover, which controls air-sea exchange, must be considered when trying to understand α-HCH concentrations in arctic air and surface waters (Jantunen and Bidleman, 1996; Jantunen and Bidleman, 1997; Jantunen *et al.*, 2005; Jantunen *et al.*, 2008; Wong *et al.*, 2011).

Here, we report levels of α-HCH in the southern Beaufort Sea region in 2003/2004 (CASES) and 2007/2008 (CFL/NAHIDIK), particularly emphasizing the influence of ice formation on the vertical distribution of α-HCH in the PML. Using these data together with historical data collected since 1986, we show the evolution of the α-HCH inventory in the PML and the PL of the Beaufort Sea. Major inputs and outputs responsible for the observed trends are discussed.

5.3 Materials and methods

5.3.1 *Sampling site*

Water column samples were collected in the southern Beaufort Sea as part of the Canadian Arctic Shelf Exchange Study (CASES; 2003-04), the Circumpolar Flaw Lead

System Study (CFL; 2007-08) and in the Mackenzie River during the 2008 NAHIDIK program (Figure 5.1). Atmospheric samples were collected during the CASES program.

Figure 5.1 Location of sampling stations during CASES (October 2003 – stations 1-4; 15 March-15 May 2004 – station 10), CFL (October-November 2007), and NAHIDIK (July 2008); dotted line shows the border between the Beaufort Sea and the Northwestern Passages defined by IHO

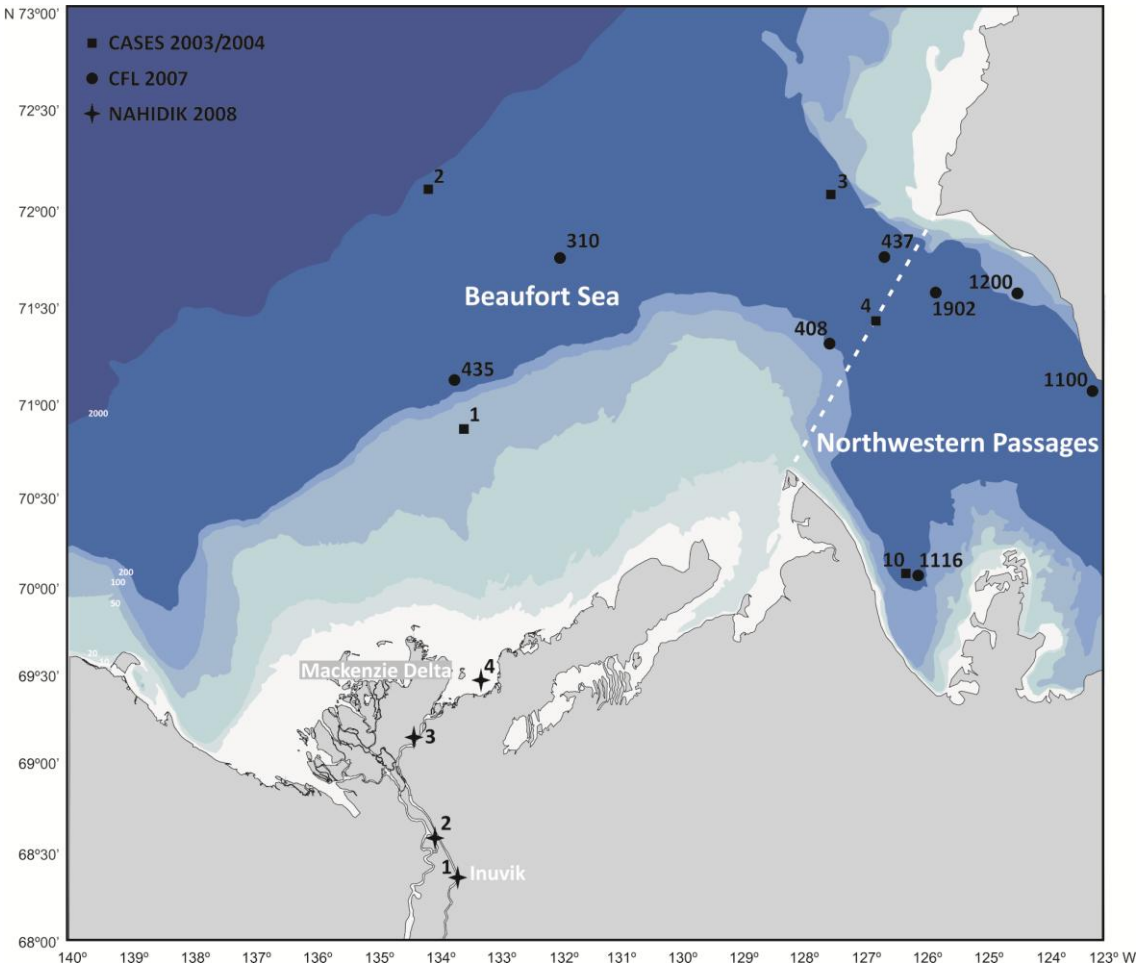

5.3.2 *α-HCH concentration*

CASES 2003/2004

Samples from CASES cruise were collected and analysed by B. R. Water samples (~90 L) were collected using 10 L Teflon Niskin bottles mounted on a Rosette

sampler/CTD system SBE 911*plus*, Sea-Bird Electronics, Bellevue, WA, USA. Samples were drained into 18 L stainless steel cans, spiked with d_6-α-HCH surrogate, and pumped through a 142 mm A/E Glass Fiber Filter, Pall Corporation, Port Washington, NY, USA, followed by a Teflon column containing Amberlite XAD-2 Resin, 20-60 mesh, Rohm and Haas Company, Philadelphia, PA, USA. Air samples were collected by pulling approximately 2500 m^3 of air through an EPM 2000 Glass Fiber Filter, Whatman, Kent, UK, followed by polyurethane foam (PUF) plugs of 7.5 cm i.d. and 6.5 cm in length (Tish Environmental, Cleves, OH, USA) using a Gast Regenair Blower (Cole-Parmer, Vernon Hills, IL, USA). The flow rate used was 7 m^3/min with an average sampling time of 7 hours. The blower was calibrated using the Sierra 620 Mass Flow Meter (Sierra Instruments, Monterey, CA, USA). Prior to further analysis, XAD-2 columns and PUF plugs were stored at -20 °C and -80 °C, respectively.

The XAD-2 columns were extracted by drawing 200 mL each of methanol and dichloromethane, respectively, through the column. The main steps of the subsequent laboratory procedure included transfer into iso-octane and clean-up with 0.5 mL of concentrated sulphuric acid (Mukherjee and Gopal, 1996). PUF filters were spiked with a recovery standard (PCB 30 congener), extracted using n-hexane on an ASE 300 Accelerated Solvent Extractor (Dionex, Sunnyvale, USA). Extract volumes were then reduced to 1 mL using rotory evaporation and cleaned-up and fractionated using Florisil column chromatography (Mukherjee and Gopal, 1996). All organic solvents used in the laboratory were distilled in glass (trace organic analysis quality, Caledon Laboratories, Georgetown, Canada).

Quantitative analysis of α-HCH was performed using a Varian 3800 Gas Chromatograph-Electron Capture (GC-ECD) equipped with a 60 m, JW DB5 column

(0.25 mm i.d., 0.25 μm film thickness). External calibration standards, obtained from Cerilliant (Round Rock, TX, USA), were run after every 5th sample. Details of quantitative methods are described elsewhere (Pućko *et al.*, 2010).

α-HCH concentrations were corrected for percent recovery. Recoveries in both the water and air samples averaged around 80 %. The Limit of Detection (LOD), calculated as the 3 standard deviation of the mean field blank, was 0.019 ng/L. All laboratory blanks were below MDL.

CFL 2007/08 and NAHIDIK 2008

Samples from CFL and Nahidik cruises were collected and analysed by M. P., W. W. And B. R. Water samples (4 L) were collected from 10 L Teflon Niskin bottles using a Rosette sampler/CTD system SBE 911*plus*, Sea-Bird Electronics, Bellevue, WA, USA, except from the under-ice water which was sampled by deploying a Wildco Kemmerer water sampler (Ben Meadows Company, Yulee, USA) through the hole immediately after ice core extraction. All samples were subsequently spiked with d_6-α-HCH surrogate and pumped through a 0.7 μm Glass Fiber Filter (Whatman, Kent, UK, 42.5 mm i.d.) which was contained in a 47 mm in-line pre-assembled single stage filter holder (Savillex, Minnetonka, MN, USA), followed by Oasis solid-phase extraction (SPE) cartridges with HLB 20 cc, 1 g (Waters, Mississauga, Canada). A Masterflex peristaltic pump (Cole-Parmer, Vernon Hills, IL, USA) was used for filtration at a flow rate < 20 mL/min. Cartridges were tested for recoveries using d_6-α-HCH surrogate (> 97 %), activated with 20 mL of methanol prior to filtration, and stored at -20 °C after filtration. The main steps of the subsequent laboratory procedure included elution of SPE cartridges with ~40 mL of acetone, transfer into iso-octane by adding 1 mL of this solvent to the acetone extract previously rotoevaporated to 3 mL,

vortexing and transferring the more non-polar phase (top phase) into the new test tube, rinsing the acetone phase with n-hexane three times, reducing the volume of the solvents mixture to 1 mL under nitrogen flow, and cleaning-up the solution with 0.5 mL of concentrated sulphuric acid (Mukherjee and Gopal, 1996).

α-HCH quantitative analysis was performed as described above (CASES 2003/2004).

5.3.3 *Data visualization*

Gridded plots of chosen variables and a map of sampling locations in the region (Figure 2) were graphed using Ocean Data View 4 software (Schlitzer, 2009).

5.3.4 *Calculations*

Sampling stations in this study were located at the border of the Beaufort Sea and the Northwestern Passages according to the boundary defined by the International Hydrographic Organization (IHO) (Jakobsson, 2002). All the calculations, including inventories of α-HCH in the PML and the PL and inputs/outputs of α-HCH to/from those layers, were performed for the Beaufort Sea.

The inventory of α-HCH in the PML of the Beaufort Sea, $PML_{\alpha\text{-HCH}}$ [t], was calculated as follows:

$$PML_{\alpha\text{-HCH}} = PML_{depth} \cdot BS_{area} \cdot C_{\alpha\text{-HCH}}^{PML} \qquad \text{(eq. 5.1)}$$

where PML_{depth} is the average depth of the PML in the Beaufort Sea [0.04 km (Macdonald *et al.*, 1989)], BS_{area} is the area of the Beaufort Sea [IHO-defined area of the Beaufort Sea, 447 000 km^2 (Jakobsson, 2002)], and $C_{\alpha\text{-HCH}}^{PML}$ is the average α-HCH concentration in the PML [t/km^3].

The inventory of α-HCH in the PL of the Beaufort Sea, $PL_{\alpha\text{-HCH}}$ [t], was calculated as follows:

$$PL_{\alpha\text{-HCH}} = (PL_{depth} - PML_{depth}) \cdot BS_{area} \cdot C_{\alpha\text{-HCH}}^{PL} \qquad \text{(eq. 5.2)}$$

where PL_{depth} is the average depth of the Pacific Mode Layer in the Beaufort Sea [0.225 km (Macdonald *et al.*, 1989)], and $C_{\alpha\text{-HCH}}^{PL}$ is the average α-HCH concentration in the Pacific Mode Layer [t/km^3].

Annual α-HCH inventories in the PML corrected for degradation (bacterial and hydrolytic), $PML_{\alpha\text{-HCH}}^{D}$ [t], were calculated as follows (Harner *et al.*, 1999):

$$PML_{\alpha\text{-HCH}}^{D} = PML_{\alpha\text{-HCH}} \cdot \exp^{(-0.158)t} \qquad \text{(eq. 5.3)}$$

where $PML_{\alpha\text{-HCH}}$ is the α-HCH inventory in the PML calculated or predicted in the previous year [t], and t is the duration of degradation [1 yr].

Annual α-HCH inventories in the PL corrected for degradation (bacterial and hydrolytic), $PL_{\alpha\text{-HCH}}^{D}$ [t], were calculated as follows (Harner *et al.*, 1999):

$$PL_{\alpha\text{-HCH}}^{D} = PL_{\alpha\text{-HCH}} \cdot \exp^{(-0.158)t} \qquad \text{(eq. 5.4)}$$

where $PL_{\alpha\text{-HCH}}$ is the α-HCH inventory in the PL calculated or predicted in the previous year [t], and t is the duration of degradation [1 yr].

To describe the saturation state of water relative to the partial pressure in air, α-HCH fugacity ratios (f_w/f_a) were calculated using the formulas of Jantunen and Bidleman (1995):

$$f_w = 10^{-9} \cdot \alpha\text{-}HCH_w \cdot H/M \qquad \text{(eq. 5.5)}$$

$$f_a = 10^{-9} \cdot \alpha\text{-}HCH_a \cdot RT_a/M \qquad \text{(eq. 5.6)}$$

where f_w and f_a are the α-HCH fugacities in the surface water and the overlying air [Pa]; $\alpha\text{-}HCH_w$ is the α-HCH concentration in the surface water [ng/m^3], $\alpha\text{-}HCH_a$ is the α-HCH concentration in air [ng/m^3]; H [Pa · m^3/mol] is the Henry's law constant; M is α-HCH molecular weight (291 g/mol); R is the gas constant (8.314 Pa · m^3/deg · mol),

and T_a is the air temperature [K]. A fugacity ratio = 1, > 1 and < 1 indicates equilibrium state, potential for volatilization and deposition, respectively.

Fluxes of α-HCH were calculated using the two-film model and the following relationships (Mackay and Yeun, 1983; Hinckley *et al.*, 1991; Jantunen and Bidleman, 1996; Jantunen and Bidleman, 1997; Wiberg *et al.*, 2000):

$$F_p = 10^9 \cdot M \cdot D_{AW} (f_w - f_a) \quad \text{(eq. 5.7)}$$

$$D_{AW} = (86400 \cdot k_a)/(R \cdot T_a) \quad \text{(eq. 5.8)}$$

$$k_a = 10^{-3} + 4.62 \cdot 10^{-4} \cdot (6.1 + 0.63 \cdot u_{10})^{0.5} \cdot u_{10} \cdot Sc_g^{-0.67} \quad \text{(eq. 5.9)}$$

where F_p is the potential α-HCH flux [ng/m^2 · day] under open water conditions, D_{AW} is the transport parameter [mol/m^2 · day · Pa], k_a is the transport velocity for α-HCH in gas phase [m/s], Sc_g is the Schmidt number for α-HCH in gas phase (2.9), u_{10} is the wind speed at 10 m above the sea surface [m/s]. Fluxes > 0 imply volatilization and < 0, deposition.

Total monthly output/input of α-HCH from/to the PML of the Beaufort Sea due to air-water gas exchange, F [t/month], was calculated as follows:

$$F = F_p \cdot BS_{area} \cdot FOW \quad \text{(eq. 5.10)}$$

where F_p is the potential α-HCH flux [t/km^2 · month], and FOW is the fraction of open water in the Beaufort Sea in a given month (estimated visually from the CIS ice weekly charts, Table 5.6).

α-HCH concentrations in the Mackenzie River water, $\alpha\text{-}HCH_{river}$ [ng/m^3], were estimated using the following equation with the assumption of equilibrium partitioning between air and water (Jantunen and Bidleman, 1995):

$$\alpha\text{-}HCH_{river} = \alpha\text{-}HCH_a \cdot R \cdot T_a/H \quad \text{(eq. 5.11)}$$

Monthly input of α-HCH from the Mackenzie River to the PML of the Beaufort Sea, $River_{\alpha\text{-HCH}}^{I}$ [t/month], was calculated as follows:

$$River_{\alpha\text{-HCH}}^{I} = R_{discharge} \cdot \alpha\text{-}HCH_{river} \quad \text{(eq. 5.12)}$$

where $R_{discharge}$ is the monthly water runoff from the Mackenzie River to the Beaufort Sea [km^3/month], and the α-HCH_{river} is the concentration of α-HCH in the river water [t/km^3], estimated using eq. 5.11.

Annual output of α-HCH from the Beaufort Sea with ice export, $Ice_{\alpha\text{-HCH}}^{O}$ [t/yr], was calculated as follows:

$$Ice_{\alpha\text{-HCH}}^{O} = IE \cdot \alpha\text{-}HCH_{ice} \quad \text{(eq. 5.13)}$$

where IE is the first-year ice export [km^3/yr], and α-HCH_{ice} is the α-HCH concentration in the first-year sea ice [t/km^3].

5.4 Results and discussion

5.4.1 *Decrease of α-HCH concentrations*

Several studies have produced α-HCH vertical profiles in the upper ocean and air in the Beaufort Sea from 1986 to 2008 (Figures 5.2, 5.3, 5.4). The earliest data, from 1986, coincide with a period of relatively high α-HCH global emissions (Figure 5.4; Li, 1999; Li *et al.*, 2002). Between 1986 and 1993 an approximate 50 % increase in α-HCH concentrations was observed in the PML (Figure 5.3). Conversely, in response to declining global usage α-HCH atmospheric concentrations declined rapidly between 1986 and 1993 (Figure 5.4; Li *et al.*, 2002).

Between 1993 and 2004, both air and water concentrations decreased (Figures 5.3, 5.4), and the mean α-HCH concentration in the Beaufort Sea at 5 m declined to 3.03 ± 0.20 (SE) ng/L (Table 5.1, Figure 5.3), which was 40 % lower than the surface water concentrations measured by Bidleman *et al.* (2007) in the summer of 1999 (4.7 ng/L), and 50 % lower than the levels in the PML in 1993 (Macdonald and Carmack,

1994). Air α-HCH concentrations in 2003 averaged 19 ± 3 (SE) pg/m^3 (Table 5.2). These values are comparable with those reported in the same year by Hung *et al.* (2010) (16 ± 8 pg/m^3), and about three times lower than those measured in 1999 by Jantunen *et al.* (2008) (67 ± 7 pg/m^3).

Figure 5.2 A comparison of α-HCH water and air sampling locations during CASES 2004 and CFL 2007 with those between 1986 and 2008 in the region; [a]Hargrave *et al.*, 1988, [b]Patton *et al.*, 1989; [c]Macdonald and Carmack, 1994; [d]Jantunen and Bidleman, 1995; [e]Halsall *et al.*, 1998; [f]Bailey *et al.*, 2000; [g]Hung *et al.*, 2010; [h]Macdonald *et al.*, 1999a; [i]Bidleman *et al.*, 2007; [j]Jantunen *et al.*, 2008; [k]Wong *et al.*, 2011; [l]Pućko *et al.*, 2011

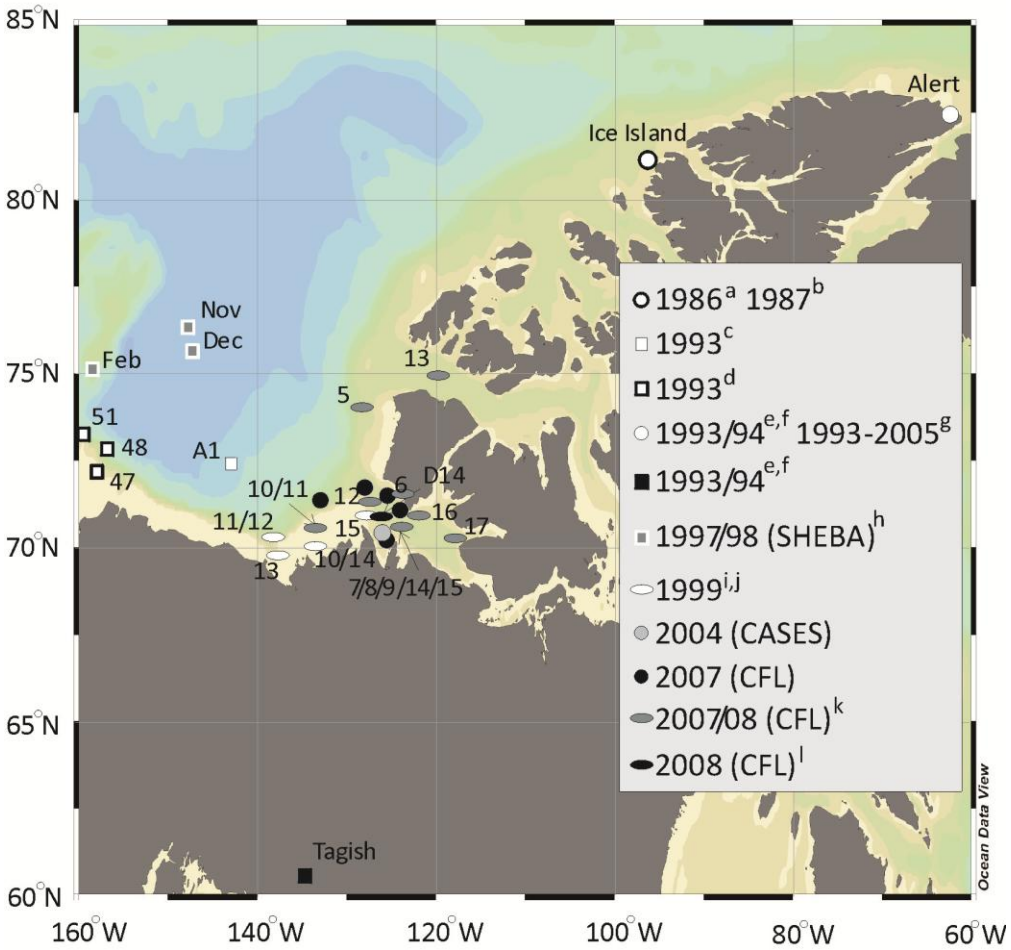

Figure 5.3 A comparison of mean α-HCH water concentrations measured during CASES 2004 (spring) and CFL 2007 (fall) with those between 1986 and 2008 in the region during summers; [a]Hargrave *et al.*, 1988, [c]Macdonald and Carmack, 1994, [h]Macdonald *et al.*, 1999a

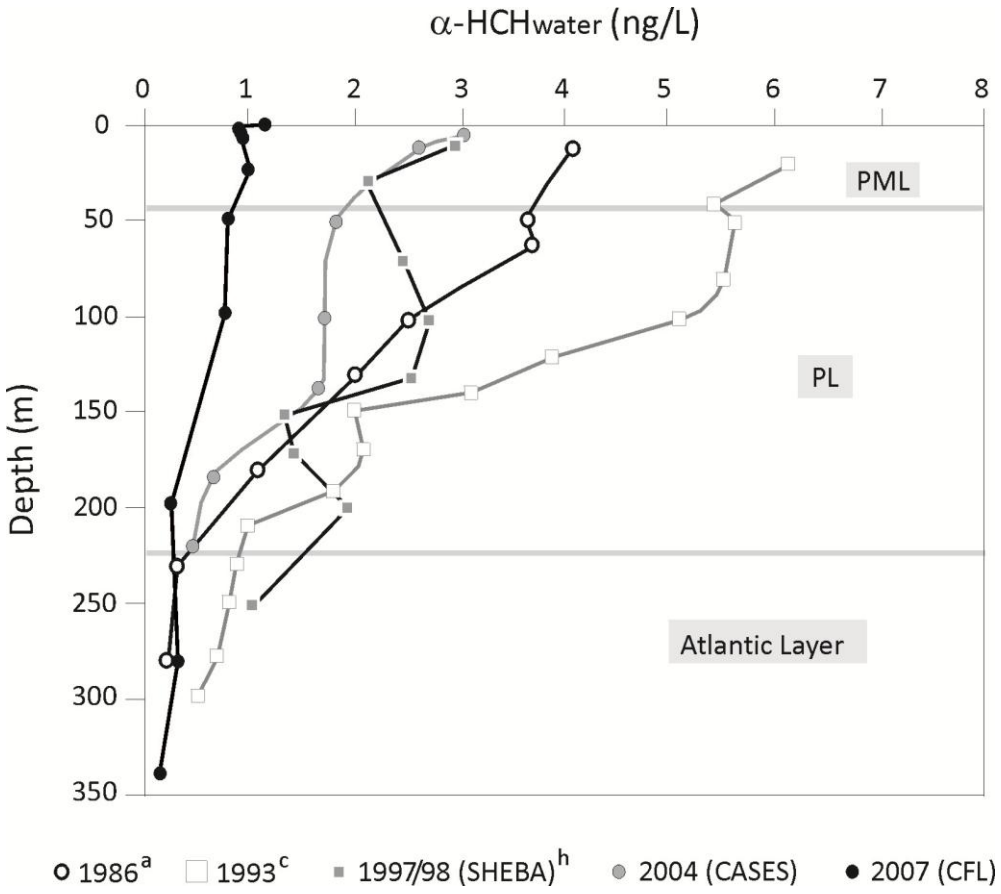

Between 2004 and 2007, we find a further decrease of surface water α-HCH concentration with values dropping by about 70 % (0.90 ± 0.08 (SE) ng/L at 5 m, Table 5.1, Figure 5.3). These levels compare very well with those measured in the surface water in 2008 by Wong *et al.* (2011). Air concentrations also decreased by half reaching 8 ± 3 pg/m^3 (Pućko *et al.*, 2011) and 7 ± 2 pg/m^3 (Wong *et al.*, 2011) in the winter of 2007/08. Significant increase in air concentration in the summer of 2008 was associated with the sea ice break-up and α-HCH volatilizing in the region (Figure 5.4, Wong *et al.*, 2011).

Figure 5.4 A comparison of α-HCH levels in air during CASES 2004 with those between 1986 and 2008 in the region along with α-HCH global emissions; [a]Hargrave *et al.*, 1988, [b]Patton *et al.*, 1989, [d]Jantunen and Bidleman, 1995, [e]Halsall *et al.*, 1998, [f]Bailey *et al.*, 2000, [g]Hung *et al.*, 2010, [j]Jantunen *et al.*, 2008, [k]Wong *et al.*, 2011, [l]Pućko *et al.*, 2011; α-HCH global emissions after [m]Li, 1999 and [n]Li *et al.*, 2002; all air measurements are from summer, except from [l]winter, [e,f,g]entire year

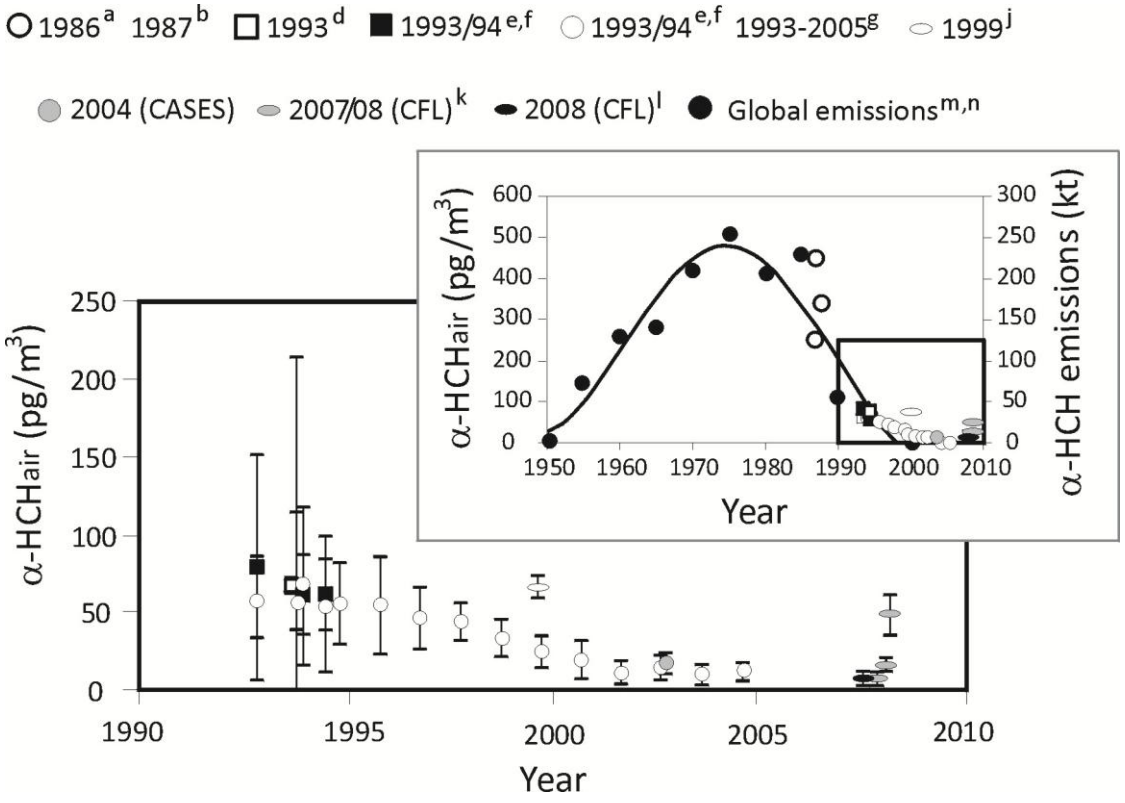

Table 5.1 Vertical profiles of α-HCH concentration measured in 2004 (CASES) and 2007 (CFL), and α-HCH concentration in the surface water of the Mackenzie River in 2008 (NAHIDIK)

CASES 2004 (measured at station 10)

α-HCH [ng/L]

Depth [m]	15-31 Mar	1-30 Apr	1-15 May	Mean	SE
5	2.828	3.236	n/a	3.032	0.204
15	n/a	2.758	2.331	2.545	0.214
50	1.949	n/a	1.697	1.823	0.126
100	1.172	2.710	1.302	1.728	0.492
140	n/a	1.618	n/a	1.618	n/a
180	0.713	n/a	n/a	0.713	n/a
220	n/a	0.727	0.249	0.488	0.239

CFL 2007

α-HCH [ng/L]

Depth [m]	11 Oct St.310	16 Oct St.435	20 Oct St.437	22 Oct St.408	26 Oct St.1100	28 Oct St.1116	31 Oct St.1200	3 Nov St.1902	Mean	SE
0	0.649	0.744	1.527	0.681	0.828	1.831	1.573	1.665	1.187	0.178
5	0.723	0.725	0.881	0.738	0.871	0.837	1.039	1.400	0.902	0.080
7.5	0.782	0.630	1.037	0.714	0.798	0.791	1.153	1.327	0.904	0.085
10	0.660	1.243	0.869	0.922	0.743	0.823	1.034	1.015	0.914	0.065
25	0.836	1.280	0.737	0.672	1.006	0.687	0.871	2.188	1.035	0.179
50	0.716	0.756	0.818	0.692	0.747	0.841	1.054	0.949	0.822	0.044
100	0.742	0.763	0.733	0.570	0.677	0.762	1.047	0.921	0.777	0.052
200	0.403	0.237	0.326	0.193	0.247	0.183	0.355	0.378	0.290	0.030
280		0.548	0.136		0.206			n/a	0.297	0.127
340								0.132	0.132	n/a

NAHIDIK 2008

α-HCH [ng/L]

Depth [m]	21 Jul (St.1)			22 Jul (St.2)			22 Jul (St.3)			23 Jul (St.4)			Mean	SE
0	0.159	0.140	0.148	0.078	0.115	0.098	0.076	0.059	0.081	0.204	0.113	0.096	0.114	0.012

SE – standard error, n/a – not available

Table 5.2 Air α-HCH concentration at different stations in October 2003 (CASES 2003)

Station	α-HCH_{air} [pg/m^3]
1	17.58
2	23.51
3	23.77
4	9.83
Mean	18.67
SE	3.28

SE – standard error

5.4.2 *Inventory of α-HCH in the PML and PL*

Average α-HCH concentrations in the PML and the PL were estimated as a mean of measurements at depths between 0 m and 50 m, and 50 m and 225 m, respectively (Table 5.3). The inventory of α-HCH in the PML of the Beaufort Sea, calculated according to eq. 5.1, equaled 68 tonnes in 1986, 102 tonnes in 1993, 46 tonnes in 1997/98, 45 tonnes in 2004, and 18 tonnes in 2007 (Table 5.3). During the same interval, the inventory of α-HCH in the PL, calculated using eq. 5.2, equaled 168 tonnes in 1986, 241 tonnes in 1993, 141 tonnes in 1997/98, 76 tonnes in 2004, and 40 tonnes in 2007 (Table 5.3).

5.4.3 *Loss of α-HCH due to degradation between 1993 and 2007*

Degradation has been shown to be a major removal mechanism of α-HCH from the Arctic Ocean, with microbial degradation and hydrolysis accounting for ~ 85 % and 15 % of the total degradation, respectively (Macdonald *et al.*, 2000). Using the kinetic rates proposed by Harner *et al.* (1999), we calculated the projected influence of degradation on the α-HCH inventories in the PML and the PL between 1986 and 2040 (eqs. 5.3 and 5.4, Table 5.3, Figure 5.5).

In the PML, α-HCH inventory decreased from 1993 to 2007 by 84 tonnes. Degradation would diminish this inventory by 91, 93, or 74 tonnes, starting the simulation from the values calculated for 1993, 1997 and 2004, respectively (Table 5.3). Thus, α-HCH inventory predicted by degradation in the PML is within 12 % of the measured decrease (Figure 5.5). In the PL, α-HCH inventory decreased from 1993 to 2007 by 201 tonnes. Degradation would diminish this inventory by 215, 213, or 194 tonnes, starting the simulation from the values calculated for 1993, 1997 and 2004,

respectively (Table 5.3). Again, α-HCH inventory predicted by degradation in the PL is within ~7 % of the measured decrease (Figure 5.5).

Figure 5.5 α-HCH inventories in the PML (A) and the PL (B) of the Beaufort Sea calculated based on available data and α-HCH inventories calculated annually based on degradation rates from [a]Harner *et al.*, 1999; for raw data and calculations see Table 5.3

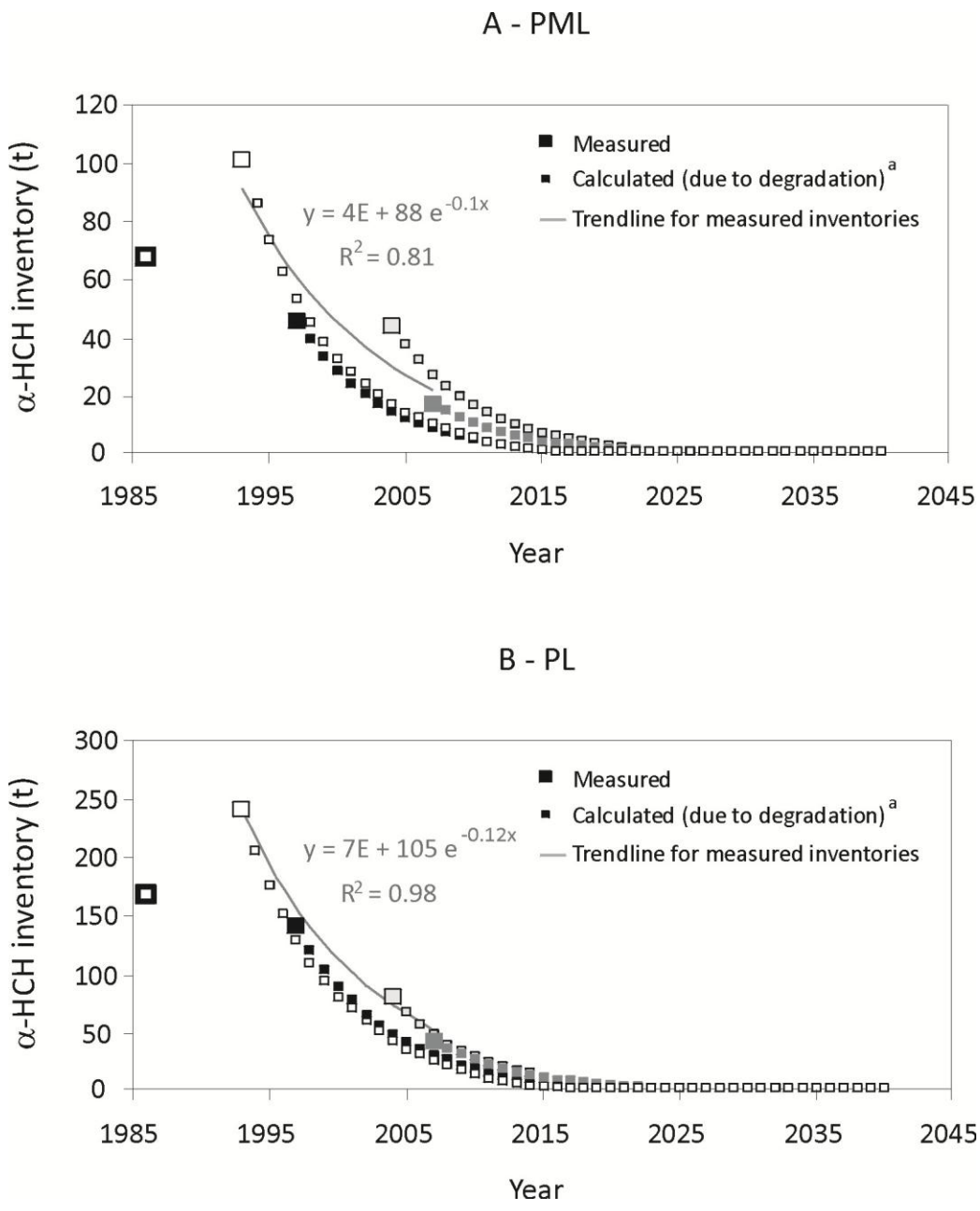

Table 5.3 Average α-HCH concentrations for the PML, $\alpha\text{-HCH}_{PML}$ and the PL, $\alpha\text{-HCH}_{PL}$ and α-HCH inventories in the PML ($PML_{\alpha\text{-HCH}}$) and the PL ($PL_{\alpha\text{-HCH}}$) in the Beaufort Sea in 1986, 1993, 1997/98, 2004, and 2007 along with modified inventories calculated for consecutive years due to degradation ($PML_{\alpha\text{-HCH}}^{D}$ and $PL_{\alpha\text{-HCH}}^{D}$)

Year	$\alpha\text{-HCH}_{PML}$ * [ng/L]	$PML_{\alpha\text{-HCH}}$ ** [t]	$PML_{\alpha\text{-HCH}}^{D***}$ [t]				$\alpha\text{-HCH}_{PL}$ * [ng/L]	$PL_{\alpha\text{-HCH}}$ ** [t]	$PL_{\alpha\text{-HCH}}^{D***}$ [t]			
1986[a]	3.754	67.9					2.485	167.6				
1987			58.0						143.1			
1988			49.5						122.2			
1989			42.3						104.3			
1990			36.1						89.1			
1991			30.8						76.1			
1992			26.3						64.9			
1993[b]	5.700	101.9	22.5				3.638	241.4	55.5			
1994			19.2		87.0				47.4		206.1	
1995			16.4		74.3				40.4		176.0	
1996			14.0		63.4				34.5		150.3	
1997[c]	2.605	46.5	11.9		54.2		2.115	140.8	29.5		128.3	
1998			10.2	46.2	39.7				25.2	109.4	120.2	
1999			8.7	39.5	33.9				21.5	93.3	102.7	
2000			7.4	33.7	28.9				18.3	79.6	87.6	
2001			6.3	28.8	24.7				15.7	67.9	74.8	
2002			5.4	24.6	21.1				13.4	57.9	63.9	
2003			4.6	21.0	18.0				11.4	49.4	54.6	
2004[d]	2.467	44.7	4.0	17.9	15.4		1.137	76.2	9.8	42.1	46.6	
2005			3.4	15.3	13.1	38.2			8.3	35.9	39.7	65.1
2006			2.9	13.1	11.2	32.6			7.1	30.6	33.9	55.6
2007[e]	0.961	17.9	2.5	11.2	9.6	27.8	0.630	40.2	6.1	26.1	28.9	47.5

2010		1.5	6.9	6.0	17.3	11.1		1.5	16.2	17.9	29.5	25.0
2020		0.3	1.4	1.2	3.6	2.3		0.3	3.3	3.6	6.1	5.2
2030		<0.1	0.3	0.3	0.7	0.5		<0.3	0.7	0.7	1.3	1.1
2040		<0.1	<0.1	<0.1	0.2	<0.1		<0.3	<0.3	<0.3	<0.3	<0.3

[*]a mean from 0 m – 50 m measurements and 50 m – 225 m measurements for the PML and the PL, respectively; [**]calculated based on eq. 5.1 and 5.2; [***]calculated based on eq. 5.3 and 5.4; α-HCH concentration profiles from [a]Hargrave *et al.*, 1988, [b]Macdonald and Carmack, 1994, [c]Macdonald *et al.*, 1999a, [d,e]this study, Table 1; $PML_{\alpha\text{-HCH}}^{D}$ and $PL_{\alpha\text{-HCH}}^{D}$ were calculated annually based on the value predicted/calculated in the previous year (shading denotes for which consecutive years the calculations were done)

5.4.4 *Degradation sensitivity analysis*

We varied the degradation constants by ± 20 % to evaluate the sensitivity of α-HCH inventories between 1993 and 2007 to the choice in degradation rate. The simulations, run annually based on equations 5.3 and 5.4, revealed that increasing the degradation constant by 20 % would increase the degradation by 36 % and 35 % in the PML and PL, respectively. A negative shift over the same time frame would decrease the final result by 55 % and 58 % in the PML and PL, respectively. Compared to the total decrease in inventories due to degradation calculated between 1993 and 2007, those variations would have negligible effect representing only 4 % and 7 % for the positive and negative shift, respectively.

5.4.5 *Increase of the α-HCH inventory between 1986 and 1993*

Between 1986 and 1993, when the global emissions of α-HCH were still relatively high (Figure 5.4; Li, 1999; Li *et al.*, 2002), inventories increased by 34 tonnes in the PML, and by 73 tonnes in the PL (Table 5.3, Figure 5.5). Additionally, roughly 45 tonnes and 112 tonnes were degraded between those years in the PML and the PL, respectively (Table 5.3). The loss of HCH by degradation implies an input of about 79 tonnes and 185 tonnes of α-HCH between 1986 and 1993 to compensate for the observed changes in the PML and the PL, respectively. Ocean currents (63 %), atmospheric deposition (30 %) and the river inflow (7 %) were shown to be the major inputs of α-HCH to the Arctic Ocean in the mid-1980s (Barrie *et al.*, 1992).

5.4.6 *The influence of the air-water exchange on the α-HCH inventory in the PML*

To calculate total outputs/inputs of α-HCH from/to the PML due to air-water exchange, fugacity ratios (Table 5.5) and potential fluxes of α-HCH, for 100 % of open

water (Table 5.6), were estimated monthly between 1986 and 2007 using eq. 5.5-5.9 and temperature data from Table 5.4. In the 1980s, surface water of the Beaufort Sea was reported to be under-saturated with α-HCH, and $f_w/f_a = 0.76$ indicated the potential for deposition (Bidleman *et al.*, 1995). Fugacity ratios in this study are consistent with findings reported by other researchers and show that the air-water α-HCH exchange direction in the Beaufort Sea has switched from deposition in the 1980s to volatilization in the early 1990s due to decreasing use and air concentrations of α-HCH (Table 5.5; Bidleman *et al.*, 1995; Jantunen and Bidleman, 1995; Jantunen and Bidleman, 1996; Jantunen and Bidleman, 1997; Jantunen *et al.*, 2008; Wong *et al.*, 2011). α-HCH fugacity ratios indicate only the direction of net exchange favoured by thermodynamics. The actual flux must take into account the exchange rates occurring for the fraction of open water (*FOW*) available for exchange.

To estimate the monthly *FOW* in the Beaufort Sea, Canadian Ice Service (CIS) sea ice concentration charts (reported weekly) were used (http://ice-glaces.ec.gc.ca). Fraction of open water (< 1/10 ice aerial extent) was estimated visually between 1986 and 2007 (Table 5.7). An ice chart from August 2004, where FOW was estimated at 40 %, is presented as an example in Figure 5.6. Total outputs/inputs of α-HCH from/to the PML due to air-water exchange were calculated monthly using eq. 5.10 and the fraction of open water estimated in Table 5.7 (Table 5.8).

Between 1986 and 1993, a net of 1.5 tonnes of α-HCH were out-gassed into the atmosphere from the PML due to air-water gas exchange, accounting for only about 2 % of the total loading of this chemical. Between 1994 and 2007, net of about 12.5 tonnes of α-HCH was out-gassed back to the atmosphere. In general, atmospheric evasion turned out to be a minor removal route of α-HCH in the Beaufort Sea between 1994 and 2007, representing about 15 % of the total loss of this chemical.

Table 5.4 Monthly average flow of the Mackenzie River (*Flow*) along with river water temperature (T_{rw}), Beaufort Sea surface water temperature (T_{sw}), air temperature (T_a) and Henry's law constant for river water (H_r) and seawater (H_{sw})

Month	*Flow* [km^3/month][a]	T_{rw} [K][b]	T_{sw} [K][c]	T_a [K][d]	H_r [Pa · m^3/mol][e]	H_{sw} [Pa · m^3/mol][f]
J	10.7	273.15	271.25	245.15	0.061	0.086
F	9.7	273.15	271.25	246.15	0.061	0.086
M	10.7	273.15	271.25	250.15	0.061	0.086
A	10.4	273.15	272.68	260.15	0.061	0.098
M	40.2	275.65	274.10	273.35	0.078	0.112
J	64.8	283.15	275.53	284.15	0.154	0.127
J	56.2	288.65	276.95	287.15	0.250	0.144
A	37.5	287.65	275.05	284.15	0.229	0.122
S	33.7	282.15	273.15	277.15	0.141	0.102
O	24.1	275.65	271.25	265.15	0.078	0.086
N	18.1	273.15	271.25	252.15	0.061	0.086
D	13.4	273.15	271.25	247.15	0.061	0.086

[a]the average flow of the Mackenzie River from 1973 to 1993 (Macdonald, 2000); [b]the temperature record from Arctic Red River from 1960 to 1993 (Macdonald, 2000); [c]between October and March it was assumed that the surface water was at freezing (~1.9 °C), in July T_{sw} was averaged from a relatively warm and cold summer of 1974 and 1975 (Macdonald *et al.*, 1987), between March and July, and July and October a linear change in T_{sw} was assumed; [d]daily average temperature recorded in Inuvik, NWT, Canada between 1971 and 2000 (www.eldoradocountyweather.com); [e]H_r as a function of T_{rw} [K] for deionized water, ($\log H = -3098/T_{rw} + 10.13$) (Sahsuvar *et al.*, 2003); [f]H_{sw} as a function of T_{sw} [K] for sea water, ($\log H = -2969/T_{sw} + 9.88$) (Kuklick *et al.*, 1991)

Table 5.5 Monthly α-HCH fugacity ratios (f_w/f_a) in the Beaufort Sea calculated using eq. 5.5 and 5.6, α-HCH concentrations in the air and surface water of the Beaufort Sea from this table, and meteorological data from Table 5.4

Year	α-HCH$_{air}$ [pg/m^3]	α-HCH$_{water}$ [ng/L]	f_w/f_a													
			J	F	M	A	M	J	J	A	S	O	N	D	Mean	SE
1986	352[a]	3.970[a]	0.48	0.47	0.47	0.51	0.56	0.61	0.68	0.58	0.50	0.44	0.46	0.47	0.52	0.02
1987	340[b]	4.236*	0.53	0.52	0.52	0.56	0.61	0.67	0.75	0.64	0.55	0.49	0.51	0.52	0.57	0.02
1988	294*	4.503*	0.65	0.64	0.63	0.69	0.75	0.82	0.92	0.79	0.68	0.60	0.63	0.64	0.70	0.03
1989	249*	4.769*	0.81	0.80	0.79	0.87	0.94	1.03	1.16	0.99	0.85	0.75	0.79	0.80	0.88	0.04
1990	203*	5.035*	1.05	1.04	1.03	1.12	1.22	1.33	1.50	1.28	1.10	0.97	1.02	1.04	1.14	0.05
1991	157*	5.301*	1.42	1.42	1.40	1.53	1.66	1.82	2.04	1.74	1.49	1.32	1.39	1.41	1.55	0.06
1992	112*	5.568*	2.10	2.09	2.06	2.25	2.45	2.67	3.00	2.57	2.20	1.94	2.04	2.08	2.29	0.09
1993	66[c,d,e]	5.834*	3.73	3.71	3.66	4.01	4.36	4.75	5.33	4.56	3.91	3.45	3.63	3.70	4.07	0.16
1994	63[c,e,f]	6.100[j]	4.09	4.07	4.00	4.39	4.77	5.21	5.84	5.00	4.29	3.78	3.97	4.05	4.45	0.18
1995	56[e]	5.073*	3.82	3.81	3.75	4.10	4.46	4.87	5.46	4.68	4.01	3.53	3.72	3.79	4.17	0.17
1996	55[e]	4.046*	3.10	3.09	3.04	3.33	3.63	3.95	4.44	3.80	3.26	2.87	3.02	3.08	3.38	0.14
1997	47[e]	3.019[k]	2.71	2.70	2.66	2.91	3.17	3.45	3.87	3.32	2.84	2.51	2.64	2.69	2.95	0.12
1998	45[e]	3.021*	2.83	2.82	2.78	3.04	3.31	3.61	4.05	3.47	2.97	2.62	2.75	2.81	3.09	0.13
1999	51[e,g]	3.023*	2.50	2.49	2.45	2.69	2.92	3.19	3.58	3.06	2.62	2.31	2.43	2.48	2.73	0.11
2000	25[e]	3.025*	5.11	2.49	2.45	2.69	2.92	3.19	3.58	3.06	2.62	2.31	2.43	2.48	2.94	0.23
2001	20[e]	3.026*	6.38	6.36	6.26	6.86	7.46	8.13	9.13	7.81	6.70	5.90	6.21	6.33	6.96	0.28
2002	11[e]	3.028*	11.62	11.57	11.38	12.47	13.57	14.80	16.60	14.22	12.19	10.74	11.29	11.52	12.66	0.51
2003	17[e,h]	3.030*	7.52	7.49	7.37	8.08	8.78	9.58	10.75	9.20	7.89	6.95	7.31	7.46	8.20	0.33
2004	11[e]	3.032[l]	11.63	11.58	11.40	12.49	13.58	14.82	16.63	14.23	12.20	10.75	11.31	11.54	12.68	0.51
2005	13[e]	2.503*	8.12	8.09	7.96	8.72	9.49	10.35	11.61	9.94	8.52	7.51	7.90	8.06	8.86	0.36
2006	11*	1.973*	4.50	4.48	4.41	4.83	5.26	5.73	6.43	5.51	4.72	4.16	4.37	4.46	4.91	0.20
2007	8[i]	1.444*	7.62	7.59	7.46	8.18	8.90	9.70	10.89	9.32	7.99	7.04	7.40	7.55	8.30	0.34

*estimated assuming linear decrease due to lack of data; [a]Hargrave *et al.*, 1988, sea water at 10 m; [b]Patton *et al.*, 1989; [c]Halsall *et al.*, 1998; [d]Jantunen and Bidleman, 1995; [e]Hung *et al.*, 2010; [f]Bailey *et al.*, 2000; [g]Jantunen *et al.*, 2008; [h]this study; [i]Pućko *et al.*, 2011; [j]Macdonald and Carmack, 1994, water at 20 m; [k]Macdonald *et al.*, 1999a, water at 10 m; [l]this study, water at 5 m; f_w/f_a – α-HCH fugacity ratio (values > 1 indicate net volatilization and values < 1 net deposition); SE – standard error

Table 5.6 Monthly α-HCH potential fluxes in the Beaufort Sea calculated using eq. 5.7-5.9

Year	F_p [ng/m^2 · day]*													
	J	F	M	A	M	J	J	A	S	O	N	D	Mean	SE
1986	-70.82	-71.08	-72.11	-66.07	-60.02	-53.20	-43.20	-56.42	-67.66	-75.67	-72.61	-71.34	-65.02	2.83
1987	-61.91	-62.18	-63.28	-56.84	-50.38	-43.10	-32.44	-46.54	-58.54	-67.08	-63.81	-62.46	-55.71	3.02
1988	-39.92	-40.22	-41.38	-34.54	-27.67	-19.93	-8.60	-23.59	-36.34	-45.42	-41.95	-40.51	-33.34	3.21
1989	-18.34	-18.65	-19.88	-12.64	-5.36	2.83	14.84	-1.04	-14.55	-24.17	-20.48	-18.96	-11.37	3.40
1990	3.63	3.30	2.00	9.65	17.33	25.98	38.66	21.89	7.63	-2.52	1.36	2.97	10.99	3.59
1991	25.59	25.25	23.88	31.93	40.02	49.13	62.47	44.82	29.81	19.12	23.21	24.90	33.34	3.77
1992	47.19	46.83	45.39	53.85	62.34	71.91	85.93	67.39	51.62	40.39	44.69	46.46	55.33	3.96
1993	69.16	68.78	67.27	76.14	85.03	95.06	109.75	90.32	73.80	62.03	66.54	68.40	77.69	4.15
1994	74.62	74.22	72.65	81.92	91.22	101.70	117.06	96.74	79.47	67.17	71.88	73.82	83.54	4.34
1995	60.67	60.34	59.03	66.74	74.47	83.19	95.97	79.07	64.71	54.47	58.39	60.01	68.09	3.61
1996	44.42	44.16	43.11	49.26	55.43	62.38	72.57	59.09	47.64	39.48	42.60	43.89	50.34	2.88
1997	30.86	30.66	29.88	34.47	39.07	44.26	51.86	41.81	33.26	27.17	29.50	30.46	35.27	2.15
1998	31.66	31.46	30.68	35.27	39.88	45.07	52.68	42.61	34.06	27.97	30.30	31.26	36.07	2.15
1999	29.39	29.19	28.41	33.00	37.61	42.81	50.42	40.35	31.79	25.69	28.03	28.99	33.81	2.15
2000	39.40	29.19	28.41	33.00	37.61	42.81	50.42	40.35	31.79	25.69	28.03	28.99	34.64	2.16
2001	41.34	41.14	40.36	44.95	49.57	54.77	62.39	52.31	43.74	37.64	39.98	40.94	45.76	2.15
2002	44.82	44.62	43.84	48.44	53.06	58.26	65.89	55.80	47.23	41.12	43.46	44.43	49.25	2.16
2003	42.55	42.35	41.57	46.18	50.80	56.00	63.63	53.54	44.96	38.85	41.19	42.16	46.98	2.16
2004	44.89	44.69	43.91	48.51	53.14	58.35	65.98	55.88	47.30	41.18	43.52	44.49	49.32	2.16
2005	35.55	35.39	34.74	38.55	42.36	46.66	52.97	44.63	37.54	32.49	34.43	35.22	39.21	1.78
2006	14.78	14.70	14.40	16.18	17.97	19.98	22.94	19.03	15.71	13.34	14.25	14.62	16.49	0.84
2007	20.32	20.22	19.85	22.04	24.25	26.73	30.36	25.55	21.47	18.55	19.67	20.13	22.43	1.03

*estimated assuming wind speed of 5 m/s, negative values mean deposition, positive volatilization; SE – standard error

Table 5.7 Monthly estimation of the fraction of open water (*FOW*) in the Beaufort Sea between 1986 and 2007

Year	*FOW*											
	J	F	M	A	M	J	J	A	S	O	N	D
1986	0	0	0	0	0.05	0.05	0.05	0.2	0.5	0.05	0	0
1987	0	0	0	0	0	0.05	0.5	0.8	0.6	0.6	0	0
1988	0	0	0	0	0	0.1	0.6	0.3	0.5	0.05	0	0
1989	0	0	0	0	0	0.1	0.05	0.15	0.5	0.6	0	0
1990	0	0	0	0	0.07	0.07	0.5	0.4	0.25	0.05	0	0
1991	0	0	0	0	0.1	0.05	0.03	0.05	0.03	0	0	0
1992	0	0	0	0	0	0	0.05	0.2	0.4	0	0	0
1993	0	0	0	0	0.05	0.15	0.8	0.8	0.75	0.6	0	0
1994	0	0	0	0	0	0	0.7	0.3	0.4	0.15	0	0
1995	0	0	0	0	0.25	0.45	0.85	0.75	0.6	0.6	0	0
1996	0	0	0	0	0	0	0.07	0.1	0.05	0	0	0
1997	0	0	0	0	0	0.15	0.1	0.2	0.7	0.1	0	0
1998	0	0	0	0	0.03	0.5	0.8	0.6	0.6	0.6	0	0
1999	0	0	0	0	0.03	0.05	0.07	0.4	0.15	0	0	0
2000	0	0	0	0	0	0	0.03	0.05	0.5	0.07	0	0
2001	0	0	0	0	0	0	0.07	0.1	0.2	0.07	0	0
2002	0	0	0	0	0.03	0	0.07	0.07	0.45	0.2	0	0
2003	0	0	0	0	0	0.15	0.15	0.2	0.2	0.15	0	0
2004	0	0	0	0	0	0.1	0.2	0.4	0.4	0.15	0	0
2005	0	0	0	0	0	0.15	0.07	0.15	0.35	0.1	0	0
2006	0	0	0	0	0	0	0.05	0.3	0.4	0.45	0	0
2007	0	0	0	0	0	0.1	0.35	0.15	0.3	0.2	0	0

Table 5.8 Monthly net α-HCH fluxes in the Beaufort Sea calculated using eq. 5.10, and data from Table 5.7

Year	*F* [t/month]*												Sum [t/yr]
	J	F	M	A	M	J	J	A	S	O	N	D	
1986	0.00	0.00	0.00	0.00	-0.04	-0.04	-0.03	-0.16	-0.45	-0.05	0.00	0.00	-0.77
1987	0.00	0.00	0.00	0.00	0.00	-0.03	-0.22	-0.52	-0.47	-0.56	0.00	0.00	-1.80
1988	0.00	0.00	0.00	0.00	0.00	-0.03	-0.07	-0.10	-0.24	-0.03	0.00	0.00	-0.47
1989	0.00	0.00	0.00	0.00	0.00	0.00	0.01	0.00	-0.10	-0.20	0.00	0.00	-0.29
1990	0.00	0.00	0.00	0.00	0.02	0.02	0.27	0.12	0.03	0.00	0.00	0.00	0.45
1991	0.00	0.00	0.00	0.00	0.06	0.03	0.03	0.03	0.01	0.00	0.00	0.00	0.16
1992	0.00	0.00	0.00	0.00	0.00	0.00	0.06	0.19	0.28	0.00	0.00	0.00	0.52
1993	0.00	0.00	0.00	0.00	0.06	0.19	1.22	1.00	0.74	0.52	0.00	0.00	3.73
1994	0.00	0.00	0.00	0.00	0.00	0.00	1.14	0.40	0.43	0.14	0.00	0.00	2.10
1995	0.00	0.00	0.00	0.00	0.26	0.50	1.13	0.82	0.52	0.45	0.00	0.00	3.69
1996	0.00	0.00	0.00	0.00	0.00	0.00	0.07	0.08	0.03	0.00	0.00	0.00	0.18
1997	0.00	0.00	0.00	0.00	0.00	0.09	0.07	0.12	0.31	0.04	0.00	0.00	0.63
1998	0.00	0.00	0.00	0.00	0.02	0.30	0.58	0.35	0.27	0.23	0.00	0.00	1.76
1999	0.00	0.00	0.00	0.00	0.02	0.03	0.05	0.22	0.06	0.00	0.00	0.00	0.38
2000	0.00	0.00	0.00	0.00	0.00	0.00	0.02	0.03	0.21	0.02	0.00	0.00	0.29
2001	0.00	0.00	0.00	0.00	0.00	0.00	0.06	0.07	0.12	0.04	0.00	0.00	0.29
2002	0.00	0.00	0.00	0.00	0.02	0.00	0.06	0.05	0.29	0.11	0.00	0.00	0.54
2003	0.00	0.00	0.00	0.00	0.00	0.11	0.13	0.15	0.12	0.08	0.00	0.00	0.59
2004	0.00	0.00	0.00	0.00	0.00	0.08	0.18	0.31	0.25	0.09	0.00	0.00	0.91
2005	0.00	0.00	0.00	0.00	0.00	0.09	0.05	0.09	0.18	0.05	0.00	0.00	0.46
2006	0.00	0.00	0.00	0.00	0.00	0.00	0.02	0.08	0.08	0.08	0.00	0.00	0.26
2007	0.00	0.00	0.00	0.00	0.00	0.04	0.15	0.05	0.09	0.05	0.00	0.00	0.37

*negative values mean deposition, positive volatilization

Figure 5.6 CIS ice chart from August 2004 presented as an example of the open water fraction estimation

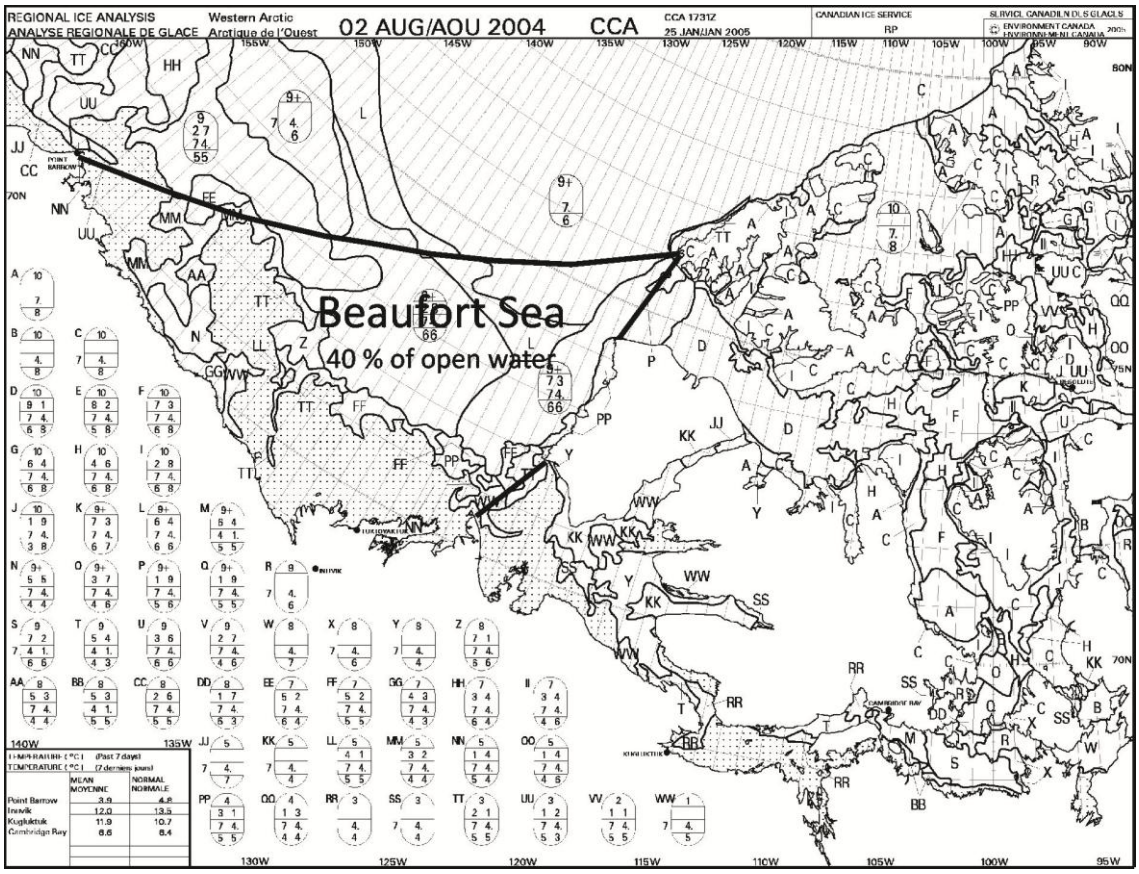

5.4.7 *The influence of river inflow on the α-HCH inventory in the PML*

The freshwater inflow from Mackenzie, Trail Valley and Anderson Rivers to the Beaufort Sea was estimated at 337 km^3/year, with the Mackenzie River accounting for almost 98 % of that value (Macdonald *et al.*, 1999b). Thus, Trail and Anderson Rivers were neglected in the further analysis. There are marked seasonal variations in continental runoff in the Beaufort Sea, where the majority of freshwater inflow takes place in May and July (Macdonald *et al.*, 1999b; McClelland *et al.*, 2010). In July 2008, we measured the α-HCH concentration in the Mackenzie River at 0.11 ± 0.01 (SE) ng/L (Table 5.1). To describe the saturation state of water relative to the partial pressure in air, α-HCH fugacity ratios (f_w/f_a) were calculated using eq. 5.5 and 5.6, the average water and air temperatures measured in this study of 15 °C and 9 °C, respectively, and

the α-HCH concentration in air of 12 pg/m^3 reported by Wong *et al.* (2011) for the region (excluding relatively high values associated with regional ice break-up). The water concentration was found to be very close to equilibrium with the overlying air as the fugacity ratio equaled 0.97. Historical α-HCH concentrations in the Mackenzie River were predicted monthly based on the available air concentrations, hydrographic and temperature data (Table 5.4) using eq. 5.11 with the assumption that α-HCH was at equilibrium partitioning with air (Table 5.9). The predicted concentrations are in good agreement with a few measurements from the Mackenzie River available in the literature (reviewed in Li *et al.*, 2004; Figure 5.7).

Figure 5.7 α-HCH concentrations in the Mackenzie River calculated in the summer (July) based on air concentrations and an assumption of equilibrium partitioning between water and air (Table 5.9), and ranges of measured values in the Mackenzie River from [a]Li *et al.*, 2004 (reviewed) and this study

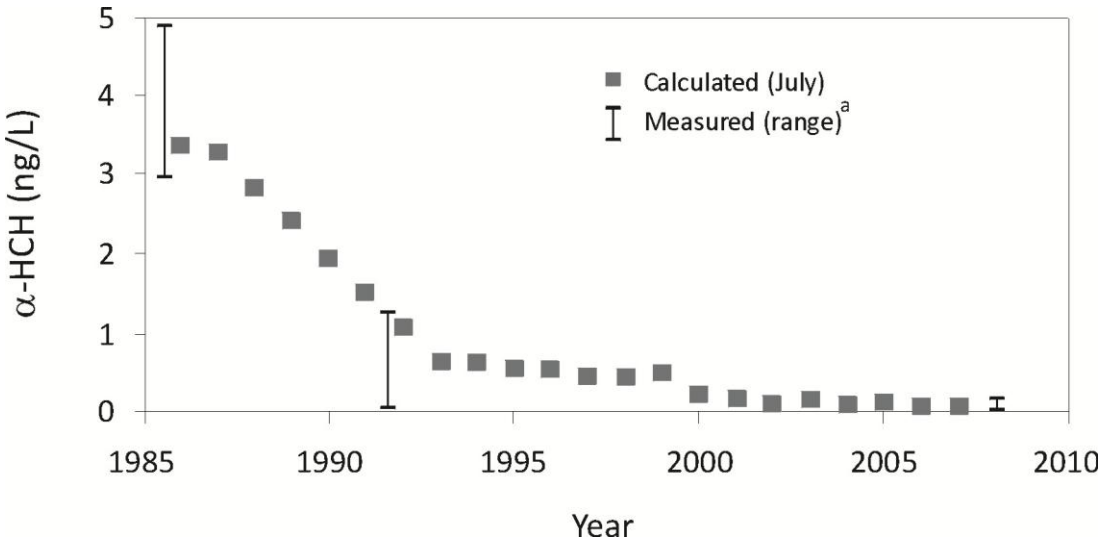

Table 5.9 Monthly α-HCH concentrations in the Mackenzie River water (α-HCH_{river}) between 1986 and 2007 estimated using eq. 5.11, α-HCH concentrations in air (α-HCH_{air}) from the literature (averaged in years with more than one study available) and hydrographic and temperature data from Table 5.4

Year	α-HCH_{air} [pg/m^3]	α-HCH_{river} [ng/L]													
		J	F	M	A	M	J	J	A	S	O	N	D	Mean	SE
1986	352[a]	11.683	11.730	11.921	12.397	10.279	5.384	3.367	3.630	5.742	9.971	12.016	11.778	9.158	1.02
1987	340[b]	11.284	11.330	11.514	11.975	9.929	5.200	3.252	3.506	5.546	9.631	11.607	11.376	8.846	0.99
1988	294*	9.758	9.797	9.957	10.355	8.586	4.497	2.812	3.032	4.796	8.328	10.036	9.837	7.649	0.85
1989	249*	8.264	8.298	8.433	8.770	7.271	3.809	2.381	2.568	4.062	7.053	8.500	8.332	6.478	0.72
1990	203*	6.737	6.765	6.875	7.150	5.928	3.105	1.941	2.094	3.311	5.750	6.930	6.792	5.282	0.59
1991	157*	5.211	5.232	5.317	5.530	4.585	2.401	1.502	1.619	2.561	4.447	5.359	5.253	4.085	0.46
1992	112*	3.717	3.732	3.793	3.945	3.271	1.713	1.071	1.155	1.827	3.173	3.823	3.748	2.914	0.33
1993	66[c,d,e]	2.190	2.199	2.235	2.325	1.927	1.009	0.631	0.681	1.077	1.870	2.253	2.208	1.717	0.19
1994	63[c,e,f]	2.091	2.099	2.134	2.219	1.840	0.964	0.603	0.650	1.028	1.785	2.151	2.108	1.639	0.18
1995	56[e]	1.859	1.866	1.896	1.972	1.635	0.857	0.536	0.578	0.913	1.586	1.912	1.874	1.457	0.16
1996	55[e]	1.825	1.833	1.863	1.937	1.606	0.841	0.526	0.567	0.897	1.558	1.878	1.840	1.431	0.16
1997	47[e]	1.560	1.566	1.592	1.655	1.373	0.719	0.450	0.485	0.767	1.331	1.604	1.573	1.223	0.14
1998	45[e]	1.494	1.500	1.524	1.585	1.314	0.688	0.430	0.464	0.734	1.275	1.536	1.506	1.171	0.13
1999	51[e,g]	1.693	1.700	1.727	1.796	1.489	0.780	0.488	0.526	0.832	1.445	1.741	1.706	1.327	0.15
2000	25[e]	0.830	0.833	0.847	0.880	0.730	0.382	0.239	0.258	0.408	0.708	0.853	0.836	0.650	0.07
2001	20[e]	0.664	0.666	0.677	0.704	0.584	0.306	0.191	0.206	0.326	0.567	0.683	0.669	0.520	0.06
2002	11[e]	0.365	0.367	0.373	0.387	0.321	0.168	0.105	0.113	0.179	0.312	0.376	0.368	0.286	0.03
2003	17[e,h]	0.564	0.567	0.576	0.599	0.496	0.260	0.163	0.175	0.277	0.482	0.580	0.569	0.442	0.05
2004	11[e]	0.365	0.367	0.373	0.387	0.321	0.168	0.105	0.113	0.179	0.312	0.376	0.368	0.286	0.03
2005	13[e]	0.431	0.433	0.440	0.458	0.380	0.199	0.124	0.134	0.212	0.368	0.444	0.435	0.338	0.04
2006	11*	0.365	0.367	0.373	0.387	0.321	0.168	0.105	0.113	0.179	0.312	0.376	0.368	0.286	0.03
2007	8[i]	0.266	0.267	0.271	0.282	0.234	0.122	0.077	0.083	0.130	0.227	0.273	0.268	0.208	0.02

[*]estimated assuming linear decrease due to lack of data; [a]Hargrave *et al.*, 1988, sea water at 10 m; [b]Patton *et al.*, 1989; [c]Halsall *et al.*, 1998; [d]Jantunen and Bidleman, 1995; [e]Hung *et al.*, 2010; [f]Bailey *et al.*, 2000; [g]Jantunen *et al.*, 2008; [h]this study; [i]Pućko *et al.*, 2011; SE – standard error

The total α-HCH loading to the PML of the Beaufort Sea from the Mackenzie River runoff, estimated monthly (Table 5.10), reached 12.1 tonnes between 1986 and 1993, 1.5 tonnes between 1994 and 1997, 1.2 tonnes between 1998 and 2004, and 0.2 tonnes between 2005 and 2007 (based on eq. 5.12). Comparison of these loadings with α-HCH inventories in the PML implies that river runoff was a minor α-HCH contributing factor prior to 1993, accounting for about 15 % of the total loading. After 1993, when atmospheric levels declined rapidly followed by lower concentrations in the rivers, river runoff became an even less significant source of α-HCH, supplying only 2.9 tonnes between 1994 and 2007 or about 3 % compared to the total loss of this molecule.

5.4.8 *The influence of the ice formation on the α-HCH levels in the PML*

The vertical distribution of α-HCH in the water column was measured in October – November 2007 (CFL). During this time, sea ice started forming in the Beaufort Sea, so that three open water stations and five ice-covered stations were sampled. At open water stations, α-HCH concentrations were uniform throughout the PML (Figure 5.8, Table 5.1). α-HCH concentration measured under newly-formed ice (1.49 ± 0.17 (SE) ng/L) was significantly higher than the levels measured at 5 m (1.00 ± 0.10 (SE) ng/L) (Figure 5.8, paired T-test, α = 95 %, p = 0.05). This phenomenon was not noted at open water stations where the average α-HCH concentration in the surface water and at 5 m were essentially the same (0.70 ± 0.05 (SE) ng/L and 0.73 ± 0.01 (SE) ng/L, respectively (paired T-test, α = 95 %, p = 0.66)).

As ice forms, only a portion of HCHs from sea water is being entrapped within the ice structure (Pućko *et al.*, 2010), and within the first several days of ice formation a significant fraction of brine enriched with HCHs is rejected from ice to the underlying

Table 5.10 Inputs of α-HCH from Mackenzie River to the Beaufort Sea, $River_{\alpha\text{-HCH}}^{I}$, estimated using eq. 5.12, and data from Table 5.9

Year	$River_{\alpha\text{-HCH}}^{I}$ [t/month]												$River_{\alpha\text{-HCH}}^{I}$ [t/year]
	J	F	M	A	M	J	J	A	S	O	N	D	
1986	0.13	0.11	0.13	0.13	0.41	0.35	0.19	0.14	0.19	0.24	0.22	0.16	2.39
1987	0.12	0.11	0.12	0.12	0.40	0.34	0.18	0.13	0.19	0.23	0.21	0.15	2.31
1988	0.10	0.09	0.11	0.11	0.34	0.29	0.16	0.11	0.16	0.20	0.18	0.13	2.00
1989	0.09	0.08	0.09	0.09	0.29	0.25	0.13	0.10	0.14	0.17	0.15	0.11	1.69
1990	0.07	0.07	0.07	0.07	0.24	0.20	0.11	0.08	0.11	0.14	0.13	0.09	1.38
1991	0.06	0.05	0.06	0.06	0.18	0.16	0.08	0.06	0.09	0.11	0.10	0.07	1.07
1992	0.04	0.04	0.04	0.04	0.13	0.11	0.06	0.04	0.06	0.08	0.07	0.05	0.76
1993	0.02	0.02	0.02	0.02	0.08	0.07	0.04	0.03	0.04	0.05	0.04	0.03	0.45
1994	0.02	0.02	0.02	0.02	0.07	0.06	0.03	0.02	0.03	0.04	0.04	0.03	0.43
1995	0.02	0.02	0.02	0.02	0.07	0.06	0.03	0.02	0.03	0.04	0.03	0.03	0.38
1996	0.02	0.02	0.02	0.02	0.06	0.05	0.03	0.02	0.03	0.04	0.03	0.02	0.37
1997	0.02	0.02	0.02	0.02	0.06	0.05	0.03	0.02	0.03	0.03	0.03	0.02	0.32
1998	0.02	0.01	0.02	0.02	0.05	0.04	0.02	0.02	0.02	0.03	0.03	0.02	0.31
1999	0.02	0.02	0.02	0.02	0.06	0.05	0.03	0.02	0.03	0.03	0.03	0.02	0.35
2000	0.01	0.01	0.01	0.01	0.03	0.02	0.01	0.01	0.01	0.02	0.02	0.01	0.17
2001	0.01	0.01	0.01	0.01	0.02	0.02	0.01	0.01	0.01	0.01	0.01	0.01	0.14
2002	0.00	0.00	0.00	0.00	0.01	0.01	0.01	0.00	0.01	0.01	0.01	0.00	0.07
2003	0.01	0.01	0.01	0.01	0.02	0.02	0.01	0.01	0.01	0.01	0.01	0.01	0.12
2004	0.00	0.00	0.00	0.00	0.01	0.01	0.01	0.00	0.01	0.01	0.01	0.00	0.07
2005	0.00	0.00	0.00	0.00	0.02	0.01	0.01	0.01	0.01	0.01	0.01	0.01	0.09
2006	0.00	0.00	0.00	0.00	0.01	0.01	0.01	0.00	0.01	0.01	0.01	0.00	0.07
2007	0.00	0.00	0.00	0.00	0.01	0.01	0.00	0.00	0.00	0.01	0.00	0.00	0.05

sea water through natural desalination mechanisms. The average concentration of α-HCH in the new and young ice (< 30 cm) was measured at 0.64 ng/L, while the α-HCH concentration in the corresponding under-ice sea water equaled 1.54 ng/L (Pućko *et al.*, 2010). Accordingly, the presence of a 30 cm thick ice cover could concentrate HCHs in the top 30 cm of the under-ice sea water by roughly 70 %. Thus, ice formation may be considered as an example of a solvent-depleting process (Macdonald *et al.*, 2002) that produces the observed 50 % increase in the α-HCH concentration in the water just beneath the ice.

Figure 5.8 Vertical profiles of α-HCH concentration in the top 120 m of the water column at different stations in October-November 2007 (CFL); stations were sorted from left to right by increasing ice thickness; 310- open water, 1200- 13 cm thick ice

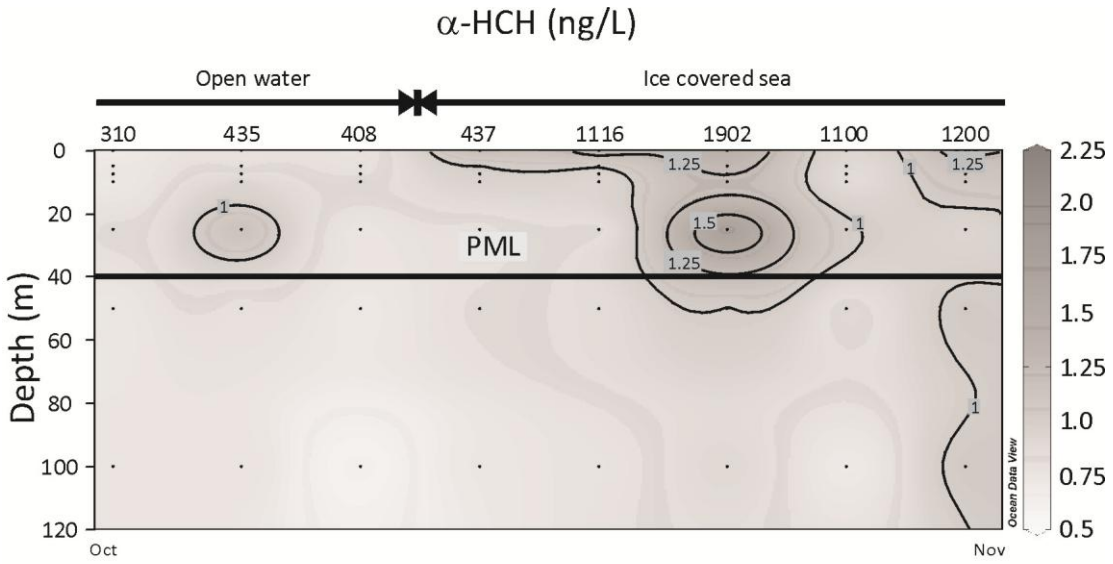

5.4.9 *The influence of ice export on the α-HCH inventory in the PML*

Ice export has been shown to account for less than 1.5 % of the total loss of α-HCH from the Arctic Ocean (Barrie *et al.*, 1992; Macdonald *et al.*, 2000). To confirm that this route is also negligible for the Beaufort Sea, annual losses of α-HCH with ice

export (Table 5.11) were calculated between 1986 and 2007 using eq. 5.13 and the first-year ice export estimated at 10 km^3/year (Macdonald *et al.*, 2010). α-HCH concentrations in the first-year sea ice meltwater were measured at 0.261 ng/L in the Beaufort Sea in 2007/2008 (Pućko *et al.*, 2010), or at 0.235 ng/dm^3 of ice correcting for ice density of about 0.9 kg/L (Timco and Frederking, 1996). Concentrations in ice prior to 2007 were estimated proportionally to the surface water concentration change presented in the Table 5.5 (Table 5.11). Ice export has been a negligible α-HCH removal route for the Beaufort Sea, equaling only 0.1 % of the total loading of this chemical between 1986 and 1993, and less than 0.1 % of its total loss between 1994 and 2007.

5.4.10 *Elimination of α-HCH from the Beaufort Sea*

Between 1993 and 2007, the decrease in α-HCH inventories could be explained almost entirely by degradation both in the PML and the PL of the Beaufort Sea (Table 5.3, Figure 5.5). An exception was a period between 1997 and 2004, when the inventories did not decrease as much as predicted by degradation kinetics. One potential explanation could be that samples in 2004 were collected from an area relatively high in α-HCH compared to the average for the Beaufort Sea. Air-water gas exchange and river runoff had minor effects on inventories of α-HCH in the PML after 1993, with a combined effect of 12 % compared to the total decline. Assuming no major changes in the degradation kinetics and hydrological conditions in the Beaufort Sea in the future, long-term elimination of α-HCH from the Beaufort Sea could be well predicted based exclusively on degradation. According to our calculations, α-HCH in the Beaufort Sea could be virtually eliminated by 2020, with concentrations in 2040 dropping to < 0.006 ng/L and < 0.004 ng/L in the PML and the PL, respectively (Table 5.3, Figure 5.5).

These results compare well with those by Li *et al.* (2004), which predicted elimination of the majority of α-HCH from the Arctic Ocean by 2020.

Table 5.11 Annual losses of α-HCH from the Beaufort Sea due the ice export ($Ice_{\alpha\text{-}HCH}^{O}$) estimated using eq. 5.13

Year	$\alpha\text{-}HCH_{ice}$* [ng/dm^3]	$Ice_{\alpha\text{-}HCH}^{O}$ [t/yr]
1986	0.646	0.01
1987	0.689	0.01
1988	0.733	0.01
1989	0.776	0.01
1990	0.819	0.01
1991	0.863	0.01
1992	0.906	0.01
1993	0.949	0.01
1994	0.993	0.01
1995	0.826	0.01
1996	0.658	0.01
1997	0.491	0.00
1998	0.492	0.00
1999	0.492	0.00
2000	0.492	0.00
2001	0.492	0.00
2002	0.493	0.00
2003	0.493	0.00
2004	0.493	0.00
2005	0.407	0.00
2006	0.321	0.00
2007	0.235[a]	0.00

*estimated proportionally to the surface water change (Table 5.5) prior to 2007; [a]Pućko *et al.*, 2011

Between 1986 and 1993, the inventory of α-HCH increased both in the PML and the PL of the Beaufort Sea (Figure 5.5, Table 5.3). The potential of air-water gas exchange and river runoff to significantly impact the inventory in the PML was relatively low, and the combined effect could account only for about 12 % of the total loading. This implies that ocean currents must have been a major source of this chemical to the Beaufort Sea at that time, and compares well with the mass balance model of α-HCH in the Arctic Ocean in mid 1980-s by Barrie and colleagues (1992).

The decrease of α-HCH emissions in the mid-1980s was followed by a remarkably rapid decline in atmospheric concentrations in the Arctic (Li, 1999; Li *et al.*, 2002; Figure 5.4). However, it has taken considerably longer for inventories in the Beaufort Sea to respond, and these even continued to increase into the 1990s. Elimination of the majority of α-HCH from sea water will take significantly longer than from the atmosphere, with the lag of approximately two decades set by degradation rates (Figures 5.4 and 5.5).

5.5 Acknowledgements

We would like to thank the crew of CCGS *Amundsen* and CCGS *Nahidik* for the field work assistance without which the collection of samples for this paper would not be possible. We thank Joanne DeLaronde, Allison MacHutchon, Paul Helm, and Debbie Armstrong for their long hours collecting the samples during the CASES and CFL expeditions. We also thank Dr. Yves Gratton and all the CTD system SBE *911plus* operators for water samples collection during CASES and CFL. Finally, we thank the Canadian program office of the International Polar Year, the Natural Sciences and Engineering Research Council (NSERC), Canada Foundation for Innovation (CFI), Canada Research Chairs (CRC), the Department of Fisheries and Oceans Canada, ArcticNet, the Nahidik program, and the University of Manitoba for funding.

5.6 References

Bailey, R.; L. A. Barrie; C. J. Halsall; P. Fellin, and D. C. G. Muir. 2000. Atmospheric organochlorine pesticides in the western Canadian Arctic: evidence of transpacific transport. *J. Geophys. Res.* **105:** 11805-11811.

Barrie, L. A.; D. Gregor; B. Hargrave; R. Lake; D. Muir; R. Shearer; B. Tracey, and T. Bidleman. 1992. Arctic contaminants: sources, occurrence and pathways. *Sci. Total Environ.* **122:** 1-74.

Bidleman, T. F.; L. M. Jantunen; L. R. Falconer; L. A. Barrie, and P. Fellin. 1995. Decline of hexachlorocyclohexane in the Arctic atmosphere and reversal of air-sea gas exchange. *Geophys. Res. Lett.* **22:** 219-222.

Bidleman, T. F.; H. Kylin; L. M. Jantunen; P. A. Helm, and R. W. Macdonald. 2007. Hexachlorocyclohexanes in the Canadian Archipelago. 1. Spatial Distribution and Pathways of α-, β-, and γ-HCHs in Surface Water. *Environ. Sci. Technol.* **41:** 2688-2695.

Carmack, E. C.; K. Aagaard; J. H. Swift; R. W. Macdonald; F. A. McLaughlin; E. P. Jones; R. D. Perkin; J. N. Smith, and K. L. K. Ellis. 1997. Changes in temperature and tracer distributions within the Arctic Ocean: results from the 1994 Arctic Ocean section. *Deep-Sea Res. II.* **44:** 1487-1502.

Halsall, C. J.; R. Bailey; G. A. Stern; L. A. Barrie; P. Fellin; D. C. G. Muir; B. Rosenberg; F. Ya. Rovinsky; E. Ya. Kononov, and B. Pastukhov. 1998. Multi-year observations of organohalogen pesticides in the Arctic atmosphere. *Environ. Pollut.* **102:** 51-62.

Hargrave, B. T.; G. A. Phillips; W. P. Vass; P. Bruecker; H. E. Welch, and T. D. Siferd. 2000. Seasonality in Bioaccumulation of Organochlorines in Lower Trophic Level Arctic Marine Biota. *Environ. Sci. Technol.* **34:** 980-987.

Hargrave, B. T.; W. P. Vass; P. E. Erickson, and B. R. Fowler. 1988. Atmospheric transport of organochlorines to the Arctic Ocean. *Tellus.* **40B:** 480-493.

Harner, T.; H. Kylin; T. F. Bidleman, and W. M. J. Strachan. 1999. Removal of a- and g-hexachlorocyclohexane and enantiomers of a-hexachlorocyclohexane in the Eastern Arctic Ocean. *Environ. Sci. Technol.* **33:** 1157-1164.

Hinckley, D. A.; T. F. Bidleman, and C. P. Rice. 1991. Atmospheric Organochlorine Pollutants and Air-Sea Exchange of Hexachlorocyclohexane in the Bering and Chukchi Seas. *J. Geophys. Res.* **96:** 7201-7213.

Hung, H.; R. Kallenborn; K. Breivik; Y. Su; E. Brorström-Lundén; K. Olafsdottir; J. M. Thorlacius; S. Leppänen; R. Bossi; H. Skov; S. Manø; G. W. Patton; G. Stern; E. Sverko, and P. Fellin. 2010. Atmospheric monitoring of organic pollutants in the Arctic under the Arctic Monitoring and Assessment Programme (AMAP): 1993–2006. *Sci. Total Environ.* **48:** 2854-2873.

Iwata, H.; S. Tanabe; N. Sakal, and R. Tatsukawa. 1993. Distribution of Persistent Organochlorines in the Oceanic Air and Surface Seawater and the Role of Ocean on Their Global Transport and Fate. *Environ. Sci. Technol.* **27:** 1080-1098.

Jakobsson, M. 2002. Hypsometry and volume of the Arctic Ocean and its constituent seas. *Geochem. Geophys. Geosyst.* **3:** doi:10.1029/2001GC000302.

Jantunen L. M. and T. F. Bidleman. 1995. Reversal of the Air-Water Gas Exchange Direction of Hexachlorocyclohexanes in the Bering and Chukchi Seas: 1993 versus 1988. *Environ. Sci. Technol.* **29:** 1081-1089.

Jantunen, L. M. and T. F. Bidleman. 1996. Air-water gas exchange of hexachlorocyclohexanes (HCHs) and the enantiomers of α-HCH in arctic regions. *J. Geophys. Res.* **101:** 28837-28846.

Jantunen, L. M. and T. F. Bidleman. 1997. Correction to "Air-water gas exchange of hexachlorocyclohexanes (HCHs) and the enantiomers of α-HCH in arctic regions". *J. Geophys. Res.* **102:** 19279-19282.

Jantunen, L. M.; P. A. Helm; T. F. Bidleman, and H. Kylin. 2005. Alpha-HCH Enantiomers Trace Sea-to-Air Gas Exchange During Ice Breakup in the Canadian Archipelago. *Organohal. Compd.* **67:** 1353-1355.

Jantunen, L. M.; P. A. Helm; H. Kylin, and T. F. Bidleman. 2008. Hexaclorocyclohexanes (HCHs) in the Canadian Archipelago. 2. Air-water gas exchange of α- and γ-HCH. *Environ. Sci. Technol.* **42:** 465-470.

Kucklick, J. R.; D. A. Hinckley, and T. F. Bidleman. 1991. Determination of Henry's law constants for hexachlorocyclohexanes in distilled water and artificial seawater as a function of temperature. *Mar. Chem.* **34:** 197-209.

Li, Y.-F. 1999. Global gridded technical hexachlorocyclohexane usage inventory using a global cropland as a surrogate. *J. Geophys. Res.* **104:** 23785-23797.

Li, Y.-F. and R. W. Macdonald. 2005. Sources and pathways of selected organochlorine pesticides to the Arctic and the effect of pathway divergence on HCH trends in biota: A review. *Sci. Total Environ.* **342:** 87-106.

Li, Y.-F.; R. W. Macdonald; L. M. M. Jantunen; T. Harner; T. F. Bidleman, and W. M. J. Strachan. 2002. The transport of β-hexachlorocyclohexane to the western Arctic Ocean: a contrast to α-HCH. *Sci. Total Environ.* **291:** 229-246.

Li, Y.-F.; R. W. Macdonald; J. M. Ma; H. Hung, and S. Venkatesh. 2004. Historical α-HCH budget in the Arctic Ocean: the Arctic mass balance model (AMBBM). *Sci. Total Environ.* **324:** 115-139.

Macdonald, R. W. 2000. Arctic estuaries and ice: a positive-negative estuarine couple. In *The Freshwater Budget of the Arctic Ocean*; Lewis, E. L., Ed.; Kluwer Academic Publishers: the Netherlands; pp. 623.

Macdonald, R. W.; L. G. Anderson; J. P. Christensen; L. A. Miller; I. P. Semiletov, and R. Stein. 2010. The Arctic Ocean. In *Carbon and Nutrient Fluxes in Continental*

Margins; Liu, K.-K.; L. Atkinson; R. Quinones, and L. Talaue-McManus, Eds.; Springer-Verlag: Berlin; pp. 744.

Macdonald, R. W.; A. L. Barrie; T. F. Bidleman; M. L. Diamond; D. J. Gregor; R. G. Semkin; W. M. J. Strachan; Y.-F. Li; F. Wania; M. Alaee; L. B. Alexeeva; S. M. Backus; R. Bailey; J. M. Bewers; C. Gobeil; C. J. Halsall; T. Harner; J. T. Hoff; L. M. M. Jantunen; W. L. Lockhart; D. Mackay; D. C. G. Muir; J. Pudykiewicz; K. J. Reimer; J. N. Smith; G. A. Stern; W. H. Schroeder; R. Wagemann, and M. B. Yunker. 2000. Contaminants in the Canadian Arctic: Five years of progress in understanding sources, occurrence and pathways. *Sci. Total Environ.* **254:** 93-236.

Macdonald, R. W. and J. M. Bewers. 1996. Contaminants in the arctic marine environment: priorities for protection. *ICES J. Mar. Sci.* **53:** 537-563.

Macdonald, R. W. and E. C. Carmack. 1994. Long-Range Transport of contaminants to the Canadian Basin. In *Synopsis of Research Conducted under the 1993/94 Northern Contaminants Program*; Murray, J. L. and R. G. Shearer, Eds., *Environ. Studies.* **72:** 104-108.

Macdonald, R. W.; E. C. Carmack; F. A. McLaughlin; K. Iseki; D. M. Macdonald, and M. C. O'Brien. 1989. Composition and Modification of Water Masses in the Mackenzie Shelf Estuary. *J. Geophys. Res.* **94:** 18057-18070.

Macdonald, R. W.; E. C. Carmack, and D. W. Paton. 1999b. Using the $\delta^{18}O$ composition in landfast ice as a record of arctic estuarine processes. *Mar. Chem.* **65:** 3-24.

Macdonald, R. W.; T. Harner, and J. Fyfe. 2005. Recent climate change in the Arctic and its impact on contaminant pathways and interpretation of temporal trend data. *Sci. Total Environ.* **342:** 5-86.

Macdonald, R. W.; D. Mackay, and B. Hickie. 2002. Contaminant amplification in the environment. *Environ. Sci. Technol.* **36:** 456A-462A.

Macdonald, R. W.; F. A. McLaughlin, and L. Adamson. 1997. The Arctic Ocean: the last refuge of volatile organochlorines. *Can. Chem. News.* **49:** 28-29.

Macdonald, R. W.; F. A. McLaughlin; G. A. Stern; E. C. Carmack; D. Paton; M. O'Brien; D. Tuele; D. Sieberg, and H. Welch. 1999a. The seasonal cycle of organochlorine concentrations in the Canada Basin. In: *Synopsis of Research Conducted under the 1998/99 Northern Contaminants Program*; Kalhok, S., Ed.; INAC: Ottawa; pp. 367.

Macdonald, R. W.; C. S. Wong, and P. E. Erickson. 1987. The distribution of nutrients in the southeastern Beaufort Sea: implications for water circulation and primary production. *J. Geophys. Res.* **92:** 2939-2952.

Mackay, D. and A. T. K. Yeun. 1983. Mass Transfer Coefficient Correlations for Volatilization of Organic Solutes from Water. *Environ. Sci. Technol.* **17:** 211-217.

McClelland, J. W.; R. M. Holmes; K. H. Dunton, and R. W. Macdonald. 2010, in press. The Arctic Ocean Estuary. *Estuar. Coast.* doi:10.1007/212237-010-9357-3.

Mukherjee, I. and M. Gopal. 1996. Chromatographic techniques in the analysis of organochlorine pesticide residues. *J. Chromatogr. A.* **754:** 33-42.

Oehme, M.; J.-E. Haugen, and M. Schlabach. 1996. Seasonal Changes and Relations between Levels of Organochlorines in Arctic Ambient Air: First Results of an All-Year-Round Monitoring Program at Ny-Ålesund, Svalbard, Norway. *Environ. Sci. Technol.* **30:** 2294-2304.

Patton, G. W.; D. A. Hinckley; M. D. Walla, and T. F. Bidleman. 1989. Airborne organochlorines in the Canadian High Arctic. *Tellus.* **41B:** 243-255.

Prasad, A. K.; N. Pant; S. C. Srivastava; R. Kumar, and S. P. Srivastava. 1995. Effect of dermal application of hexachlorocyclohexane (HCH) on male reproductive system in rat. *Human and Experimental Toxicol.* **14:** 484-488.

Pućko, M.; G. A. Stern; D. G. Barber; R. W. Macdonald, and B. Rosenberg. 2010. The International Polar Year (IPY) Circumpolar Flaw Lead (CFL) System Study: the importance of brine processes for α- and γ-hexachlorocyclohexane (HCH) accumulation or rejection in sea ice. *Atmos.-Ocean.* **48:** 244-262.

Pućko, M.; G. A. Stern; R. W. Macdonald; B. Rosenberg, and D. G. Barber. 2011. The influence of the atmosphere-snow-ice-ocean interactions on the levels of hexachlorocyclohexanes (HCHs) in the Arctic cryosphere. *J. Geophys. Res.* **116:** C02035, doi:10.1029/2010JC006614.

Sahsuvar, L.; P. A. Helm; L. M. Jantunen, and T. F. Bidleman. 2003. Henry's law constants for α-, β-, and γ- hexachlorocyclohexanes (HCHs) as a function of temperature and revised estimates of gas exchange in Arctic regions. *Atmosph. Environ.* **37:** 983-992.

Schlitzer, R. 2009. Ocean Data View, http://odv.awi.de.

Shen, L.; F. Wania; Y. D. Lei; C. Teixeira; D. C. G. Muir, and T. F. Bidleman. 2004. Hexachlorocyclohexanes in the North American atmosphere. *Environ. Sci. Technol.* **38:** 965-975.

Timco, G. W. and R. M. W. Frederking. 1996. A review of sea ice density. *Cold Reg. Sci. Technol.* **24:** 1-6.

Wania, F. and D. Mackay. 1993. Global fractionation and cold condensation of low volatility organochlorine compounds in polar regions. *Ambio.* **22:** 10-18.

Wania, F. and D. Mackay. 1999. Global chemical fate of α-hexachlorocyclohexane. 2. Use of a global distribution model for mass balancing, source apportionment, and trend prediction. *Environ. Toxicol. Chem.* **18:** 1400-1407.

Wiberg, K.; R. J. Letcher; C. D. Sandau; R. J. Norstrom; M. Tysklind, and T. F. Bidleman. 2000. The Enantioselective Bioaccumulation of Chiral Chlordane and α-HCH Contaminants in the Polar Bear Food Chain. *Environ. Sci. Technol.* **34:** 2668-2674.

Willett, K. L.; E. M. Ulrich, and R. A. Hites. 1998. Differential toxicity and environmental fates of hexachlorocyclohexane isomers. *Environ. Sci. Technol.* **32:** 2197-2207.

Wong, F.; L. M. Jantunen; M. Pućko; T. Papakyriakou; G. A. Stern, and T. F. Bidleman. 2011, in press. Air-Water Exchange of Anthropogenic and Natural Organohalogens on International Polar Year (IPY) Expeditions in the Canadian Arctic. *Environ. Sci. Technol.* doi:10.1021/es1018509.

Chapter 6

Synopsis of findings

6.1 Summary of research findings

Sea ice may have a potential to transport and redistribute contaminants in the Arctic Ocean (Pfirman *et al.*, 1995, 1997; Korsnes *et al.*, 2002). Rapidly declining sea ice extent and thickness will probably have cascading effects on many aspects on the Arctic environment including contaminant transport and exposures through altered pathways within the Arctic marine environment (Schiedek *et al.*, 2007). In-depth knowledge of the accumulation, transport, and rejection of contaminants in the Arctic cryosphere as well as their cycling between various abiotic compartments in the environment is needed to predict the potential for ice to redistribute contaminants effectively and measure potential impacts of climate change in the years to come.

This thesis provides the first insight into the understanding of the pathways of hexachlorocyclohexane (HCH) in the Arctic marine environment, with particular emphasis on the cryosphere. The null hypothesis of this thesis (cryospheric processes have no significant potential to impact HCH levels in the Arctic marine environment) can be rejected. Findings of this research point to the potential of the cryospheric processes to redistribute HCHs in the Arctic marine environment effectively. Below, the major findings of this thesis are summarized.

As the ice forms, HCHs are being rejected in conjunction with brine. Levels of HCHs in the first year ice (30-200 cm) from the Amundsen Gulf were measured at 0.261 ± 0.015 (SE) ng/L and 0.040 ± 0.002 (SE) ng/L for the α- and γ-isomer, respectively. They were roughly four times lower than the levels reported in the under-ice water of the Amundsen Gulf. This circumstance suggests that ice formation may be considered as a solvent depleting process leading to increased levels of HCHs in the under-ice sea water through brine rejection. Analysis of α-HCH vertical distribution in the PML of the Beaufort Sea revealed that ice formation can increase concentrations of

this HCH isomer in the water just beneath the ice significantly. Taken together, ice formation and transport may lead to significant vertical redistribution of HCHs within the PML through brine rejection in the area of ice formation. It can also lead to large-scale horizontal redistribution of HCH through concentration in the area of ice formation and dilution in the area of ice melt. Concentrating processes would mainly take place in shallow coastal regions, e.g. Kara Sea, and diluting processes in marginal ice zones where majority of ice melts, e.g. within Beaufort Sea or Barents Sea (Pfirman *et al.*, 1995).

The relationships between HCH in sea ice and the geophysical and thermodynamic state of the ice are crucial in understanding HCH pathways in the Arctic cryosphere. Average α-HCH concentrations in the ice column were highly dependent on initial entrapment of brine and later desalination. γ-HCH levels were less predictable by geophysical parameters of the sea ice. Old ice samples had relatively high levels of HCHs despite significant desalination, likely due to deposition of HCHs onto the ice during its survival of the spring season. Three distinct thermodynamic states of first year ice appeared to be important to understand HCH behaviour: growing, warming and melting. Vertical distribution of α-HCH depended strongly on depth in the ice core, salinity and texture during growing phase, on the depth in the ice core and salinity in the warming state, and was independent of these variables during the melting state. Unlike α HCH, γ-HCH vertical distribution in the ice was not strongly related to geophysical variables during any of the thermodynamic ice states. Our results point to the possibility of atmospheric deposition to the ice or small-scale spatial variability of γ-HCH. During melting, which corresponds to the algal bloom period, biological processes within the bottom part of the ice manifests itself as a significant decrease in γ-HCH concentration and α-HCH EF, possibly due to algal uptake and enantioselective

bacterial degradation. Redundancy Analysis confirmed the presence of a factor, additional to geophysical variables, determining levels of α- and γ-HCH in the bottom of the ice during the algal bloom period.

This research points to the role of sea ice brine for exposures to HCHs, especially in the case of ice-associated biota. Brine contained within sea ice currently exhibits the highest HCH concentrations in any abiotic Arctic environment, exceeding under-ice water concentrations by a factor of approximately 3 in the spring, and 4 in the winter. On average, in the winter first-year sea ice HCH brine concentrations reached 4.013 ± 0.307 (SE) ng/L and 0.423 ± 0.013 (SE) ng/L for the α- and γ-isomer, respectively. This circumstance implies that ice-associated biota, e.g. ice algae or sympagic amphipods, have been and continue to be the most exposed to HCHs. This, in turn, translates into higher biological exposures all the way up through the Arctic marine food web.

Sump-hole technique has been proven to be a reliable means of collecting brine for HCH measurements in the Arctic under winter and spring conditions. Ice crystal matrix melting, sea water or upper layers brine seeping, and air-brine gas exchange were shown not to have a significant impact on the HCH levels measured directly in the sea ice brine. Using basic calculations, it was estimated that roughly 50 % of the total HCH burden in sea ice was entrapped within the sea ice crystal structure. This phenomenon could explain relatively high levels of HCHs recorded in the old ice samples. In the spring, HCHs in the brine decreased gradually with time, with increasing brine volume fraction and decreasing brine salinity. These decreasing concentrations could be accounted for by both the dilution with the ice crystal matrix and under-ice sea water. However, it was proposed that the former process plays a more significant role considering brine volume fractions were below 20 %.

The complexity of the physical interactions between atmosphere, snow and sea ice provide for equal complexity in the exchange of HCH between these media. The physical processes, which depend strongly on the season, and the chemical exchanges, which depend on snow and ice physical characteristics, atmospheric conditions, and age of the snow, are depicted schematically in Figure 6.1. In the fall, HCH concentrations in newly-forming sea ice depend primarily on the rate of ice formation (HCH accumulation) and desalination (concurrent HCH rejection) until the combination of declining atmospheric temperature and increasing insulation by a thickening ice cover permit the ice to cool sufficiently for its brine volume fraction to drop below 5 %. In the winter, most of the ice column exhibits a brine volume fraction below 5 %; throughout this time the accumulating HCH concentrations at the bottom of the ice will become locked as the ice grows, thereby reflecting HCH concentration of the water beneath the ice. After the first snow deposition, upward migration of brine from the surface of the ice will affect levels of salt and HCHs in the snow by diffusion out of the shallow 'slush' layer, which maintains a brine volume fraction greater than 5 %. In contrast, ventilation under windy conditions will lead to a decrease in HCH concentrations in the snow pack due to the loss of snow surface area. The atmospheric environmental conditions discussed above, clearly have a significant influence on HCH variability in snow. The extent to which snow can affect HCH levels in sea ice is significantly smaller, and restricted to a short period in spring when the ice warms enough for its brine volume fraction to exceed 5 %.

Decline of α-HCH in the PML and the PL of the Beaufort Sea due to degradation provides important insight into elimination rates of this chemical from the Arctic Ocean. It shows that roughly 80 % decrease in α-HCH inventories observed between 1993 and 2007 can be accounted for exclusively by degradation (bacterial and

hydrolytic). If the degradation rates do not change significantly in the nearest future, the majority of α-HCH could be eliminated from the Beaufort Sea by 2020. Putting this observation in a broader context, there appears to be a lag of about half a century between peak loadings of α-HCH and its elimination from the water.

Figure 6.1 Schematic diagram of atmosphere-snow-sea ice-ocean processes affecting HCH concentrations in various compartments of the Arctic environment in various seasons

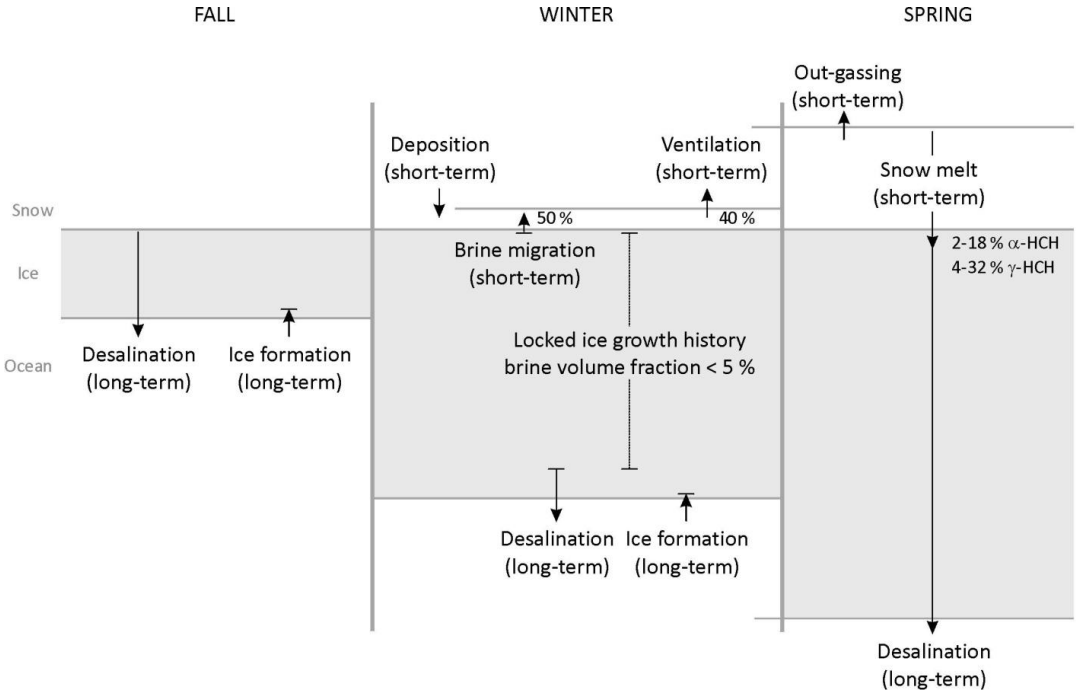

6.2 Potential implications of climate change on HCH exposures and pathways

There are several observations in this thesis, based on which indirect impacts of climate change on HCH exposures can be predicted. Although the nature of such predictions will be speculative to a certain extent, they present an important platform to start this kind of debate. The impacts on exposures discussed here will act primarily through changed HCH pathways within the Arctic marine cryosphere.

One of the major changes modeled between 1950 and 2050 for the Arctic Ocean includes major shifts in sea ice transport and storage, ocean transport and storage, and net surface flux exchange (Holland *et al.*, 2007). Undoubtedly such shifts will have implications for HCH exposures by affecting ice routes, and in turn, the capacity to redistribute HCHs horizontally within the Arctic environment and beyond. Also, changes in timing of ice formation/decay as well as increased rates of melting will probably impact vertical redistribution of HCHs in the PML.

Climate change will also affect the structure of the Arctic marine food web significantly (Gradinger, 1995). Open water regions of enhanced primary productivity (polynyas and marginal ice zones, MIZ) will occur in areas that until now have been characterized by a perennial ice cover and an extremely low biological productivity. This shift will most likely decrease the annual percentage contribution to the food web by sea-ice primary producers in favor of pelagic producers. In turn, this will most likely affect the entire Arctic food web exposures to HCHs by changed proportions of ice algae (exposed to relatively high levels of HCHs in the brine) versus phytoplankton at the base of this food web.

Finally, changes in the perennial versus annual types of sea ice will affect the temperature distribution at the surface of the ice (Barber *et al.*, 2009), making the interaction of snow cover and sea ice more widespread in the Arctic both geographically and seasonally. Subsequently, the exchange rates of HCHs between different compartments of the Arctic cryosphere will most likely shift.

6.3 Future research directions

As shown in this thesis, atmosphere-snow-ice-ocean interactions as well as ice geophysical and thermodynamic properties are crucial in understanding pathways of

HCHs, and most likely other contaminants, in the Arctic marine environment. This research fills in a gap in knowledge about HCH cycling in the Arctic cryosphere, however, there is still a lot to be discovered regarding other contaminant pathways in sea ice, snow and brine. Future research should focus on entrapment, transport, and rejection of other contaminants by sea ice and snow highlighting differences between water soluble (e.g. HCHs) versus particle-bound contaminants (e.g. PCBs). Ultimately, climate change effects on ice and snow transport and thermodynamics should be further investigated and linked to potential direct and indirect consequences for contaminant exposures.

Experimental approach would also greatly contribute to the understanding of contaminant pathways in the Arctic cryosphere. Freezing of ice from artificial sea water spiked with different contaminants under varying conditions (e.g. turbulent versus quiescent, very low temperatures versus ones just below freezing) could provide insight into those chemicals entrapment in and rejection from ice in various environmental scenarios. Using experimental cryospheric set-up, particularly one with controlled atmosphere, would be of enormous benefit to conduct research on contaminats partitioning and transport between various environmental compartments including different climate change scenarios.

6.4 References

Barber, D. G.; R. Galley; M. G. Asplin; R. De Abreu; K.-A. Warner; M. Pućko; M. Gupta; S. Prinsenberg, and S. Julien. 2009. Perennial ice pack in the southern Beaufort Sea was not as it appeared in the summer of 2009. *Geophys. Res. Lett.* **36:** L24501, doi:10.1029/2009GL041434.

Gradinger, R. 1995. Climate change and biological oceanography of the Arctic Ocean. *Philos. Trans. R. Soc. London, Ser. A.* **352:** 277-286.

Holland, M. M.; J. Finnis; A. P. Barret, and M. C. Serreze. 2007. Projected changes in Arctic Ocean freshwater budgets. *J. Geophys. Res.* **112:** G04S55, doi:10.1029/2006JG000354.

Korsnes, R.; O. Pavlova, and F. Godtliebsen. 2002. Assessment of potential transport of pollutants into the Barents Sea via sea ice – an observational approach. *Mar. Pollut. Bull.* **44:** 861-869.

Pfirman, S. L.; H. Eicken; D. Bauch, and W. F. Weeks. 1995. The potential transport of pollutants by Arctic sea ice. *Sci. Total Environ.* **159:** 129-146.

Pfirman, S.; J. Kogler, and I. Rigor. 1997. Potential for rapid transport of contaminants from the Kara Sea. *Sci. Total Environ.* **202:** 111-122.

Schiedek, D.; B. Sundelin; J. W. Readman, and R. W. Macdonald. 2007. Interactions between climate change and contaminants. *Mar. Pollut. Bull.* **54:** 1845-1856.